UiT The Arctic University of Norway

Faculty of Biosciences, Fisheries and Economics

Exploring the Performance Space of a Genetic Toggle Switch across Host and RBS context

Lena Winter

Master's thesis in Marine Biotechnology (BIO-3901), May 2024

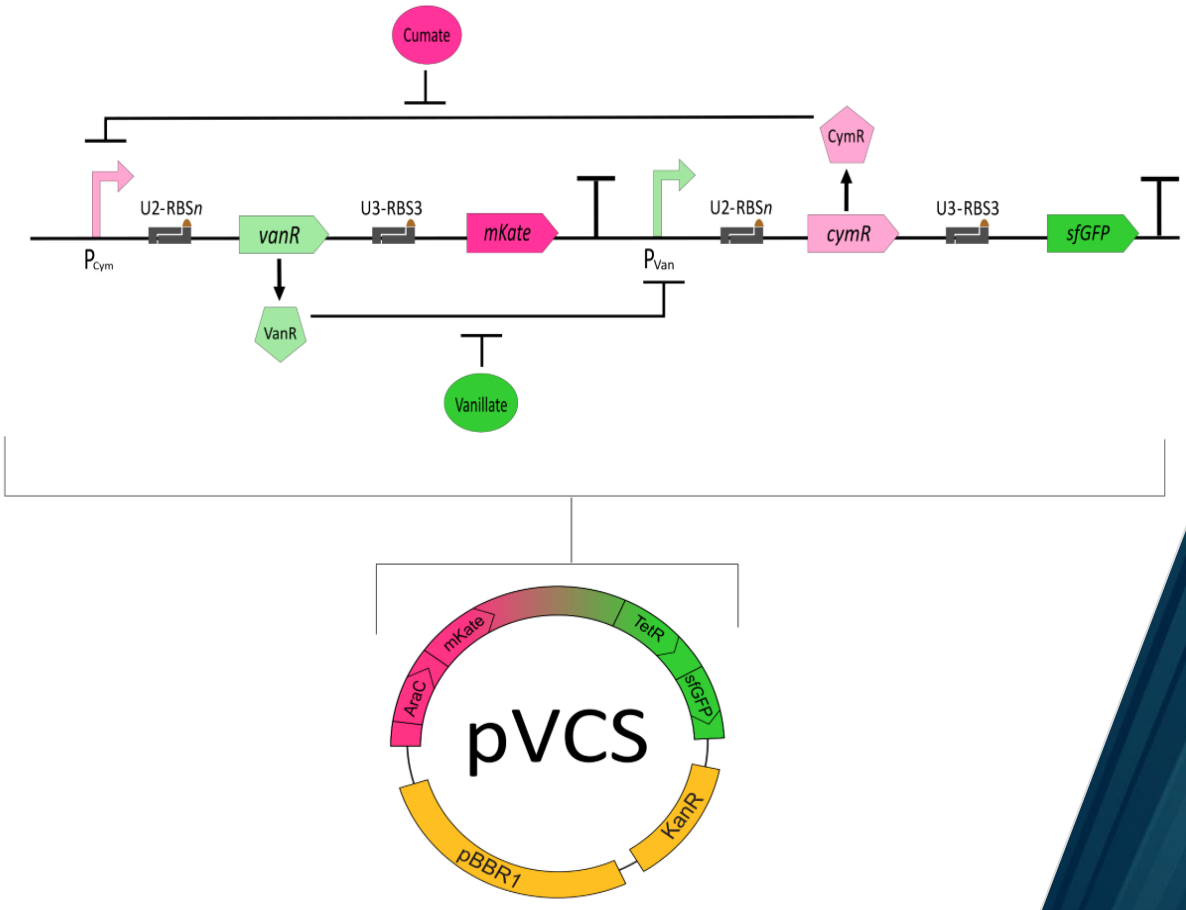

Acknowledgements

This Master's Thesis was conducted in the Microalgae and Microbiomes Research Group (M2RG) at the Faculty of Bioscience, Fisheries and Economics at UiT - The Arctic University of Norway under supervision of Professor Hans Christopher Bernstein and PhD candidate Dennis Tin Chat Chan. The thesis comprises 60 ECTS and was submitted to the UiT to fulfill the requirements for the Master of Science (M.Sc.) in Marine Biotechnology.

Reflecting on this challenging but incredibly rewarding journey, I would like to take the opportunity to express my gratitude to the people who continuously supported me.

I would like to thank my supervisor Hans for giving me the opportunity to work on this project in the M2RG research group. Your expertise and encouragement have been invaluable assets to me during the process of writing my thesis. Thank you for your mentorship and your dedication to fostering a supportive and stimulating environment within the research group.

I also want to reinforce my immense gratitude to my amazing co-supervisor Dennis for his invaluable support, not only during laboratory work, but also during the intense process of data analysis and writing. I deeply appreciate your willingness and patience to answering all my questions and providing insightful feedback that helped me to shape my ideas and refine this work.

Furthermore, I would like to thank the entire M2RG research group for creating such a pleasant working atmosphere in which I could learn and grow. The team spirit has been a constant inspiration to me and has reinforced my belief in the collective benefits of collaboration, which I would not want to miss on my professional journey.

I am also incredibly grateful to my friends, family, and my partner who have been a source of unwavering motivation and emotional support to me. I appreciate your belief in my abilities and your willingness to mentally guide me on this journey to completing my Master's degree.

Lena Winter

UiT, The Norwegian College of Fishery Science

Tromsø, May 2024

Hans Christopher Bernstein

Abstract

Synthetic biology applies engineering principles onto biological systems to rationally create novel devices with desired properties. The behavior of an engineered genetic circuit is influenced by a complex multitude of factors, including regulatory elements and the cellular environment it operates within. This thesis delves into the impact of ribosome binding site (RBS) configurations and host context on shaping the performance space of a synthetic genetic toggle switch. A total of nine toggle switches were assembled using the BASIC DNA assembly platform, incorporating different combinations of three RBS strengths regulating the translation efficiency of the transcriptional repressors. Analysis of quantifiable performance parameters revealed differing performance profiles across toggle switches with varying RBS combinations. Moreover, this work investigated the impact of host-context on toggle switch performance (i.e. the chassis-effect) by transforming the genetic circuits into *Escherichia coli* DH5α and *Pseudomonas putida* KT2440. Strong clustering of performance profiles was observed along host organisms, suggesting a clear chassis-effect dominating over RBS context in driving toggle switch performance. This work unveils the opportunity of the chassis-effect to expand the design space of a genetic circuit, underlining the pivotal role of selecting an appropriate chassis as a crucial variable in synthetic biodesign. Furthermore, harnessing the fine-tuning potential of RBS can serve as an efficient strategy to regulate and optimize gene expression levels. Considering a multitude of design parameters that allow for strategical tuning will pave the way for precise control over gene expression, enhancing the functionality of genetic circuits, and expanding the repertoire of tools available for synthetic biology endeavors.

Keywords: Synthetic biology, genetic toggle switch, RBS, chassis-effect, performance space

Table of Contents

List of Tables

List of Figures

Abbreviations

RBS	Ribosome binding site
WT	Wild-type
BASIC	Biopart Assembly Standard for Idempotent Cloning
SEVA	Standard European Vector Architecture
BB	Backbone
Km^R	Kanamycin resistance marker
Cm^R	Chloramphenicol resistance marker
iS / iP	integrated Suffix / integrated Prefix
(c)PCR	(colony) Polymerase Chain Reaction
PCA	Principal Component Analysis
UTR	Untranslated region
OSTIR	Open Source Translation Initiation Rate Prediction
OSF	Open Science Framework
Cym	Cumate
Van	Vanillate
NI	No Inducer
A	Carrying capacity
μ	Specific growth rate
Fss	Maximum fluorescence steady-state intensity
DR	Dynamic range
β	Maximal expression level
n	Hill coefficient
C	Basal expression / leakage
K	Activation coefficient
RFU	Relative fluorescence unit

1 Introduction

Synthetic biology involves the utilization of modular and standardized biological parts sourced from natural systems to redesign nature. Modularity of an element refers to the capacity of maintaining its inherent characteristics, even when extracted from its original context. The resulting interchangeability is a fundamental criterion for reprograming cellular behavior and has predominantly been achieved at the genetic level using DNA parts, such as protein coding sequences and regulatory units (Benner & Sismour, 2005). These modules are rationally assembled to create genetic circuits capable of processing input signals and respond accordingly with a defined output in a predictable manner. Due to the modularity of DNA parts, the rewiring of cellular processes is facilitated by altering input and output constructs to obtain highly adaptable and versatile devices for tailored applications. Efficient biodesign requires not only an understanding of the functions of individual components but also their interactions as a whole. Furthermore, an increasing genetic toolbox of cloning techniques, assembly methods, and sequencing data, complemented by a growing number of well-characterized parts, allows for the construction of gene networks of increasing complexity, capable of addressing broader biological challenges. Emerging application fields for these engineered devices include bioremediation (Gilbert et al., 2003), biosynthesis of valuable compounds, such as polymers and antimicrobial precursors (Benner & Sismour, 2005), diagnostic tools (Elbeik et al., 2004), biosensors (Khalil & Collins, 2010), and biofuel production (Waks & Silver, 2009).

The efficacy and performance of a synthetic device strongly relies on the host organism in which it operates (Cardinale & Arkin, 2012). Consequently, the phenomenon of host-specific performance arises, denoting the altered behavior of a genetic device within the context of its host, often termed the chassis-effect (Khan et al., 2020). Chan et al. (2023) and others have described the emergence of a clear chassis-effect, wherein diverse performance profiles were displayed by the same genetic circuit when operating within different host organisms under standardized conditions. The observed differences in performance parameters correlated notably with differences in the physiological properties between hosts (Chan et al., 2023). The performance of a genetic circuit is dependent on the cellular environment provided by the host, as it becomes coupled to the host's metabolic flux and relies on the host-specific machinery, as well as on the availability of cellular resources (Cardinale & Arkin, 2012). Furthermore, operation of heterologous and endogenous elements within the same cell opens up the possibility of direct and indirect interactions between cellular components, as well as cross-talk with metabolic pathways, and competition with endogenous processes, all intricately linked to

cellular growth dynamics (Klumpp et al., 2009; Tas et al., 2021). Although host-context dependencies can impede the predictability and interoperability of genetic circuits (Kushwaha & Salis, 2015), they also offer a compelling opportunity to expand the circuits' performance space and optimize expression levels (Tas et al., 2021). Consequently, to effectively explore the performance space of a genetic circuit, it is imperative to consider the intricate nature of host-context effects.

Undesired cross-talk and indiscriminate interactions between individual components can impede the predictability of a genetic circuit (Cardinale & Arkin, 2012). The expression of heterologous pathways also competes with endogenous processes in the host organism for cellular resources (Ow et al., 2006). The resulting imbalances in gene expression can lead to decreased productivity, the accumulation of toxic intermediates, or significant growth burdens, all of which impact the performance, robustness, and predictability of a device (Tas et al., 2021; Zelcbuch et al., 2013). To address these challenges, precise fine-tuning of gene expression within genetic circuits is highly desirable. This involves adjustments of regulatory modules, such as promoters and ribosome binding sites (RBSs), regulating gene expression at the transcriptional and translation levels, respectively, to achieve an optimized performance space (Chen et al., 2018; Salis et al., 2009). However, determining the optimal expression levels necessary for desired circuit behavior is challenging, due to the innumerable potential interactions among individual components, making rational design a non-trivial task. Combinatorial approaches offer a promising solution by simultaneously exploring the effects of multiple regulatory elements, thereby spanning a broader expression space in a time-efficient manner without requiring extensive prior knowledge of optimal expression levels (Naseri & Koffas, 2020; Zelcbuch et al., 2013). This approach allows for the creation of library parts covering a broad expression range and expanding the genetic toolbox beyond conventional modules (Ellis et al., 2009; Lu et al., 2009). However, even subtle alterations in regulatory elements can considerably impact gene expression levels, which, paired with innumerable possible combinations, results in combinatorial explosion, which is defined as a condition, in which the experimental space is undoubtedly outnumbered by the sequence space (Farasat et al., 2014). To address this challenge, *in silico* tools have been developed to streamline the exploration of the experimental space and circumvent combinatorial explosion (Farasat et al., 2014; Jeschek et al., 2016). These computational efforts, which generate optimized libraries through intelligent algorithms, complement combinatorial and fine-tuning design principles.

They have demonstrated success in enhancing biosynthetic pathways, as evidenced in boosting the production of violacin, a medically valuable compound (Jeschek et al., 2016).

While the majority of combinatorial research aimed at optimizing pathway flux has concentrated on transcriptional control (Naseri & Koffas, 2020), tuning at the translational level has also been recognized as a highly effective and customizable strategy for modifying and expanding the performance space of genetic devices (Jiang et al., 2023). For instance, in a study conducted by Anderson et al. (2007) it was found that the inherent activities of certain promoters failed to encompass the range required for desired circuit performance. However, by manipulating the strengths of RBSs, the anticipated performance was achieved, underlining the fine-tuning potential of this regulatory element (Anderson et al., 2007). Moreover, the possibility to regulate multiple genes within an operon (Zelcbuch et al., 2013), the versatility across diverse host organisms (Farasat et al., 2014), and the significant impact on translational rates resulting from minimal alterations within these short sequences (Salis et al., 2009) render RBSs particularly attractive targets for expression fine-tuning. RBSs play a central role in translation initiation, the rate-limiting step of the translational cascade (Laursen et al., 2005). The RBS recruits the 30S ribosomal subunit through molecular interactions between the Shine-Dalgarno (SD) sequence embedded within the RBS and the anti-SD sequence present in the 16S rRNA of the ribosomal subunit (Shine & Dalgarno, 1974). The degree of complementarity between the SD and anti-SD sequences determines the binding affinity, thereby dictating the efficiency of translation initiation complex formation, which reflects the strength of the RBS. Furthermore, factors such as the distance between the RBS and the start codon, the choice of the start codon itself, and the presence of secondary structures proximal to the RBS have been shown to impact translation initiation rates (Na & Lee, 2010; Salis et al., 2009; Seo et al., 2013; Studer & Joseph, 2006). Consequently, the optimal RBS strength varies for each gene coding sequence (Salis et al., 2009; Thiel et al., 2018). Combinatorial modifications of RBS strengths can therefore be an effective strategy to explore a broader expression space and attain desired performance profiles. Illustrating the practical utility of this approach, Zelcbuch et al. (2013) employed combinatorial variations of RBSs to significantly enhance the biosynthesis of astaxanthin, a high-value industrial carotenoid (Zelcbuch et al., 2013). Furthermore, several computational tools have been developed to complement the design process and streamline experimental endeavors by predicting translation initiation rates based on given mRNA sequences, or design *de novo* RBS sequences that yield desired expression levels (Na & Lee, 2010; Salis et al., 2009; Seo et al., 2013).

Ultimately, a comprehensive understanding of how individual DNA modules interact within their regulatory network and considering the chassis-effect will empower innovative biodesign towards genetic circuits operating in a robust, predictable, and efficient manner (Lu et al., 2009).

1.1 Main Objectives

This work aims to explore the performance space of a genetic toggle switch across both, RBS configurations and host context. A total of nine toggle switches were assembled, varying in combinations of RBS strengths that regulate the expression of transcriptional repressors. Performance metrics of each toggle switch were quantified through a series of assays, delineating the combinatorial RBS performance space for each toggle switch. Furthermore, this work explores the chassis-effect, the impact of host context on the behavior of a genetic circuit. By introducing the nine toggle switches into the two distinct host organisms *E. coli* DH5α and *P. putida* KT2440, host-specific performance profiles are compared. Consequently, this thesis evaluates the importance of RBS and host context used as design parameters to shape the performance space of a genetic circuit.

2 Background

2.1 Synthetic Biology and the Design-Build-Test Cycle

By deconstructing genomes into modular parts and restructuring these characterized parts into novel constructs, synthetic biology aims to understand fundamental biological processes and apply this knowledge to create innovative designs. While reconstructing modular DNA parts can yield in various types of gene expression systems, the term genetic circuit is used to describe devices capable of processing an input and responding with a defined output (Benner & Sismour, 2005). The development of synthetic genetic circuits often employs a systematic and iterative engineering strategy known as the design-build-test cycle (Liu et al., 2015). The design phase focuses on the exploration of a theoretical construct's design space and is highly dependent on characterization of genome structures, metabolic fluxes, and regulatory networks. The usage of databases, repositories, and *in silico* tools facilitates identifying DNA parts required to design desired input-output properties. During the build process, the genetic circuit is physically constructed and integrated into a host organism, using various DNA assembly techniques and transformation methods. Testing protocols are tailored to the function and the measurable input-output parameters of the device. Results of the performance analysis can guide subsequent rational changes to improve the design and achieve desired functionality.

2.1.1 Design: The Toggle Switch

The design process involves choosing an appropriate expression system, defining the type of desired input and output variables and the mechanism in which these inputs will ultimately be computed into output. With an expanding repository of well-characterized parts and assembly methods, more complex devices can be designed, such as logic gates (Jiang et al., 2023), oscillators (Elowitz & Leibler, 2000) or toggle switches (Gardner et al., 2000). Often, these input-output properties are inspired by regulatory networks ubiquitously found in nature. Bistable switches have been found to play critical roles in cellular decision making and cell differentiation (Strasser et al., 2012; Wu et al., 2013), for instance, governing the lysis-lysogeny fate of a bacteriophage (Khalil & Collins, 2010). The genetic toggle switch, a bistable regulatory gene network and one of the inaugural synthetic circuits was first described by Gardner et al. (2000). The design involves two gene cassettes that, upon induction, express transcription factors that mutually repress each other's promoters. Hence, if one gene is activated, the transcriptional repressor of the opposing gene cassette is produced, creating a feedback loop that allows the switch to attain a stable induction state. This state is retained,

even in absence of the inducing signal, displaying the biological equivalent of memory storage, until a certain threshold of the opposing inducer is present, which causes activation of the contrary gene cassette, switching the device to its alternative induction state (Cherry & Adler, 2000; Gardner et al., 2000).

The modular design of the genetic toggle switch allows to replace and customize regulatory DNA parts. The toggle switches created in this work combine two gene cassettes, each regulated by an inducible system consisting of a negatively inducible promoter and its cognate repressor, P_{Van}-VanR and P_{Cym}-CymR, respectively. In contrast to constitutive expression structures, inducible systems allow for more precise control over gene expression levels, making them particularly valuable in synthetic circuits (Martin-Pascual et al., 2021). The produced repressor proteins, CymR and VanR, bind to a recognized site in the operator region within their cognate promoter, thereby preventing the RNA polymerase complex from binding, inhibiting transcription initiation. Binding of cumate or vanillate, to their respective repressor proteins causes an allosteric change, releasing the repressor molecule from the operator binding site and allowing transcription to occur. VanR is part of the PadR-like transcriptional regulator family, naturally occurring in the *vanR-vanABK* system of *Caulobacter crescentus* (Thanbichler et al., 2007). Active VanR operates in dimers, blocking operator sites adjacent to −35 and −10 regions upstream of the transcription initiation site (Kunjapur & Prather, 2019). While vanillate has been identified as the only effector of VanR (Morabbi Heravi et al., 2015), minimal toxicity was shown for induction with up to 5 mM vanillate in an *E. coli* host (Kunjapur & Prather, 2019). CymR acts as a transcription factor of promoter P_{Cym}, which is flanked by two operator sites (CuO) allowing CymR to bind. The corresponding *p-cmt/p-cym* operon was originally described in *P. putida F1* (Eaton, 1997). According to current knowledge, no growth inhibiting effects of cumate were reported from studies employing cumate-inducible expression systems (Eaton, 1997; Kaczmarczyk et al., 2013; Meyer et al., 2019), with the highest concentration tested being 0.1 mM (Meyer et al., 2019). Given the systems dual inducible nature, it is crucial to prevent cross interactions between the individual components, and to ensure that the respective promoters and repressors solely react to their designated stimuli. Results of Kaczmarczyk et al. (2014) combining P_{Van}/VanR and P_{Cym}/CymR inducible systems in a *Sphingomonas* host suggest no cross reactivity while each system responded to their cognate inducer (Kaczmarczyk et al., 2014).

To ensure transferability, maintenance, and stable operability in multiple host organisms, genetic devices are built into plasmid vectors, providing the scaffold for the synthetic

constructs. Efforts towards uniform cloning vector design principles resulted in the Standard European Vector Architecture (SEVA), promoting standardization and reproducibility of broad-host plasmid designs (Silva-Rocha et al., 2013). The genetic toggle switch used in this work is incorporated into a SEVA-based backbone encompassing a kanamycin antibiotic resistance marker (Km^R) and the broad-host pBBR1 origin of replication (Haines et al., 2022), allowing for selection of transformed hosts and maintenance of the synthetic construct.

2.1.2 Build: BASIC Biopart Assembly

The ability to precisely assemble modular DNA parts to create genetic constructs with desired functions is a crucial aspect in synthetic biology. Various assembly methods with different properties have been developed, while each method is based on the complementary base-pair binding property of DNA (Casini et al., 2015). In this work, the Biopart Assembly Standard for Idempotent Cloning (BASIC) method is applied, which has standardization and part-library construction as a core property, while also allowing for simultaneous one-pot assembly (Storch et al., 2015). DNA parts are integrated into the BASIC standard by flanking them with the BASIC Prefix (*i*P; 5'-TCTGGTGGGTCTCTGTCC- 3') and the BASIC Suffix (*i*S; 5'-GGCTCGGGAGACCTATCG- 3') sequences. DNA parts of interest can be synthesized with the *i*P and *i*S sequences already flanking. Alternatively, PCR with designed primers containing the respective sequences can be performed. The obtained universal BASIC format allows the biopart to be assembled in any genetic context. As BASIC assembly is a restriction-ligation based method, it uses restriction enzymes that recognize defined sequences and introduce cuts in a specific pattern. Specifically, BSAI, a type IIS restriction enzyme, is used, characterized by its ability to cut outside of its recognition site located in the *i*P and *i*S sequences, releasing the biopart from its storage vector and leaving it with a four base pair overhang. Subsequently, BASIC Prefix and Suffix half linkers are clipped to the DNA part of interest by complementary annealing to the four base pair overhang, respectively. During the annealing process, DNA ligase seals the nicks and subsequent purification yields the final DNA part clipped with half linkers. Simultaneously, the linkers contain single stranded regions that are complementary to other linkers, thus guiding the accurate final order of assembly in a one-pot reaction. BASIC linker sequences are designed by an algorithm, allowing orthogonal functionality, while avoiding undesirable sequence motifs, such as restriction recognition sites and minimizing presence of secondary structures (Storch et al., 2015). Furthermore, BASIC linkers include a double stranded region, called adapter region that allow incorporation of specific sequences that provide the linker with special functions: In this work, linkers with integrated functional

RBS sequences of different strengths are used to regulate translation of the transcriptional repressors in the toggle switch.

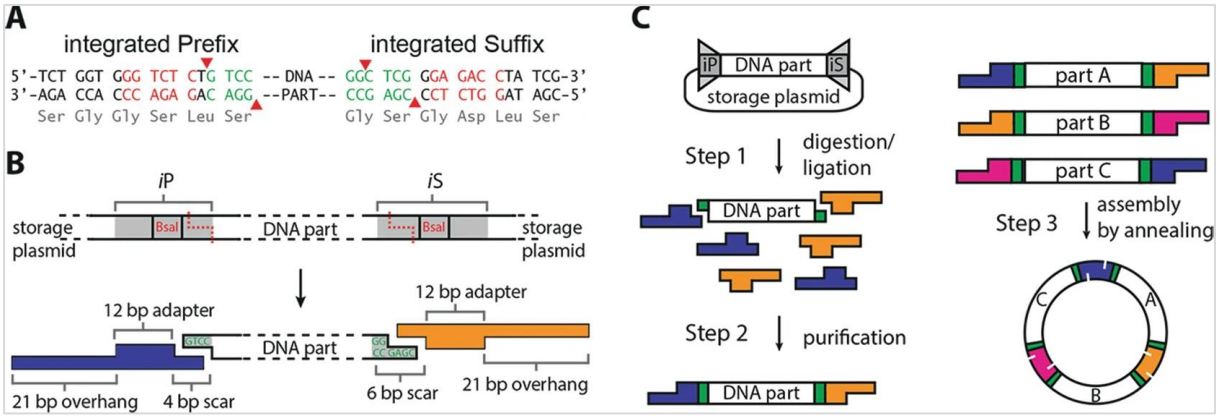

Fig. 1. **BASIC assembly allows for joining of DNA parts in a modular and standardized manner, based on their complementary base-pair binding property.** (A) DNA parts are integrated into the BASIC standard by flanking them with a Prefix and Suffix sequence that include a recognition site for the restriction enzyme BsaI. (B) The DNA part is separated from its storage plasmid through BsaI digestion, leaving a 4bp overhang to which a linker anneals by complementary base-pair binding. (C) Workflow of the BASIC assembly. After isolation of the DNA part from its storage vector and attaching of the desired linker, the linker-flanked DNA part is purified. In a one pot reaction, the desired DNA parts are assembled in a linker-guided order, revealing the final plasmid. Figure adapted from Storch et al. (2015).

2.1.3 Test: Quantifying Device Performance

Genetic circuits are designed to process an input signal and respond with a measurable output, used to characterize performance. The reporter genes built into the toggle switches produce fluorescence proteins whose measurable fluorescence signal intensity correlates to fluorescent protein concentration. Measurements can be conducted in an automated and high-throughput manner using modern plate readers. Quantitative characterization of the performance profiles is achieved by fitting appropriate models to calculate comparable performance parameters. Consequently, differences in the behavior of the toggle switches can be determined across RBS and host context. As fluorescence response measured over time correlates with bacterial growth dynamics, fitting a growth model to the fluorescence curves yields in the parameters rate of fluorescence (Rate) and maximum fluorescence at steady-state of growth (Fss), equivalent to specific growth rate (μ) and carrying capacity (A), respectively.

Measured fluorescence signal in response to inducer concentration resembles a dose-response curve that can be modelled by the Hill function (Ang et al., 2013). This empirical approach describes complex non-linear ligand-receptor interactions and was originally developed by A. V. Hill in order to characterize binding interactions between oxygen and hemoglobin (Hill, 1913). The Hill function is presently recognized to express input-output relations, capturing the

fundamentals of the way changing inputs alter the response of a biological system. The resulting output curve retains the Michaelis-Menten pattern, where the response increases linearly with increasing input until reaching a saturated level. However, unlike Michaelis-Menten kinetics, the Hill function describes a logarithmic, rather than a linear response at low input levels (Frank, 2013). Hence, the Hill function provides a reasonably well fit to numerous biological input-output reactions and is particularly used in the context of gene regulatory mechanisms at the transcriptional level (Alon, 2006). In this work, the Hill function is fitted to induction curves, yielding performance parameters K, C, β, and n, describing induction kinetics of the genetic circuits. The maximum expression level, represented by β, indicates the maximum fluorescence signal displayed at saturating inducer concentration levels. The activation coefficient K expresses the concentration of inducer required to achieve half maximal expression, hence is related to the chemical binding affinity between the repressor and its cognate inducer. Thus, K describes the sensitivity of a system. The Hill coefficient n governs the steepness of the function and is considered to indicate cooperativity between ligand and macromolecule binding. Performance parameter C accounts for basal gene expression in absence of the inducer.

Furthermore, the dynamic range (DR) was calculated, which is defined as the ratio of maximum fluorescence levels between the induced and non-induced state, hence, expressing the overall responsiveness of the toggle switch.

2.2 Computational Tools to Predict Translation Initiation Rates

Predictability of performance is a critical aspect when designing synthetic devices, particularly when modifying regulatory elements. *In silico* strategies can complement the design process of genetic circuits and reduce experimental efforts by circumventing inefficient trial and error optimization (Lu et al., 2009). Several algorithms have been developed allowing the prediction of translation initiation rates of given mRNA sequences, and even to design RBS sequences that achieve desired protein expression levels (Na & Lee, 2010; Salis et al., 2009; Seo et al., 2013). Translation initiation rate prediction is based on a thermodynamic model, characterizing sequence-based molecular interactions during the formation of the translation initiation complex between mRNA transcript and 30S ribosomal subunit. The strength of molecular interactions is quantified by calculating the change in total Gibbs free energy (ΔG_{tot}) between the unbound initial state and the assembled initiation complex. Decreasing ΔG_{tot} indicates that a reaction is more favorable to occur, due to the system's striving to reach a lower energy state.

As the energy of the product (initiation complex) is lower than the energy of the reactants (mRNA, 30S subunit), the decreasing ΔG_{tot} results in favorable interactions between mRNA and 30S complex, enhancing translation initiation rates (Salis et al., 2009). Applying the thermodynamic model to any given RBS sequence upstream a protein coding sequence determines translation initiation rates and therefore RBS strengths in a reverse engineering manner. Furthermore, the combination of the thermodynamic model with an optimization algorithm provides a forward engineering approach, in which RBS sequences are designed to achieve desired translation initiation rates. However, the computational approach has its limitations, for instance, the RBS Calculator developed by Salis et al. (2009) is not accounting for interactions between locally close sequences within an operon, like translational coupling, or other mRNA structural elements that contribute to translation initiation (Reeve et al., 2014). Consequently, *in vivo* approaches are still required to confirm translational efficiency (Lu et al., 2009; Thiel et al., 2018). In this work, the open source software OSTIR (open source translation initiation rate prediction) was applied in this work (Roots et al., 2021). Derived from the RBS Calculator codebase, OSTIR provides means to detect differences in translation initiation rate according to the RBS and its surrounding sequences, namely the upstream untranslated region (UTR) and the downstream protein coding sequence (*vanR*, *cymR*, *sfGFP* and *mKate*, respectively).

2.3 The Open Science Framework

Transparency and collaboration stand as crucial cornerstones in research, indispensable for effectively directing the lifecycle of scientific projects. Launched by the Center of Open Science, a non-profit organization, the Open Science Framework (OSF) serves as an open-source platform, facilitating the management and sharing of research endeavors. The free use of this tool, promotes accessibility, while fostering an environment of transparency and collaboration, in which centralized workflows, spanning from study design and methodology to data analysis and written reports can be developed. To contribute to a reproducible and transparent research practice, all experimental raw data obtained during this study as well as R Markdown scripts used for analysis and visualization was published in the OSF project “Exploring the performance space of a genetic toggle switch across RBS and host context ”, accessible through the following link: https://osf.io/pknmz/

3 Material and Methods

3.1 Bacterial Strains and Culturing Conditions

All bacterial strains used in this work are listed and described in Table 1. Wild-type (WT) strains, if not stated otherwise, were cultivated in sterile lysogeny broth (LB) at 37 °C under constant shaking (1000 rpm). Transformed bacteria hosting the pVCS plasmid or backbone (BB23) were grown in LB-medium containing kanamycin (50 mM). Single colonies of the respective strains were picked from LB-agar plates (containing kanamycin, when applicable) for inoculation of overnight cultures. A negative control consisting of sterile medium was added to check for contamination during each round of cultivation. Freezer stocks were prepared in a cryogenic vial by adding 80% glycerol to an overnight culture (1:3) and stored at -80 °C. Inducer stock solutions (500 mM cumate and 1 M vanillate) were prepared by dissolving cumic acid (Sigma-Aldrich, Germany, 536663) and vanillic acid (Thermo Fisher Scientific, USA, 10228789) in 70% EtOH, respectively. Dissolving vanillate required the gradual addition of 5 M NaOH until precipitants were cleared and a pH of 6-7 was reached (by adding ca. 600 µL NaOH to 10 mL stock solution). Cumate stock solutions were stored at -20 °C, while vanillate stock solutions were kept at room temperature.

Performance analysis required cultivation of bacteria in black 96-well plates with flat and clear bottom (Thermo Fisher Scientific, 165305). Therefore, 199 µL of medium with the respective inducer concentration was added per well and inoculated with 1.5 µL of overnight culture. The plate was sealed using a Breathe-Easy film (Sigma-Aldrich, Germany, Z380059) and cultivated in a plate reader (BioTek Synergy H1 Microplate Reader, Agilent, USA, 21031715) under continuous linear shaking for up to 24 h.

Table 1. Description of bacterial strains used throughout this study.

Strain	Genotype	Culture Collection	NCBI Accession	Reference
E. coli DH5α	WT	DSMZ (6897)	ASM289947v1	(Anton & Raleigh, 2016)
E. coli DH5α	BB23	This study	This study	This study
E. coli DH5α	pVCS1-9	This study	This study	This study
P. putida KT2440	WT	DSMZ(6125)	ASM756v2	(Belda et al., 2016)
P. putida KT2440	BB23	This study	This study	This study
P. putida KT2440	pVCS1-9	This study	This study	This study

3.2 Plasmid Extraction

Overnight liquid cultures of bacterial strains hosting the desired cloning vector were prepared. Plasmid extraction was performed using the QIAprep Spin Miniprep Kit (QIAGEN, Germany, 27106) according to the manufacturer's protocol. Therefore, 5 mL of overnight culture was centrifuged (4000 rpm, 5 min), the supernatant discarded and the cell pellet resuspended with 250 µL Buffer P1. Subsequently, the mixture was transferred into a micro tube, and mixed, first with 250 µL Buffer P2 and second with 350 µL Buffer N3 by inverting the tube. After a 10 min centrifugation at 13000 rpm, 750 µL of supernatant is transferred to a spin column and centrifuged again for 1 min at 13000 rpm. Subsequently, 500 µL Buffer PB is added to the column, centrifuged (1 min, 13000 rpm) followed by addition of 750 µL Buffer PE and centrifugation (1 min, 13000 rpm). To elute the DNA, 30 µL of Ultra Pure Water (Biochrome GmbH, Germany, 0934F) was pipetted onto the spin column before a last centrifugation step (1 min, 13000 rpm). Concentrations of eluted DNA were measured with the NanoDrop ND-1000 Spectrophotometer (Saveen Werner, Sweden).

3.3 BASIC Assembly

The plasmids pVCS1-9 were created using the BASIC DNA assembly method as described by Storch et al. (2015). The assembly workflow consists of four steps, described in 3.3.1-3.3.4. DNA parts used to assemble plasmid pVCS are described in Table 2, while a detailed list of the sequences is provided in Appendix A. Prior to assembly, the individual parts were integrated into the BASIC standard, flanked by BASIC prefix and suffix sequences. A pSEVA331-derived backbone with a chloramphenicol resistance marker (Cm^R) served as vector for each BASIC part and half switch (promoter-RBS1/2/3-repressor coding sequence-RBS3-reporter gene), and was stored in *E. coli* DH5α. Storage plasmids containing the desired contigs, as well as the pSEVA231-based backbone (Km^R) were isolated (3.2) prior to pVCS assembly.

Table 2. Summary of BASIC DNA parts used to create plasmid pVCS1-pVCS9.

Gene/Part	Function	Source	Reference
P_{Van}	Promoter	Donated*	(Haines et al., 2022)
P_{Cym}	Promoter	Donated*	(Haines et al., 2022)
mKate	Fluorescent reporter gene	Donated*	(Haines et al., 2022)

sfGFP	Fluorescent reporter gene	Donated*	(Haines et al., 2022)
VanR	Van inducible repressor	Donated*	(Haines et al., 2022)
CymR	Cym inducible repressor	Donated*	(Haines et al., 2022)
BB23	BASIC intergrated pSEVA231 backbone with pBBR1 ori and Km^R	Cloned from pSEVA231 using B_pSEVA_F and B_pSEVA_R primers primers	(Chan et al., 2023)
BASIC Linkers	BASIC assembly of parts and adding RBS	Purchased from BIOLEGIO (BBT-18500)	(Storch et al., 2015)

*parts donated by Geoff S. Baldwin, Department of Life Science, Imperial College Center for Synthetic Biology, Imperial College London

3.3.1 BASIC Clip Reaction

During clip reaction, specific linkers are ligated to the BASIC parts, that determine the order in which the final pVCS plasmid is assembled. The restriction sites within the prefix and suffix sequences were digested by BSAI, yielding overhangs that are complementary to the prefix and suffix linkers, respectively. For each BASIC part, clip reaction was performed in PCR tubes by mixing 17 µL dH2O, 3 µL 10X T4 DNA Ligase Reaction Buffer (New England Biolabs, USA, B0202S),1 µL prefix linker, 1 µL suffix linker, and 200 nmol of BASIC part (50 ng per 1 kb total plasmid size). Subsequently, 1 µL BsaI-HFv2 20 U/µL (New England Biolabs, USA, R3733) and 0.5 µL T4 DNA Ligase 1-3 U/µL (New England Biolabs, USA, M0202L) were added to each reaction, topped up with dH2O to 30 µL and mixed by pipetting up and down. Finally, each reaction tube was incubated in a PCR thermal cycler under the following program: cycle 20× [37 °C for 2 min, 20 °C for 1 min], 60 °C for 20 min and further used for purification.

3.3.2 BASIC Purification

In this step, unligated DNA parts and excess linkers were removed from restriction-ligation reactions using a magnetic beads purification system based on Mag-Bind TotalPure NGS (Omega Bio-Tek, Georgia, M1378-01). Therefore, 54 µL of magnetic beads were added to each reaction and mixed by pipetting ten times, avoiding formation of that no air bubbles. After a 5 min incubation, the PCR tubes were placed on a magnetic stand, causing the magnetic beads to immobilize and the solution to clear up. Not removing the tubes from the magnetic stand, the solution was discarded using a pipette and subsequently washed by adding 190 µL of 70% EtOH. Following an incubation period of 30 sec, the EtOH was removed, and the washing

procedure was repeated one more time. Subsequently, the tubes were left open without a lid for the magnetic beads to dry (ca. 5 min) before being removed from the magnetic stand. The magnetic beads were resuspended in 32 µL dH_2O and incubated for 1 min allowing DNA to elute. Finally, the tubes were placed on the magnetic stand again to immobilize the magnetic beads and transfer 30 µL of the clear and purified DNA containing solution into a microtube for further use in assembly.

3.3.3 BASIC Clip Assembly

BASIC clip assembly allows annealing of up to seven linker-adapted BASIC parts to generate the final plasmid. Therefore, 2 µL dH_2O, 1 µL 10X CutSmart Buffer (New England Biolabs, USA, B6004S), and 1 µL of each purified linker-ligated part were mixed in a PCR tube by pipetting up and down and topped up with dH_2O to reach a final reaction volume of 10 µL. Finally, the tube was incubated in a PCR thermocycler running the BASIC assembly program: 50 °C for 45 min. The constructed pVCS plasmid was immediately transformed to competent *E. coli* cells (3.3.4).

3.3.4 Heat-shock Transformation

Heat shock transformation was performed to introduce the pVCS plasmids into *E. coli* cells. Chemically competent cells were previously prepared according to the Inoue method (Sambrook & Russell, 2006). In a micro tube, 100 µL competent cells were mixed with 10 µL of the assembled plasmid and incubated on ice for 20 min. No plasmid DNA was added to the negative control. For heat-shocking the cells, the tube was placed in a 42 °C water bath for 45 sec following a 2 min incubation on ice. Subsequently, 400 µL of LB-medium was added to the tube. After an incubation of 1 h, the cells were plated out on LB-agar containing appropriate antibiotics (50 mM kanamycin) and incubated overnight.

3.4 Electroporation

Transformation of plasmid pVCS into the *P. putida* host was achieved by electroporation. Therefore, overnight cultures of *P. putida* were diluted with LB-medium (3:1) and incubated under constant shaking for 1-2 h at 37 °C. Subsequently, the culture was centrifuged for 5 min at 4000 rpm and room temperature. After discarding the supernatant, the pellet was re-suspended in SM buffer (300 mM sucrose, 1 mM MgCl) and centrifuged again, as previously stated for a total of two washes. The pellet was then resuspended in the remaining buffer and 80 µL were transferred to 1 mm gap electroporation cuvettes (VWR International, Belgium,

732-1135). Plasmid DNA was added to a final volume of ca. 50 ng/mL, while 1.5 mL sterile Ultra Pure Water was added to the negative control. Following a 15-30 min incubation, electroporation was conducted using the ECM 399 Exponential Decay Wave Electroporation System (BTX Harvard Apparatus, 45-0000) at 1250 V. Immediately afterwards, 750 µL LB-medium was added to the cuvette, mixed, and transferred to a sterile tube containing 5 mL LB-medium. After an incubation for 1-2 h, transformed cells were plated out on LB-agar containing appropriate antibiotics (50 mM kanamycin) and incubated overnight.

3.5 Colony PCR (cPCR) and Gel Electrophoresis

Each pVCS transformation was followed by cPCR with subsequent gel electrophoresis to verify correct incorporation of the plasmid. Thereby, a targeted section within the plasmid was amplified using cPCR and the amplification products were visualized by gel electrophoresis.

3.5.1 cPCR

Forward and reverse primers targeting specific sequences within the pVCS structure are listed in Appendix A. Generally, the toggle switch gene cassette excluding the backbone structure was amplified during cPCR using the primers LMP-F and LMS-R. In some cases however, stepwise cPCR was performed with primers targeting consecutive units of the plasmid. For every transformed strain, four colonies were picked and screened by cPCR. Negative controls included the respective WT colony lacking the plasmid, and a DNA-free control, whereas a colony confirmed to carry the desired plasmid, and 1 µL of extracted pVCS served as positive controls. All preparation work was performed on ice. Each cPCR reaction required a master-mix consisting of 6.5 µL dH_2O, 7.5 µL Taq Plus 2 x Master Mix (VWR Life Science, Belgium, 733-2599), 0.5 µL forward primer and 0.5 µL reverse primer. Colonies were picked with a sterile pipette tip, tapped on a labeled spot on a LB-agar plate containing kanamycin (50 mM) and finally dipped into the reaction mixture. Finally, the samples were incubated in a PCR thermocycler under the following temperature settings: initial denaturation: 95 °C for 5 min, cycle 25 x (denaturation: 95 °C for 30 sec, annealing: 57 °C for 30 sec, elongation: 72 °C for 2 min), final elongation: 72 °C for 5 min. Subsequently, the cPCR products were further analyzed by gel electrophoresis (3.5.2). The LB-agar plate was incubated overnight at 37 °C, allowing to pick and inoculate positive colonies that were detected by gel electrophoresis.

3.5.2 Gel electrophoresis

After performing cPCR, the amplification products are separated based on size and charge by gel electrophoresis to screen for colonies bearing the desired plasmid. Gel Loading Dye (6 x) (New England Biolabs, USA, B7024S) was used to dye the cPCR products by adding 1.5 µL to each sample. Therefore, a 0.8% agarose gel was prepared by dissolving UltraPureTM Agarose (Invitrogen, USA, 16500500) in 1 x TAE (Tris-acetate-EDTA) buffer under boiling until a clear solution was obtained. GelRed® Nucleic Acid Stain (10000 x) (Biotium, USA, 41003) was added to the gel solution (5 µL/100 mL) and mixed gently before being poured into a gel chamber with combs. Once the gel has solidified, the combs were removed and 10 µL of dyed sample were pipetted into the resulting gel pockets. In addition, the GeneRuler 1 kb Plus DNA Ladder (ThermoFisher Scientific, USA, SM1331) was added to a gel pocket as a reference to determine the size of the separated DNA fragments. Electrophoresis was performed at 150 V for 35 min with subsequent evaluation under UV light in a VWR Gel Documentation System Smart3 (VWR, USA, 1730-1459). Visible DNA bands with a size of ca. 3800 bp indicate the presence of the toggle switch within the bacterial colony. In case of step-wise cPCR, the resulting DNA bands were expected to form a characteristic ladder pattern in the gel according to the increasing size of DNA fragments. This allows for every subunit to be confirmed of correct assembly.

3.6 Plasmid Sequencing

To further verify the accurate assembly and transformation of pVCS, extracted plasmids of selected bacterial strains used in this work were sent to plasmidsaurus for whole plasmid sequencing using the latest sequencing technology (Oxford Nanopore Technologies). Samples were prepared according to the company's requirements (10 µL sample with DNA concentration of ca. 30 ng/µL).

3.7 Performance Characterization

Three different assays were performed to analyze the influence of combinatorial RBS on the toggle switch behavior. Thereby, the measurable output, sfGFP (485/515, gain = 75) and mKate (585/615, gain = 125) fluorescence, and OD_{600} was continuously recorded during incubation in the plate reader, as outlined in 3.1. Data analysis was performed in R (v4.3.2). Fluorescence signals recorded using different plate readers were in each case standardized as described in

3.7.1. Furthermore, fluorescence signals were normalized to OD_{600} prior to calculating metrics and estimating parameters. All plotting was accomplished using *ggplot*, a data visualization system included in the *tidyverse* package.

3.7.1 Plate Reader Calibration

Fluorescence was recorded as measurable output of toggle-switch performance using three different Synergy H1 plate readers. Calibration and standardization are required, since fluorescence signals are reported using relative fluorescence units (RFU) that heavily depend on type, settings and life span of the instrument (De Wannemaeker et al., 2023). For calibration, two appropriate fluorophores sodium fluorescein (Sigma-Aldrich, Germany, 518478) and sulforhodamine 101 (Sigma-Aldrich, Germany, 60311026), resembling the excitation and emission spectra of sfGFP (485 nm, 515 nm) and mKate (585 nm, 615 nm), respectively, were selected. Each fluorophore was serial diluted in a 96-well plate (eight replicates per concentration) and measured with each plate reader under the same conditions used to conduct following performance assays. Ultimately, a conversion factor was determined for each machine and fluorophore by linear regression of the RFU outputs against a reference instrument. Thereby, RFU signals were standardized across different instruments.

3.7.2 Ethanol Assay

Inducer stock solutions used throughout performance characterization assays were dissolved in 70% EtOH. Accordingly, an ethanol assay was conducted to define the maximum concentration of ethanol that can be used without considerably impeding bacterial growth. Overnight cultures of *P. putida* WT and *E. coli* WT were therefore exposed to a range of ethanol concentrations according to volumes of inducer solutions used in further assays. A total of four replicates were tested for each strain and cultivated in the plate reader recording OD_{600} for subsequent calculation and comparison of growth rates (μ) and carrying capacities (A) across ethanol concentrations.

3.7.3 Prediction of Translation Initiation Rates with OSTIR

OSTIR (Open-Source Translation Initiation Rates, v1.1.2, https://github.com/barricklab/ostir) was run with default settings, using the highly conserved anti-Shine-Dalgarno (anti-SD) sequence of *E. coli* (5'-ACCTCCTTA-3') (Shine & Dalgarno, 1974). Briefly, the OSTIR employs a thermodynamic model (ViennaRNA, (Lorenz et al., 2011)) of bacterial translation initiation to calculate the Gibbs free energy of ribosome binding, which infers the Gibbs free energy change to a protein coding sequence's translation initiation rate and thereby expression

strength (Salis, 2011). As input sequence, the 33 bp 5'-UTR linker region upstream of the 14 bp RBS was included. The RBS is followed by a 4 bp (5'-GTCC-3') spacer region and the respective gene coding sequence, beginning with the start codon ATG. Genes *cymR* and *vanR* have the 5'-UTR2 (5'-TGTTACTATTGGCTGAGATAAGGGTAGCAGAA-3') sequence upstream of their RBS, while the RBS of genes *sfGFP* and *mKate* are linked to the 5'-UTR3 (5'-GTATCTCGTGGTCTGACGGTAAAATCTATTGT-3').

3.7.4 Experimental Verification of RBS Strengths

Preliminary experimental verification of the pre-defined RBS strengths was performed by assembling a constitutive promoter, J23104, each RBS linker variant used in the toggle switch (combining UTR2 and UTR3 with RBS1, RBS2, and RBS3, respectively), a *sfGFP* reporter gene and the BB23 backbone to yield a total of six different plasmids. Eight replicates were tested per UTR-RBS variant, measuring sfGFP signals during incubation in the plate reader. Subsequently, fluorescence response was compared to assess the expected correspondence of increasing RBS strength to enhanced translational performance (RBS1 < RBS2 < RBS3).

3.7.5 Toggle Assay

The capability of attaining and switching between stable induction states and the impact of the previous induction state on toggle switch performance was analyzed conducting a toggle assay. The induction conditions (Van-ON, Cym-ON, NI) were obtained by exposing four replicates of each pVCS strain to 0.75 mM vanillate, 0.75 mM cumate, or no inducer, respectively. Medium supplemented with the respective inducer concentration was inoculated with overnight cultures, grown in absence of inducer, to perform the first toggling. Following a 20 hour incubation under periodic shaking and initial measuring (First Toggle ON) of OD_{600}, sfGFP and mKate signal intensity, the cells were centrifuged at 4000 rpm for 15 min. The supernatant was discarded, and the cells were resuspended in an equal volume of LB-medium. This washing step was repeated for a total of two washes, to remove the initial inducer. Finally, the induction states were inverted by diluting the resuspended cells in medium containing the opposite respective inducer. Subsequent measurements (Second Toggle ON) of OD_{600}, sfGFP and mKate were taken during a second incubation period of about 20 h under periodic shaking. Maximum steady-state fluorescence intensity (Fss) was used to measure device performance and estimated at stationary growth phase using the *all_growthmodels* function to fit the Gompertz growth model (Gompertz, 1815). Additionally, using the *all_easylinear* function from the *growthrates* R package and predicated on a rolling regression method, maximum rates

of fluorescence (Rate) were estimated. Finally, the dynamic range (DR) of a toggle switch was defined as ratio between induced Fss and non-induced Fss.

3.7.6 Induction Assay

Bacterial strains bearing the pVCS plasmid were exposed to various inducer concentrations to measure inducer sensitivity and fluorescence intensity. Concentrations for vanillate ranged from 0-1 mM for *E. coli* and 0-12 mM *P. putida*, while for cumate, concentrations varied between 0-1 mM for *E. coli* and 0-5 mM for *P. putida*. Eight technical replicates were tested for each inducer concentration. During incubation in the plate reader OD_{600}, sfGFP and mKate were continuously recorded for subsequent generation of induction curves: For each bacterial strain and inducer, steady-state fluorescence intensity recorded at stationary phase (time ≥ 12 h) was averaged and plotted against inducer concentration. Furthermore, the Hill function (1) was fitted to induction curves of each replicate using the *growthmodel* function from the *growthrates* R package. For optimized fitting, start values, as well as upper and lower bounds of each parameter were defined. Consequently, the following performance parameters could be estimated by the model: Hill coefficient (n), activation coefficient (K), maximum steady-state fluorescence (β), and basal fluorescence in absence of inducer (C).

$$y_{ss} = (\beta x^n/(K^n + x^n)) + C \quad (1)$$

3.7.7 Growth Assay

A growth assay was performed to determine potential growth inhibiting effects caused by the presence of inducers, and maintenance and expression of the pVCS plasmid. Overnight cultures of the bacterial WT and WT + BB were therefore exposed to the same inducer concentrations used in the hysteresis assay for a total of eight technical replicates per condition. OD_{600}, and fluorescence intensity of sfGFP and mKate were continuously measured throughout incubation. Similar to the analysis used for assessing hysteresis, the maximum carrying capacity and maximum rates based on OD_{600} curves were estimated using the *all_growthmodels* and *all_easylinear* functions, respectively. Finally, metrics $\Delta\mu_{NI}$, $\Delta\mu_{Van}$ and $\Delta\mu_{Cym}$ describing potential growth burdens were calculated using equations (2), (3), and (4), respectively.

$$\Delta\mu_{NI} = \left(\left(\mu_{WT\_NI} - \mu_{pVCS\_NI}\right)/\mu_{WT\_NI}\right) * 100 \quad (2)$$

$$\Delta\mu_{Van} = \left({(\mu_{pVCS\_NI} - \mu_{pVCS\_Van})} \Big/ {\mu_{pVCS\_NI}} \right) * 100 \quad (3)$$

$$\Delta\mu_{Cym} = \left({(\mu_{pVCS\_NI} - \mu_{pVCS\_Cym})} \Big/ {\mu_{pVCS\_NI}} \right) * 100 \quad (4)$$

3.7.8 Flow Cytometry

Physical characteristics of single cells within the population can be revealed by flow cytometry. In this work, flow cytometry is used to detect variability and distribution of fluorescence intensity within the bacterial culture. Therefore, four replicates of each strain were exposed to the respective inducer concentrations used in 3.7.3 resulting in the induction states Van-ON, Cym-ON, and NI. Cells were incubated in a plate reader until late exponential phase (OD_{600} around 0.6 - 0.7). After verifying that the inducers triggered the desired fluorescence response, cells were diluted using PBS (1x) and fixed with formaldehyde to a final concentration of 1.5% and a standardized OD_{600} of 0.2. Flow cytometry was performed using the BD LSRFortessa Cell Analyzer (BD Sciences, USA) equipped with an HTS autosampler (BD Sciences, USA) measuring sfGFP signals with a 488 nm laser and 530/30 nm detector and mKate with a 561 nm laser and 610/20 nm detector. Voltages for detecting forward scatter, side scatter, sfGFP and mKate were adjusted to 420, 270, 460 and 530, respectively. To reduce background debris, thresholds for forward and side scatter were set to 5,000, while 20,000 events were recorded, if applicable, for each sample. Logarithmic transformation was applied to all documented events before plotting smoothed density estimates for all strains in each induced state.

3.7.9 PCA

Multiple performance parameters are introduced throughout this work, spanning several dimensions in which toggle switch performance can be characterized. The principal component analysis (PCA) provides an operation to reduce dimensionality and summarize the variance in toggle switch performance based on identifying variables that explain maximal variability between the switches, referred to as principle components. PCA was applied to the scaled induction performance parameters (K, β, and C), using the *prcomp* function from the *stats* R package.

4 Results

This thesis aims to characterize the performance space of a genetic toggle switch across different combinations of RBS strengths, driving the translational efficiency of the repressive transcriptional factors that regulate circuit function. Various assays were conducted to characterize the impact of different RBS combinations on the performance profile displayed by the respective toggle switch. Furthermore, host-specific toggle switch behavior is compared between two different bacterial species, *E. coli* and *P. putida* to determine the role of the chassis-effect on device performance. Ultimately, these results allow for assessing the efficiency of employing RBS and host context as a design strategy to shape circuit behavior.

4.1 The Genetic Toggle Switch Design spans a two-dimensional Expression Space in two distinct Bacterial Hosts

4.1.1 Plasmid Structure and Toggle Switch Functionality

A total of nine toggle switches comprising unique combinations of RBSs that regulate the translation of two repressive transcriptional factors were constructed within the BASIC assembly environment. This method allows for linker-guided modular joining of standardized DNA parts. The BASIC assembly linker library used in this study contains linkers with RBS parts of three different translational strengths integrated into their adapter regions. The RBS parts are designated RBS1, RBS2, and RBS3, which differ in their SD-sequences and, in the given order, have increasing translational efficiencies. The modular property of BASIC assembly streamlines the exploration of a combinatorial design space with respect to RBS sequences and was therefore the method of choice to construct the genetic toggle circuits.

The nine toggle switches designed for this study take inspiration from the canonical toggle switch by Gardner et al. (2000), but employing different regulatory elements. The toggle switches consist of two expression cassettes, each associated with a negatively inducible promoter, P_{Van} and P_{Cym}, and their cognate repressors, VanR and CymR, respectively. Each promoter regulates the expression of the opposing promoter's transcriptional repressor gene, establishing a motif of mutual inhibition. By binding the operator site of their cognate promoters, the transcriptional repressors VanR and CymR act as a physical steric hindrance to RNA polymerase, thus preventing transcription initiation. The addition of either vanillate or cumate shifts the expression level of the two cassettes. The inducer ligands bind their cognate repressor molecules, inducing a conformational change, which impedes the repressor's capacity

to bind to their associated promoters, thus allowing RNA polymerase to initiate transcription. Each gene cassette incorporates a distinct fluorescent reporter protein that allows for the practical detection of an output signal in response to promoter activation. Hence, sfGFP output serves as an indicator of P_{Van} activation and consequently, *cymR* expression, whereas mKate is the indicative signal for *vanR* expression upon P_{Cym} activation (Fig. 2A). The toggle switch constructs were assembled into a pSEVA231-derived backbone containing a pBBR1 origin of replication and a kanamycin selection marker (Fig. 2B), resulting in the plasmid series (pVCS1-pVCS9) (Fig. 2C).

The strengths of RBS relate to their affinity to recruit and bind ribosomes, a critical step in translation initiation (Salis et al., 2009). Given the different RBS combinations, a two-dimensional RBS design space is established, in which a variety of performance profiles displayed by the nine toggle switch variants can be expected. Furthermore, the pVCS series was transformed into *E. coli* and *P. putida*, allowing for comparative characterization with respect to the chassis-effect across two model synthetic biology hosts.

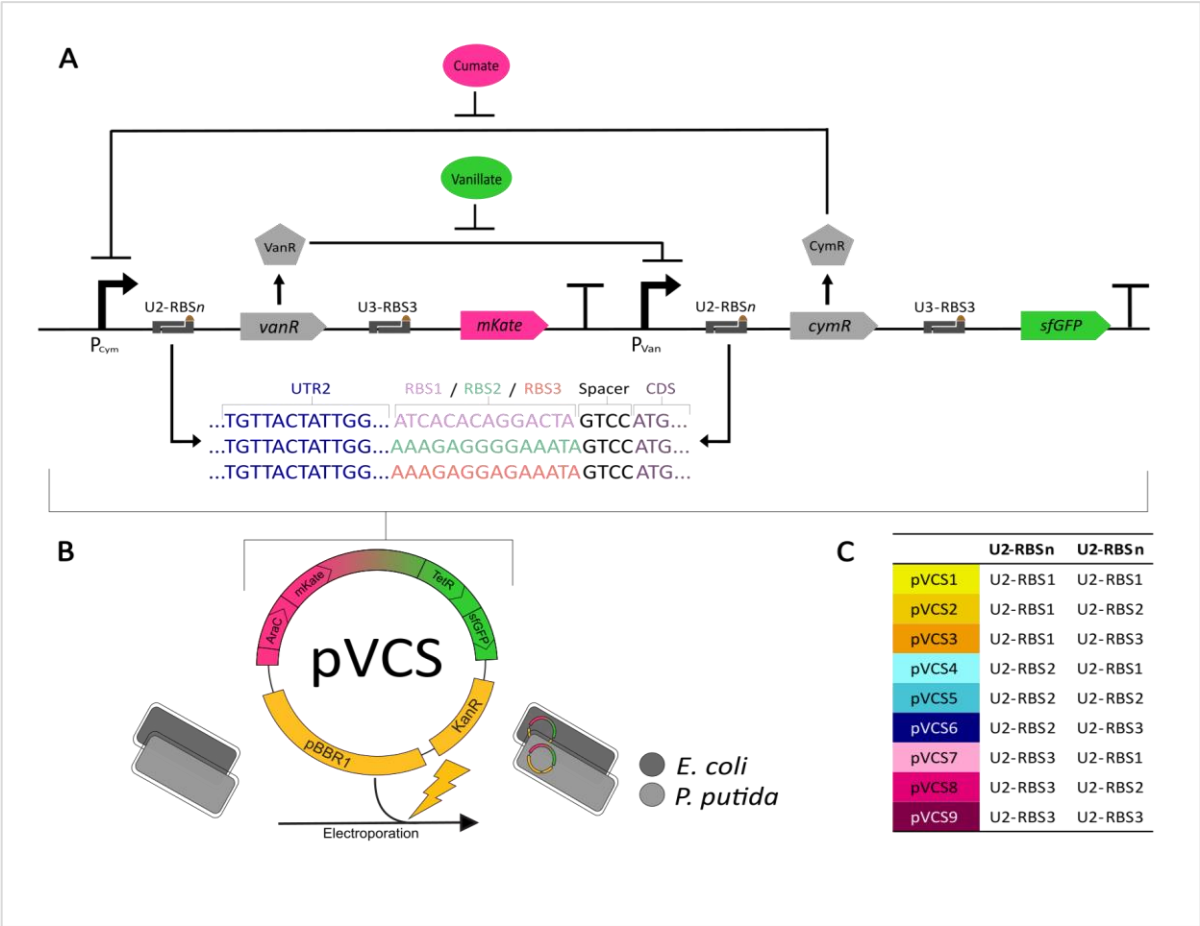

Fig. 2. The pVCS toggle switch series with different RBS combinations of varying strengths was successfully introduced into the *E. coli* and *P. putida* hosts. (A) Schematic overview of the van and cym inducible toggle switch series. The gene products of *vanR* and *cymR* act as transcriptional repressors by binding to their respective cognate promoters. In presence of van, vanillate-bound VanR undergoes a conformational change that prevents its ability to bind P_{Van} promoter, positively biasing transcription from the P_{Van} promoter and thereby expression of *cymR* and *sfGFP*. CymR production will in turn lead to repression of P_{Cym} promoter. In a similar manner, presence of cumate promotes expression from P_{Cym} promoter, leading to expression of *mKate* and a negative feedback regulation of P_{Cym}. The toggle switch series vary in the combination of RBS strengths regulating for the translation of both transcription factor, while the RBS site regulating for reporter protein is kept constant. (B) The toggle switch series were cloned into a pSEVA231-derived backbone with a kanamycin resistance gene to form plasmids pVCS1 to pVCS9. All nine plasmids were transformed into *E. coli* and *P. putida* hosts. (C) Overview of the pVCS toggle switch series and their RBS strength combinatorial composition. Higher number indicates higher translational efficiency.

4.1.2 Predicted Translation Initiation Rates depend on the Genetic Context

The strength of a RBS refers to its affinity to recruit ribosomes, while varying RBS strength has been shown to serve as an efficient strategy for tuning translational efficiency and gene expression (Salis et al., 2009; Zelcbuch et al., 2013). The BASIC library provides linkers with pre-defined RBS strengths, which were verified using the Open Source Translation Initiation Rate prediction software (OSTIR) (Roots et al., 2021). This software is based on previous work from Salis et al. (2009), who developed a method for predicting translation initiation rates based on RBS and adjacent DNA sequences. The thermodynamic model assumes that the strength of molecular interactions between mRNA transcript and 30S ribosomal subunit, reflected by

change in total Gibbs free energy (ΔG_{tot}), determines translation initiation rates. Predicted translation initiation rates increase as the level of favorable interactions between mRNA and the 30S complex rises, reflected by a lower ΔG_{tot} (Salis et al., 2009). OSTIR prediction results reveal that as the strength of the RBS upstream of *vanR* increases, the expected translation efficiency aligns with predicted values, showing an increase in translation rate and decrease in ΔG_{tot} (Fig. 3). However, RBS upstream of *cymR* exhibit a different pattern: While RBS3 is associated with a higher predicted translation initiation rate compared to RBS1 and RBS2, RBS2 is predicted to have a lower rate than RBS1. Furthermore, the RBS upstream of *mKate* is predicted to display considerably higher translation efficiency than upstream of *sfGFP*, despite both coding sequences being linked to identical RBS strengths. These results indicate that the effective translational strength associated with an RBS is dependent on the gene-context, in particular the untranslated region and the protein coding sequence. Experimental verification of RBS strengths was conducted by linking all RBS variants to a *sfGFP* reporter and measuring the fluorescence output. The results indicate that pre-defined RBS strengths follow the expected pattern, displaying increased sfGFP fluorescence intensity with stronger RBS (Appendix D).

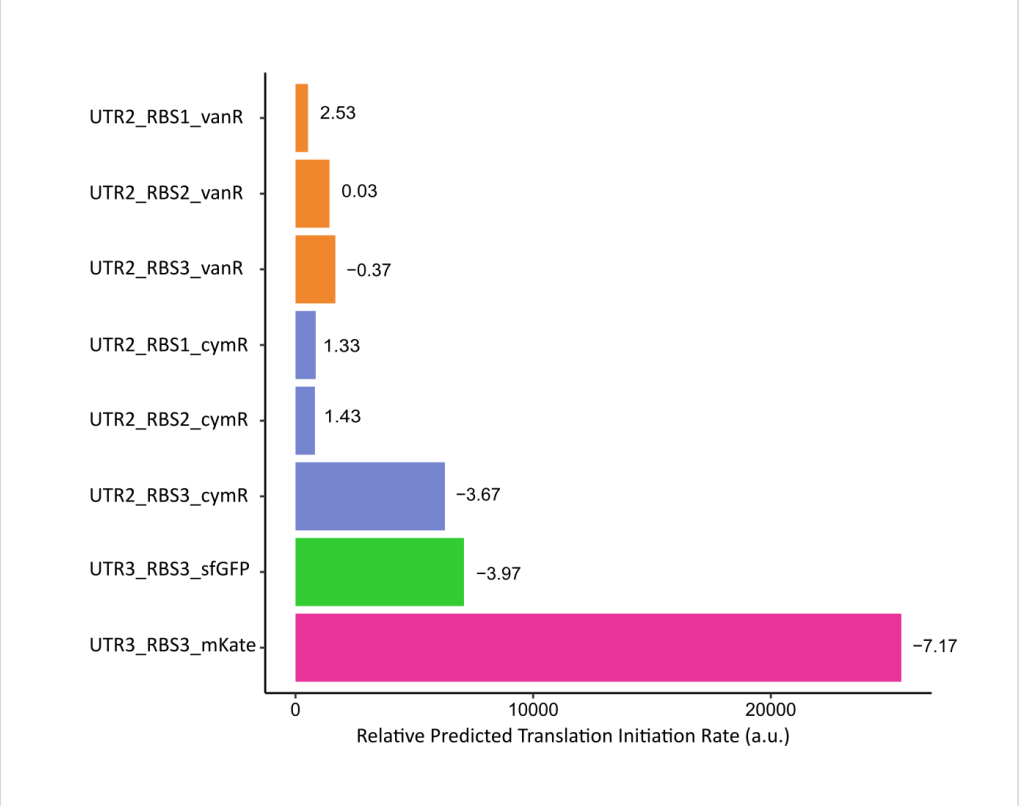

Fig. 3. Predicted translation initiation rates vary with RBS strengths and downstream protein coding sequence. Color coding refers to protein coding sequence. Lower ΔG_{tot} (next to bars) indicates stronger molecular interactions between the mRNA sequence and the 16S rRNA of the ribosomal subunit and is associated with a higher predicted translation initiation rate. Predictions were conducted with OSTIR, based on the RBS calculator (Salis et al., 2009).

4.1.3 Inducer Toxicity and Growth Burden vary across Plasmid-Bearing Hosts

The maintenance and expression of plasmids requires cellular resources and is competing with endogenous processes, consequently imposing a metabolic burden onto the host organism (Ow et al., 2006). To assess the growth altering effects of the pVCS toggle switches, OD_{600} curves of plasmid-carrying bacteria and their WT counterpart were measured in absence of inducers to return and compare the specific maximum growth rates (μ).

The results show that the extent of growth burdens imposed by the same genetic device vary in context of the host. In the *E. coli* host, all plasmid bearing strains, expect for pVCS6, exhibit significantly lower specific growth rates (p-values < 0.005) compared to *E. coli* WT (Fig. 4C). Growth burdens, as determined by a reduction in μ, range from 7.8 ± 7.8% to 29.2 ± 2.2% on average, with pVCS7 demonstrating the highest degree of growth inhibition in *E. coli* (Fig. 4B). The extent of a growth burden is even more evident in *P. putida*, where all plasmid carrying strains show highly significant reduced specific growth rates ($p < 0.001$) compared to the WT strain (Fig. 4E) and average growth burdens range from 21.6 ± 4.8% to 37.1 ± 4.6%. However, the severe impact on growth specifically caused by the pVCS7 device, as observed from *E. coli*, is not as prominent in *P. putida*. Instead, pVCS9 (3-3) appears to cause the strongest growth burden in the *P. putida* host (Fig. 4D).

Previous studies reported minimal inducer toxicity of vanillate (Kunjapur & Prather, 2019), while no growth-inhibiting effects could be associated with cumate (Kaczmarczyk et al., 2013). Results of a preliminary ethanol toxicity test indicate no growth inhibtory effects for the range of EtOH concentrations used in this work as a solvent for the inducers (Appendix C). To further assess potential growth inhibitory effects of the inducers on the host strains due to inducer toxicity, the specific growth rates were measured for both, *E. coli* and *P. putida* WT strains under each induction condition (0.75 mM cumate/vanillate, no inducer) (Fig. 4F). The specific growth rate of *P. putida* showed no significant response ($p > 0.05$) to vanillate and cumate. However, the presence of vanillate appeared to impact the growth of the *E. coli* WT strain, significantly ($p < 0.001$) (Fig. 4G) reducing the maximum specific growth rate by 9.6 ± 4.6 % on average. These results are indicative of a chassis-specific phenomenon, meaning that the choice of host can determine how much the inducer effect on growth must be considered in further analysis.

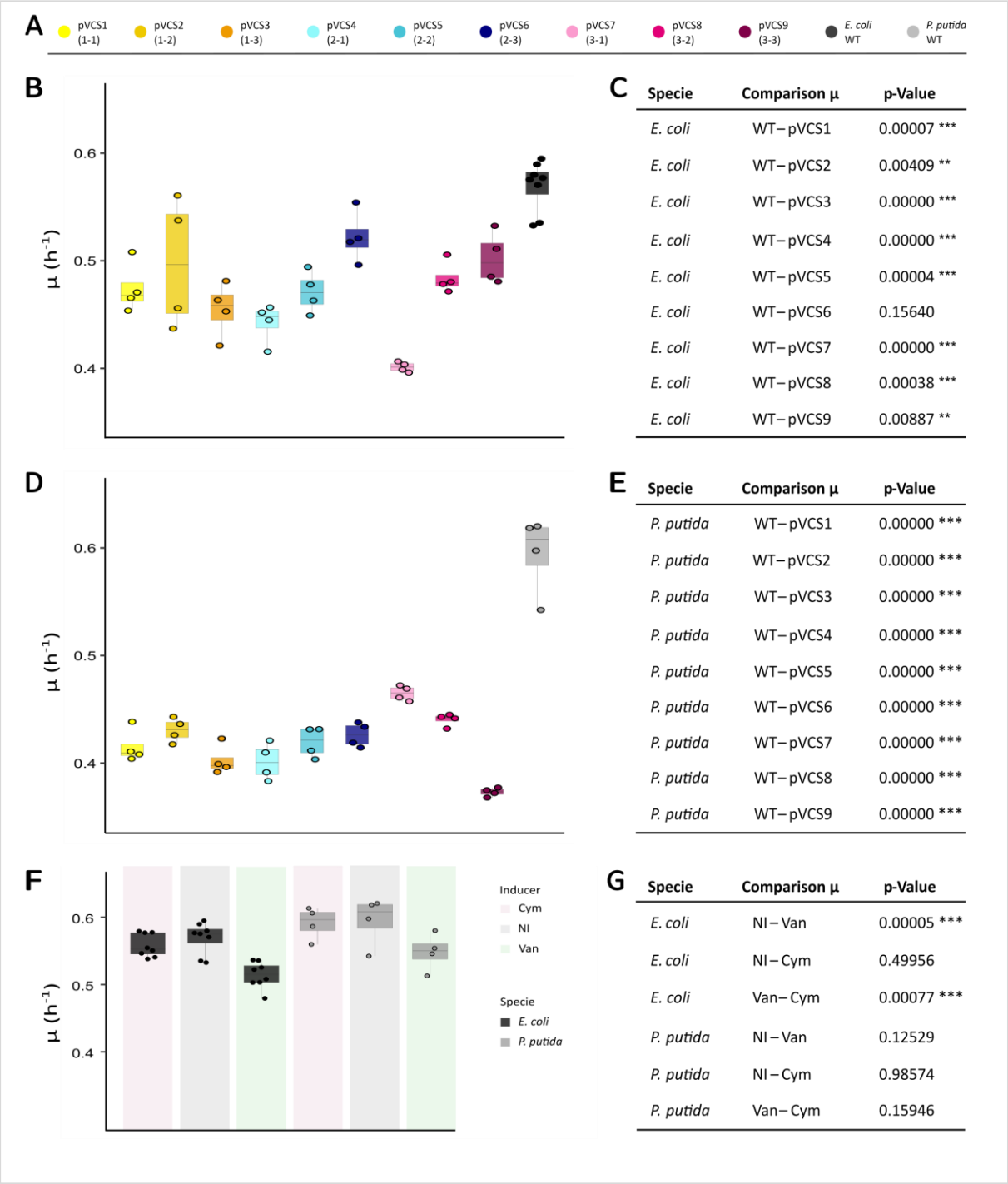

Fig. 4. Plasmid carriage and inducer toxicity impact growth dynamics in *E. coli* and *P. putida* to a varying extent. (A) Colour coding scheme for bacterial strains. (B) Maximum specific growth rate μ (h^{-1}) of pVCS strains and *E. coli* WT bacteria after cultivation in absence of inducer. (C) Significance of differences in maximum specific growth rates compared to *E. coli* WT, Tukey HSD test was carried out with a 95% confidence level. (D) Maximum specific growth rate μ (h^{-1}) of pVCS strains and *P. putida* WT bacteria after cultivation in absence of inducer. (C) Significance of differences in maximum specific growth rates compared to *P. putida* WT, Tukey HSD test was carried out with a 95% confidence level. (F) Maximum specific growth rate μ (h^{-1}) of *E. coli* WT and *P. putida* WT when exposed to different inducers (0.75 mM van/cym). (C) Significance of differences in maximum specific growth rates with respect to the inducer, Tukey HSD test was carried out with a 95% confidence level.

4.2 Toggle Switch Performance Characterization in *E. coli*

To investigate the impact of varying RBS strength on the performance of a genetic toggle switch, the fluorescence output response dynamics of the pVCS plasmids were determined in *E. coli* under standardized conditions through the assays described in 3.7.4-3.7.8. To decouple growth effects from fluorescence output, fluorescence response was normalized by OD_{600}.

4.2.1 RBS Combinations impact Toggle Dynamics

The pVCS toggle switches are comprised of two negatively inducible promoters, whose transcriptional activity is dependent on the abundance of unbound cognate repressor. The aim of the toggle dynamics assay is to verify the ability of the toggle switch to attain a stable induction state according to the present inducer as well as to compare fluorescence response across the combinatorial RBS landscape. Therefore, cells were toggled from a non-induced (NI) state to the three possible induction states (Cym-ON, Van-ON, and NI) by dilution to pre-induced media. As cells grow, the sfGFP fluorescence response is expected to increase upon addition of vanillate, while mKate signals are expected to increase when induced with cumate, in a pattern resembling the growth curve. Given the mutual inhibitory motif of the genetic circuit, the fluorescence response linked to the opposing gene cassette is expected to decrease or remain unchanged from the fluorescence response exhibited in a non-induced state.

Examining the results from the toggle assay, all toggle switches display the expected fluorescence response according to the corresponding inducer. Cells diluted to vanillate-supplemented media demonstrate an increased sfGFP response, higher than non-induced control cells, while mKate output is decreasing. In a similar manner, upon cumate induction, an increasing mKate response is observed with simultaneously decreasing sfGFP fluorescence (Fig. 5B). Furthermore, the results suggest that fluorescence response varies with different RBS combinations. To quantify the differences in fluorescence dynamics, performance metrics were estimated based on the normalized fluorescence curves. These metrics include the maximum rate of fluorescence (Rate), the maximum fluorescence at stationary phase of growth (Fss) and the dynamic range (DR), which is the ratio of Fss between induced and non-induced cells.

The results reveal a range of varying performance metrics, indicating that fluorescence dynamics are affected by different RBS combinations (Table 3). In absence of inducer, toggle switches display different levels of fluorescence output, also referred to as leakage or basal expression. While pVCS1 (1-1), pVCS2 (1-2), and pVCS3 (1-3) show high initial sfGFP intensities, pVCS4 (2-1) and pVCS7 (3-1) exhibit remarkably high basal mKate signals.

Notably, the high basal *mKate* expression is reflected in the DR_{mKate} levels as well, with pVCS4 and pVCS7 exhibiting much lower values compared to the other variants. This indicates that, under unbiased conditions, these two toggle switch designs are more toggled towards the P_{Van} direction, with all other variants are more toggled towards the P_{Cym} cassette. This is further supported by the high DR_{sfGFP} values of pVCS4 and pVCS7.

Upon vanillate induction, sfGFP intensities ranged from 5200 ± 200 RFU to 9700 ± 200 RFU, with pVCS2 (1-2), pVCS6 (2-3), and pVCS9 (3-3) displaying some of the highest Fss_{sfGFP} responses (Table 3). When induced with cumate, Fss_{mKate} intensities range from 23700 ± 1500 RFU to 52700 ± 1300 RFU, with some of the highest can be observed in pVCS5 (2-2), pVCS8 (3-2), and pVCS9 (3-3). Interestingly, these switches are characterized by a combination of two stronger RBS regulating the transcriptional repressors, suggesting enhanced translational efficiency, thus tighter control over the opposing gene cassette.

These initial toggle assay results suggest that upon addition of the respective inducer, the toggle switches are able to attain a stable induction state, while toggle dynamics vary across the combinatorial RBS landscape. To further characterize the ability of the genetic circuits to toggle between stable states and assess if past induction states affect performance, cells were toggled again by first washing and then diluting them to the respective opposite inducer. Additionally, the non-induced control state was maintained.

A brief examination of the fluorescence output upon the second toggling event reveals that all switches allow for toggling between two stable induction states, displaying the expected fluorescence response according to the corresponding inducer (Fig. 5C). Performance metrics were estimated to further quantify the behavior of the inverted toggle switch. The results suggest that performance metrics vary across the combinatorial RBS landscape, while some metrics indicate the influence of past induction states on toggle dynamics (Table 4). In absence of inducer, all toggle circuits display a slightly increased level of leakage, compared to the first toggling event. Additionally, expression levels of *mKate* upon vanillate induction are slightly increased compared to the previous toggle event, introducing a second type of leakage that is fluorescence response in the presence of the antagonistic inducer. Throughout both toggling points mKate fluoresce at a higher rate than sfGFP. While no remarkable change in sfGFP rate can be observed between both toggling points, the rate of mKate fluorescence increases in the second toggle, particularly evident in pVCS4 and pVCS7. Compared to the first toggle event, a slight increase in DR values is displayed in most of the toggle switches upon cumate induction

and Fss_{mkate} values range from 25400 ± 1600 RFU to 52900 ± 3000 RFU. Vanillate induction appears to result in slightly lower DR values across most plasmids and Fss_{sfGFP} levels range from 4600 ± 100 RFU to 9300 ± 600 RFU. Although the fluorescence output follows the general trend observed during the first toggle event and RBS combinations with the highest F_{SS} and DR values still show the highest values in the second toggle state, the findings suggest a subtle dependence of toggle performance on previous induction states.

The fluorescence output observed for the toggle assay is the average fluorescence produced by the whole population of cells, which, even if genetically identical, can display high degrees of heterogeneity (Fedr et al., 2023; Kærn et al., 2005). To investigate this, flow cytometry was performed to measure fluorescence intensities at the single cell level, thereby gaining insight of the fluorescence distribution of the population. The toggle assay was repeated and the cells were harvested at late exponential phase of growth. Density plots obtained from flow cytometry reveal that the average fluorescence intensities measured in the toggle assay are driven by a homogenous response at the population level, verifying that the observed fluorescence response is representative of the population (Fig. 5D).

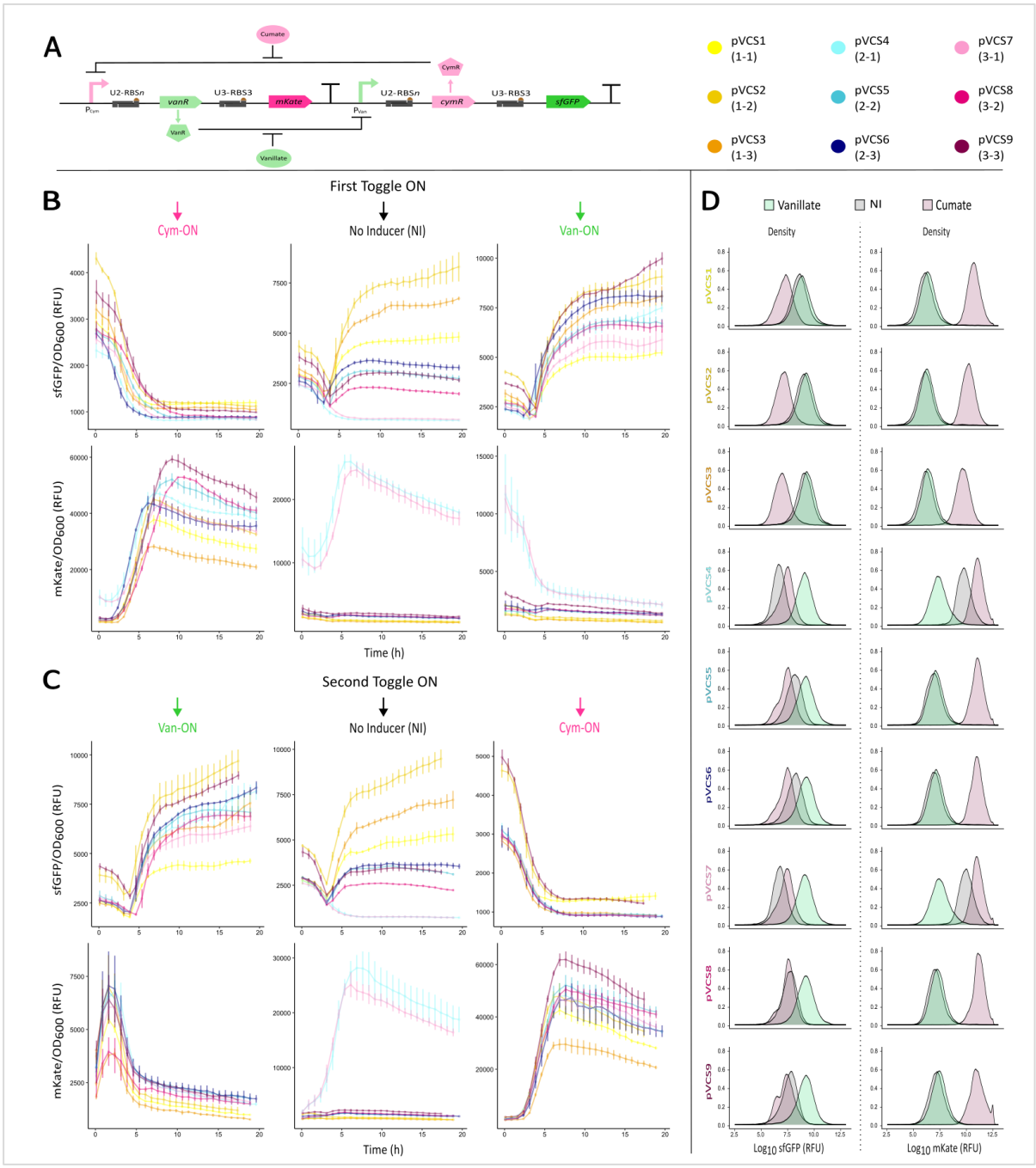

Fig. 5. Toggle switch fluorescence dynamics in *E. coli* as observed through a toggling assay and according fluorescence distribution. (A) Toggle scheme and colour coding scheme of plasmids varying in RBS combinations. (B) The switches were toggled from initial OFF state (no inducer) to ON state (First Toggle ON) with 0.75 mM vanillate and cumate, respectively. Normalized sfGFP and mKate fluorescence signals are shown (n=4) including error bars indicating standard deviation. (C) Washed and diluted cells were toggled to their respective opposite state (Second Toggle ON) using the same inducer concentrations (n=4). (D) Population density plots across induced states (0.75 mM van, 0.75 mM cym, NI) based on sfGFP and mKate measurements are shown for each plasmid carrying strain (n=4), while 20000 events were recorded per sample.

Table 3. Summary of estimated and rounded performance metrics based on fluorescence output measured during the first toggle event in *E. coli* (First Toggle ON). Rate = maximum rate of fluorescence (h^{-1}), F_{ss} = maximum fluorescence steady-state intensity at stationary growth phase (RFU) (rounded), Dynamic Range = F_{ss} ratio between induced (ON) and non-induced (OFF) state. All parameters are reported with standard deviations.

	Vanillate			Cumate			No Inducer		Dynamic Range	
	sfGFP		mKate	sfGFP	mKate		sfGFP	mKate	Vanillate	Cumate
	Rate	F_{ss}	F_{ss}	F_{ss}	Rate	F_{ss}	F_{ss}	F_{ss}	sfGFP	mKate
pVCS1	0.26 ± 0.02	5200 ± 200	700 ± 30	1200 ± 60	1.08 ± 0.03	30800 ± 1500	4800 ± 300	700 ± 10	1.08 ± 0.08	42.53 ± 1.92
pVCS2	0.30 ± 0.00	8900 ± 400	800 ± 40	1200 ± 40	1.10 ± 0.05	37100 ± 800	8100 ± 600	800 ± 30	1.10 ± 0.05	46.58 ± 2.72
pVCS3	0.30 ± 0.01	8000 ± 300	700 ± 10	1100 ± 30	1.26 ± 0.07	23700 ± 1500	6600 ± 200	600 ± 30	1.21 ± 0.06	37.13 ± 2.92
pVCS4	0.34 ± 0.01	7300 ± 300	2500 ± 400	800 ± 20	0.47 ± 0.06	40700 ± 500	700 ± 20	20800 ± 600	10.89 ± 0.73	1.96 ± 0.07
pVCS5	0.33 ± 0.01	6800 ± 200	1300 ± 60	900 ± 40	0.90 ± 0.04	45900 ± 2400	2900 ± 100	1400 ± 60	2.38 ± 0.11	33.52 ± 2.19
pVCS6	0.34 ± 0.03	8100 ± 300	1400 ± 50	900 ± 30	1.09 ± 0.06	36500 ± 2000	3400 ± 100	1400 ± 60	2.37 ± 0.07	25.32 ± 1.02
pVCS7	0.29 ± 0.01	5800 ± 300	2200 ± 700	900 ± 30	0.44 ± 0.04	36800 ± 1200	700 ± 20	19800 ± 1100	7.95 ± 0.51	1.84 ± 0.25
pVCS8	0.31 ± 0.00	6600 ± 200	1400 ± 70	900 ± 20	0.78 ± 0.02	47900 ± 900	2100 ± 70	1500 ± 30	3.09 ± 0.15	33.15 ± 0.24
pVCS9	0.32 ± 0.01	9700 ± 200	1700 ± 20	1000 ± 20	0.82 ± 0.03	52700 ± 1300	3000 ± 120	1800 ± 80	3.31 ± 0.12	29.73 ± 1.32

Table 4. Summary of estimated and rounded performance metrics based on fluorescence output measured during the second toggle event in *E. coli* (Second Toggle ON). Rate = maximum rate of fluorescence (h^{-1}), F_{ss} = maximum fluorescence steady-state intensity at stationary growth phase (RFU) (rounded), Dynamic Range = F_{ss} ratio between induced (ON) and non-induced (OFF) state. All parameters are reported with standard deviations.

	Vanillate			Cumate			No Inducer		Dynamic Range	
	sfGFP		mKate	sfGFP	mKate		sfGFP	mKate	Vanillate	Cumate
	Rate	F_{ss}	F_{ss}	F_{ss}	Rate	F_{ss}	F_{ss}	F_{ss}	sfGFP	mKate
pVCS1	0.26 ± 0.02	4600 ± 100	1200 ± 30	1400 ± 90	1.28 ± 0.04	34200 ± 1600	5200 ± 400	700 ± 30	0.87 ± 0.05	52.19 ± 4.17
pVCS2	0.31 ± 0.01	9300 ± 600	1400 ± 200	1300 ± 40	1.35 ± 0.08	39000 ± 3200	9200 ± 500	800 ± 20	1.02 ± 0.09	48.88 ± 3.63
pVCS3	0.34 ± 0.01	7200 ± 600	1000 ± 50	1000 ± 10	1.56 ± 0.08	25400 ± 1600	7200 ± 200	600 ± 20	1.00 ± 0.1	42.41 ± 3.72
pVCS4	0.32 ± 0.00	8000 ± 500	1800 ± 100	900 ± 20	1.05 ± 0.04	40500 ± 1200	800 ± 40	22300 ± 2700	10.02 ± 1.23	1.95 ± 0.23
pVCS5	0.33 ± 0.01	7200 ± 300	2000 ± 100	900 ± 30	1.37 ± 0.09	46200 ± 3200	3400 ± 30	1300 ± 30	2.12 ± 0.08	35.74 ± 1.95
pVCS6	0.34 ± 0.01	8100 ± 200	2100 ± 200	900 ± 20	1.29 ± 0.07	40600 ± 4700	3700 ± 100	1300 ± 100	2.21 ± 0.06	30.40 ± 3.13
pVCS7	0.29 ± 0.01	6300 ± 200	1900 ± 100	900 ± 20	1.23 ± 0.06	43200 ± 3200	800 ± 40	19500 ± 700	8.43 ± 0.33	2.22 ± 0.23
pVCS8	0.34 ± 0.00	6900 ± 200	1700 ± 100	900 ± 20	1.28 ± 0.03	45000 ± 2200	2500 ± 700	1400 ± 1700	2.78 ± 0.15	32.19 ± 1.21
pVCS9	0.28 ± 0.00	8600 ± 200	1900 ± 100	1300 ± 30	1.22 ± 0.06	52900 ± 3000	3400 ± 200	1800 ± 100	2.50 ± 0.06	28.66 ± 1.75

4.2.2 Induction Kinetics vary across RBS Combinations

Previous results indicate that the toggle switch is invertible upon addition of the respective inducer, while a single inducer concentration was used to toggle the pVCS series. The toggle assay also unveiled the different performance profiles displayed by RBS combinations, demonstrating the effect of varying RBS strength to tune circuit performance. However, the toggle assay takes only a single inducer concentration into consideration. To gain deeper insights into toggle switch performance profiles, induction dynamics were further characterized. The pVCS series was therefore exposed to increasing concentrations of inducer ligands until reaching saturated output levels, which is when all repressor molecules are ligand-bound (Alon, 2006). Estimated maximum fluorescence signals were used as induction response variables and plotted against inducer concentrations to obtain induction curves. As the activation of the negatively inducible promoters is dependent on the abundance of unbound cognate repressor, fluorescence output of mKate or sfGFP, is expected to increase accordingly until reaching a saturation point, resulting in device-specific induction curves. Simultaneously, given the mutual inhibitory motif of the toggle switches, fluorescence output of the antagonistic gene cassette is expected to decrease or remain unchanged.

Induction assay results reveal that all nine toggle switches demonstrate the expected dosage-dependent response of a negatively inducible promoter, exhibiting increasing fluorescence output with increasing inducer concentration until eventually reaching a saturation level (Fig. 6B,C). Examining the fluorescence output controlled by expression of the opposing gene cassette (*mKate* under van induction/ *sfGFP* under cym induction), most toggle switches exhibit a decreasing or not considerably changing fluorescence response.

A brief inspection of each induction curve reveals a difference in the scale of fluorescence across devices, indicating variation in performance within the combinatorial RBS landscape. To formally quantify induction behavior and verify a difference in performance, the Hill equation was fitted to each curve. Parameters C, K and β are used to describe induction kinetics of each toggle switch, with the hill coefficient n serving as a fitting parameter. The metrics derived from the Hill function consider a wider range of toggle switch states across inducer concentrations, thus providing more comprehensive information about each toggle switch system as a whole.

A range of Hill function parameters are observed across the toggle switches, indicating how varying the combinatorial RBS strength can cause drastic changes in toggle switch performance

(Table 5). All plasmids display a basal fluorescence expression in absence of inducer, expressed by the metric C, which is also referred to as leakage. C appears to correlate to increasing RBS strength. Plasmids pVCS4 and pVCS7, which harbor stronger RBSs regulating *vanR* expression combined with a weaker RBS controlling *cymR* exhibit a considerably high *mKate* expression in absence of inducer. Furthermore, plasmids pVCS2 and pVCS3 show high initial sfGFP response, while both plasmids combine a weak RBS controlling for *vanR* and a stronger RBS regulating *cymR* expression.

The performance parameter β describes the maximal expression level quantified by maximum fluorescence intensity at steady state, and varies between the RBS combinations. When induced with cumate, β ranges from 24400 ± 500 RFU to 59800 ± 1900 RFU (Table 5). Plasmids pVCS5, pVCS6, and pVCS8, which bear toggle switches combining two stronger RBSs, show some of the highest β values, indicative of a tighter control over the opposing promoter due to enhanced translational efficiency. Vanillate induction results in a range of β values from 2900 ± 50 RFU to 10200 ± 300 RFU, while some of the highest sfGFP intensities are displayed by pVCS2, pVCS3, and pVCS6, all combining a weaker RBS controlling for *vanR* and a stronger RBS regulating *cymR* expression.

The activation coefficient, denoted as K, corresponds to the inducer concentration required to achieve half maximum expression and thereby indicates the chemical binding affinity between the inducer and its cognate repressor. Thereby, K also describes the inducible concentration range of the toggle switch. The results demonstrate that the metric K varies within the RBS design space (Table 5). Upon cumate induction, toggle switches combining stronger RBSs controlling for *vanR* and weak RBSs regulating *cymR* expression show the lowest K values. Conversely, pVCS2 and pVCS3 combining the weakest RBSs controlling for *vanR* and a stronger RBSs tuning *cymR* expression display the highest K values. For toggle switches with RBSs of the same strength upstream of *vanR*, K is increasing with stronger RBSs controlling for *cymR*. This suggests that higher translational efficiency associated with by stronger RBSs leads to increased CymR abundance, thus requiring higher cumate concentration for repressor deactivation. Conversely, upon vanillate induction, combinations of weak RBSs regulating *vanR* and stronger RBSs tuning *cymR* expression were expected to show the lowest K values. However this trend is not observed for pVCS1 (1-1), pVCS2 (1-2) and pVCS3 (1-3), displaying the highest K values. Among the remaining plasmids, increased K values are observed when *cymR* is linked to a weak RBS (pVCS4, pVCS7), whereas combinations of RBS2 and RBS3 within a toggle switch shows no association with a change in K.

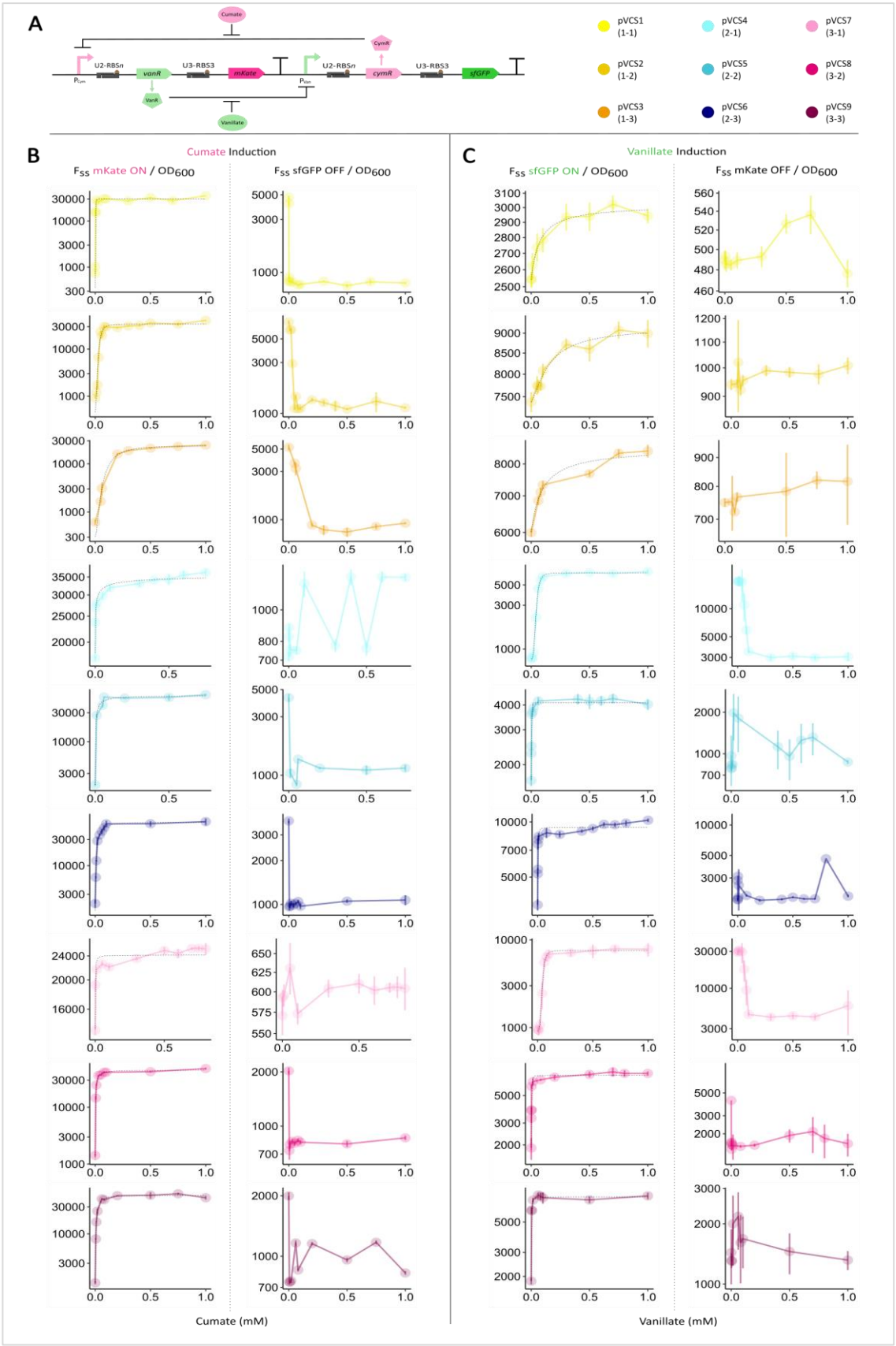

Fig. 6. Toggle switch induction kinetics vary across different RBS combinations in *E. coli*. (A) Toggle scheme and colour coding scheme of plasmids varying in RBS combinations. (B) Cumate and (C) vanillate induction curves with parameter fitted Hill function (dashed line) and the respective opposing fluorescence signal are shown (n=8) with error bars. Fluorescence signals recorded at steady-state are plotted on a log-transformed Y-axis and are standardized and normalized to OD_{600}. Error bars show standard deviation.

Table 5. Estimated and empirical performance parameters obtained by fitting the Hill function to the respective induction curve in *E. coli* toggle switches. K=activation coefficient (mM) (estimated), β=maximal expression level (RFU) (empirical, rounded), n=Hill coefficient (estimated), C=basal expression level (RFU) (estimate, rounded). All parameters are reported with standard deviations.

	Cumate Induction				Vanillate Induction			
	K	β	n	C	K	β	n	C
pVCS1	0.003 ± 0.00	35400 ± 500	1.82 ± 0.07	500 ± 0.00	0.08 ± 0.04	2900 ± 50	2.14 ± 1.23	2500 ± 70
pVCS2	0.05 ± 0.01	40800 ± 800	2.92 ± 0.62	600 ± 300	0.21 ± 0.09	9000 ± 400	1.91 ± 0.85	7500 ± 200
pVCS3	0.16 ± 0.01	24400 ± 500	2.17 ± 0.16	300 ± 0.00	0.12 ± 0.03	8500 ± 200	1.00 ± 0.00	6000 ± 100
pVCS4	0.005 ± 0.00	36600 ± 1000	0.50 ± 0.00	18000 ± 500	0.05 ± 0.00	7000 ± 500	3.54 ± 0.52	800 ± 50
pVCS5	0.01 ± 0.00	59800 ± 1900	1.06 ± 0.09	2300 ± 600	0.002 ± 0.00	4100 ± 300	2.11 ± 1.04	1700 ± 100
pVCS6	0.02 ± 0.00	56400 ± 1100	1.45 ± 0.19	1800 ± 700	0.002 ± 0.00	10200 ± 300	1.36 ± 0.45	3500 ± 300
pVCS7	0.001 ± 0.00	25300 ± 1300	1.00 ± 0.00	13700 ± 700	0.05 ± 0.00	9200 ± 200	3.51 ± 0.62	800 ± 100
pVCS8	0.01 ± 0.00	48000 ± 2000	1.11 ± 0.13	1300 ± 100	0.002 ± 0.00	7500 ± 400	2.45 ± 1.36	2000 ± 500
pVCS9	0.02 ± 0.00	43600 ± 3400	1.36 ± 0.15	1400 ± 300	0.001 ± 0.00	7800 ± 500	1.05 ± 0.09	1900 ± 100

4.2.3 Plasmid Maintenance and Expression impose Growth Burdens

Preliminary tests revealed minor levels of vanillate toxicity, and no impact of cumate on growth of the *E. coli* WT strain (Fig. 4). In pVCS carrying strains, plasmid maintenance and expression requires cellular resources and energy and is therefore expected to affect cell growth (Ow et al., 2006). In particular, strong RBSs are expected to display a considerable growth burden upon induction as a result of high translational efficiency. To determine how growth is affected by RBS combinations in the toggle switch, plasmid maintenance and inducer toxicity, a growth assay was conducted. According to the toggle assay, a single concentration of the respective inducer was added to toggle the pVCS series to the three possible induction levels (Van-ON, Cym-ON, NI), under standardized conditions and OD_{600} values were measured.

The RBS combinations display different growth behaviors as indicated by OD_{600} curves (Fig. 7B). For a better comparison and quantification of growth impacts, the maximum specific growth rate (μ) and carrying capacity (A) was estimated for each toggle switch based on the growth curves. The results suggest not only an impact on growth due to different RBS strengths, but also in dependence of the inducer (Table 6). While no growth inhibiting effects can be observed in presence of vanillate, induction with cumate clearly reduces μ for all nine toggle switches. Particularly, pVCS5, pVCS8 and pVCS9, that hold a combination of stronger RBSs and had previously been associated with highest maximum fluorescence (Fss_{mKate}) upon cumate induction, show the lowest μ values. Consequently, with respect to previous results suggesting

no cumate toxicity, these findings indicate that the impact on growth can be associated with the expression of the cognate gene cassette.

To further determine growth dynamics upon toggle inversion, the inducer was washed out and the pVCS series was toggled to their respective opposite induction state or kept in a non-induced condition (Fig. 7C). Measuring OD_{600} generated growth curves based on which μ and A were estimated to quantify and compare growth kinetics between varying RBS combinations and upon toggle inversion. Toggle switches once more demonstrated diminished μ values following cumate induction, however no considerable variation can be detected between different RBS combinations (Table 7).

Furthermore the growth assay serves to determine the extent of growth burden across the combinatorial RBS design space and induction state. Growth burdens were characterized through the Δμ metric, defined as the relative percentage difference in growth rate between two conditions, where a negative value indicates reduction in growth and vice versa. Growth burdens resulting from the comparison between the pVCS series to the *E. coli* WT in a non-induced state are referred to as $\Delta\mu_{NI}$. This revealed that hosting the toggle switch reduces growth by -16.7 ± 6.4% on average. In particular, pVCS7 (3-1) appears to be affected by growth impairment (Fig. 7D). Upon vanillate induction, a less considerable growth burden $\Delta\mu_{Van}$ is observed when compared to non-induced states (Fig. 7E). Interestingly, some pVCS strains, namely pVCS4 and pVCS7 show higher μ values when induced with vanillate, compared to their non-induced state. However, in the presence of cumate, all toggle switches display a noticeable growth burden compared to their respective non-induced state, which is indicated by $\Delta\mu_{Cym}$, ranging from -15.2 ± 4.2 % to -51.9 ± 2.4 % on average (Fig. 7F). Once again, pVCS5, pVCS8 and pVCS9 are particularly subject to a considerable growth restriction upon cumate induction, indicating a growth diminishing effect that potentially is related to the expression of the cognate gene cassette and inducer toxicity.

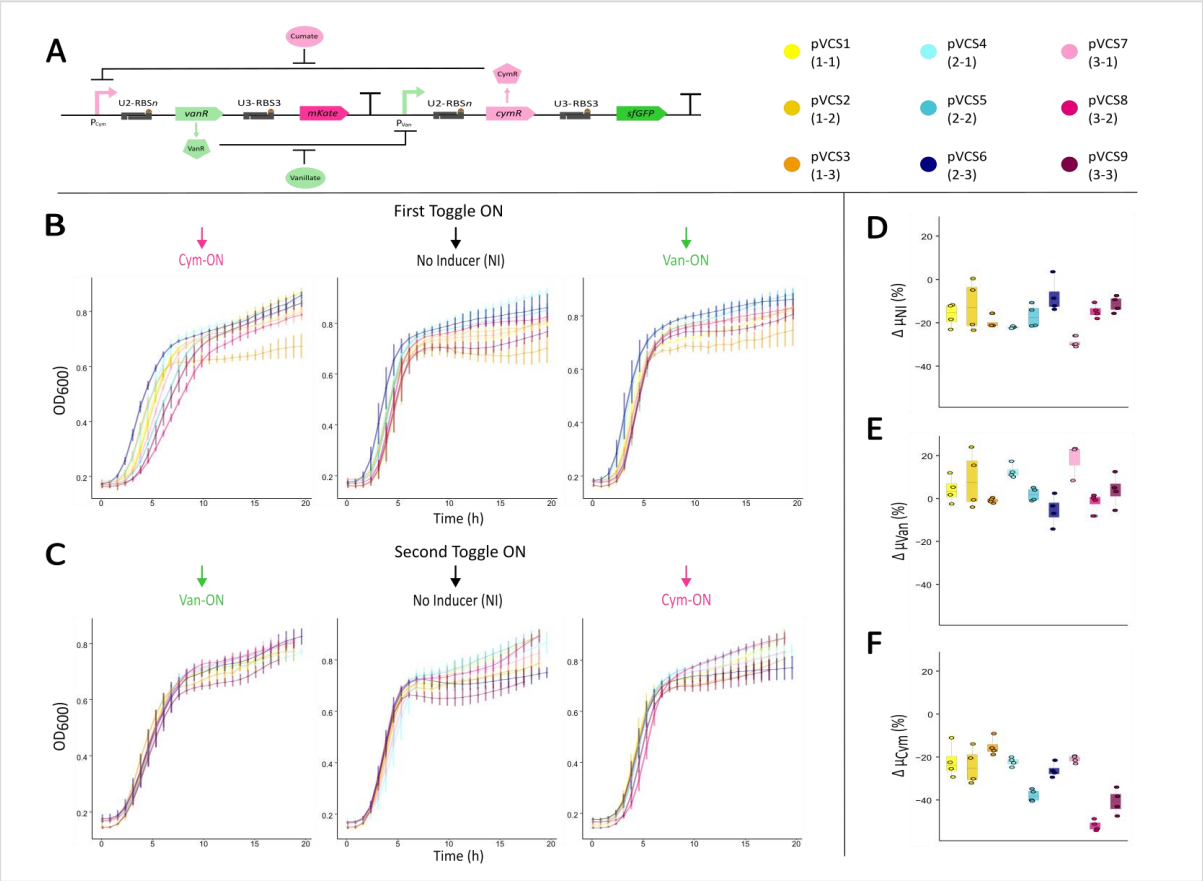

Fig. 7. Growth dynamics displayed by toggle switches in *E. coli* and the extent of growth burdens vary across RBS combinations and inducer. (A) Toggle scheme and colour coding scheme of plasmids varying in RBS combinations are introduced. (B) OD_{600} curves of switches as recorded during the toggle assay: First toggled from initial OFF state (no inducer) to ON state (First Toggle ON) and then (C) to the respective opposite state (n=4). Error bars show standard deviation. (D) Growth burden exhibited by the plasmid bearing strains in the absence of inducer compared to WT counterpart (n=4). (E) Growth burden of plasmid bearing strains as a result of vanillate and (F) cumate induction compared to non-induced state (n=4).

Table 6. Summary of estimated growth metrics based on OD_{600} output measured during the first toggle event in *E. coli* (First Toggle ON). μ = maximum specific growth rate (h^{-1}), A = carrying capacity (OD_{600}). All parameters are reported with standard deviations.

	Vanillate		Cumate		No Inducer	
	μ	A	μ	A	μ	A
pVCS1	0.49 ± 0.03	0.77 ± 0.01	0.37 ± 0.04	0.76 ± 0.03	0.47 ± 0.02	0.76 ± 0.02
pVCS2	0.53 ± 0.01	0.79 ± 0.01	0.37 ± 0.02	0.81 ± 0.02	0.50 ± 0.01	0.77 ± 0.02
pVCS3	0.45 ± 0.02	0.70 ± 0.03	0.39 ± 0.01	0.65 ± 0.02	0.45 ± 0.03	0.69 ± 0.03
pVCS4	0.50 ± 0.01	0.82 ± 0.02	0.34 ± 0.02	0.79 ± 0.01	0.45 ± 0.02	0.87 ± 0.02
pVCS5	0.48 ± 0.02	0.83 ± 0.02	0.29 ± 0.01	0.79 ± 0.02	0.47 ± 0.02	0.81 ± 0.02
pVCS6	0.49 ± 0.02	0.83 ± 0.02	0.38 ± 0.01	0.80 ± 0.02	0.51 ± 0.01	0.82 ± 0.04
pVCS7	0.48 ± 0.04	0.79 ± 0.01	0.32 ± 0.01	0.76 ± 0.03	0.40 ± 0.00	0.77 ± 0.18
pVCS8	0.47 ± 0.01	0.79 ± 0.02	0.23 ± 0.01	0.77 ± 0.00	0.48 ± 0.01	0.79 ± 0.01
pVCS9	0.52 ± 0.02	0.76 ± 0.01	0.29 ± 0.02	0.80 ± 0.01	0.50 ± 0.03	0.72 ± 0.02

Table 7. Summary of estimated growth metrics based on OD_{600} output measured during the second toggle event in *E. coli* (Second Toggle ON). μ = maximum specific growth rate (h^{-1}), A = carrying capacity (OD_{600}). All parameters are reported with standard deviations.

	Vanillate		Cumate		No Inducer	
	μ	A	μ	A	μ	A
pVCS1	0.44 ± 0.01	0.82 ± 0.04	0.34 ± 0.01	0.75 ± 0.02	0.47 ± 0.03	0.83 ± 0.03
pVCS2	0.48 ± 0.01	0.76 ± 0.03	0.40 ± 0.02	0.73 ± 0.03	0.52 ± 0.01	0.73 ± 0.01
pVCS3	0.42 ± 0.01	0.74 ± 0.02	0.37 ± 0.03	0.74 ± 0.04	0.46 ± 0.01	0.74 ± 0.03
pVCS4	0.44 ± 0.02	0.79 ± 0.02	0.33 ± 0.01	0.74 ± 0.01	0.40 ± 0.03	0.80 ± 0.04
pVCS5	0.45 ± 0.01	0.83 ± 0.02	0.33 ± 0.02	0.77 ± 0.02	0.47 ± 0.01	0.83 ± 0.03
pVCS6	0.43 ± 0.02	0.75 ± 0.03	0.32 ± 0.03	0.78 ± 0.02	0.48 ± 0.02	0.72 ± 0.02
pVCS7	0.46 ± 0.03	0.79 ± 0.01	0.34 ± 0.01	0.77 ± 0.02	0.41 ± 0.02	0.78 ± 0.03
pVCS8	0.45 ± 0.01	0.84 ± 0.02	0.32 ± 0.01	0.77 ± 0.01	0.49 ± 0.01	0.79 ± 0.19
pVCS9	0.48 ± 0.01	0.73 ± 0.03	0.34 ± 0.02	0.69 ± 0.02	0.51 ± 0.02	0.67 ± 0.03

4.3 Performance Characterization in *P. putida*

The impact of varying RBS strengths regulating translation of transcriptional repressors in the genetic toggle switch has previously been investigated in the *E. coli* host. Although the toggle switches were intentionally constructed and optimized to operate in *E. coli*, the pVCS series is transferable across multiple bacterial species. To investigate device performance within the unique RBS design space in a second host, the pVCS series was transformed into *P. putida* and tested under standardized conditions through the assays described in 3.7.4-3.7.8.

4.3.1 Fluorescence Dynamics in the Toggle Assay vary across RBS Combinations

The purpose of the toggling assay was to verify the ability of the toggle switch to attain a stable induction state according to the presence of the corresponding inducer. Furthermore, the assay aims to investigate the degree in which RBS combinations affect device performance. The pVCS series was therefore grown under non-induced conditions and upon adding the respective inducer, fluorescence dynamics of each toggle switch was determined across three induction states (Van-ON, Cym-ON, NI). The fluorescence response exhibited by the toggle switches, according to the respective inducer is predicted to increase over time until reaching a stationary phase, mirroring growth dynamics. Simultaneously, fluorescence output associated with the opposing gene cassette is expected to decline or remain unchanged from the non-induced state.

Observing the fluorescence output when exposed to the respective inducer, the results verify the expected operation of all toggle switches: Cumate induction causes mKate output, while sfGFP response is decreasing, whereas vanillate generates a rise in sfGFP fluorescence levels, while mKate fluorescence remains unchanged compared to the non-induced level (Fig. 8B). Furthermore, different fluorescence dynamics are observed among varying RBS combinations, indicating the impact of RBS strengths on toggle behavior. To further characterize fluorescence dynamics, maximum rate of fluorescence (Rate), the maximum fluorescence at stationary phase of growth (Fss) and the dynamic range (DR) were estimated based on the fluorescence output.

Comparing the different performance metrics across the pVCS series reveals that varying RBS strengths appear to impact fluorescence dynamics (Table 8). Basal fluorescence expression, particularly of mKate, in absence of inducer varies across the toggle switches, with pVCS4 (2-1) and pVCS7 (3-1) displaying comparatively low levels of mKate leakage. Interestingly, when induced with vanillate, a slight increase in mKate fluorescence is observed for most toggle switches compared to their non-induced state. This fluorescence expression upon induction

with the antagonistic inducer is noticeable for some devices at both induction states, albeit to a lesser extent for cumate induction.

In presence of vanillate, Fss_{sfGFP} ranges from 1400 ± 20 RFU to 3900 ± 100 RFU. Toggle switches pVCS2 (1-2) and pVCS7 (3-1) show some of the highest sfGFP fluorescence levels, while the high DR values and high sfGFP rate can be observed in pVCS2 (1-2), pVCS3 (1-3), pVCS4 (2-1) and pVCS7 (3-1). These results are surprising, given that these plasmids combine opposing combinations of RBS strengths, however they might be correlated to the initial level of VanR: Toggle switches pVCS2 and pVCS3 combine a weak RBS upstream of the *vanR* gene, potentially resulting in less efficient VanR production. Similarly, pVCS4 and pVCS7 show low mKate response in the non-induced state compared to other plasmids, corresponding to an intrinsically low level of VanR. When induced with cumate, Fss_{mKate} ranges from 7000 ± 300 RFU to 13900 ± 200 RFU, while pVCS5 (2-2), pVCS6 (2-3), pVCS8 (3-2) and pVCS9 (3-3), all with combinations of strong RBS, show some of the highest Fss_{mKate}. Maximum fluorescence rates vary across the RBS combinations, while the rate of sfGFP fluorescence is consistently lower compared to the rate of mKate fluorescence across all toggle switches (Table 8).

The results suggest that while varying RBS strengths appear to affect fluorescence dynamics, all toggle switches show the ability to attain a stable induction state. The toggle assay aims to further demonstrate the bistable behavior of the pVCS series, which manifests in switching between two stable induction states in correspondence of the inducer, while assessing the influence of past induction states on fluorescence dynamics. To test this, cells, after washing, were diluted in pre-supplemented media containing the respective opposite inducer. Measured fluorescence response is shown in Fig. 8C.

A range of varying performance parameters indicate noticeable change of fluorescence dynamics compared to the first toggling event, as well as across the RBS combinations (Table 9). On average, Fss_{mKate}, Fss_{sfGFP}, and rates of mKate decrease, while rates of sfGFP slightly increase in the second toggle event, suggesting that device performance is influenced by its past induction state. In the second toggle event and upon vanillate induction, the trend remains consistent, with RBS combinations that showed the some of the highest Fss_{sfGFP}, $Rate_{sfGFP}$, and DR_{Van} values in the first event still displaying the highest values. When induced with cumate, pVCS3 (1-3) and pVCS6 (2-3) display high Fss_{mKate} values, and a high DR value, besides plasmids pVCS4 and pVCS7, where the DR value may be attributed to low basal *mKate*

expression. Interestingly, plasmids pVCS5, pVCS8, and pVCS9 show a considerable reduction of their Fss_{mKate} response, leading to reduced DR_{Cym} values compared to the first toggle event.

Flow cytometry was performed to measure fluorescence responses at the single cell level, thereby demonstrating how average fluorescence response is reflected by fluorescence distribution within the population. Noticeably, the density plots obtained from flow cytometry show a slightly irregular distribution for some of the toggle switches, indicating a more heterogenic response at the population level (Fig. 8D).

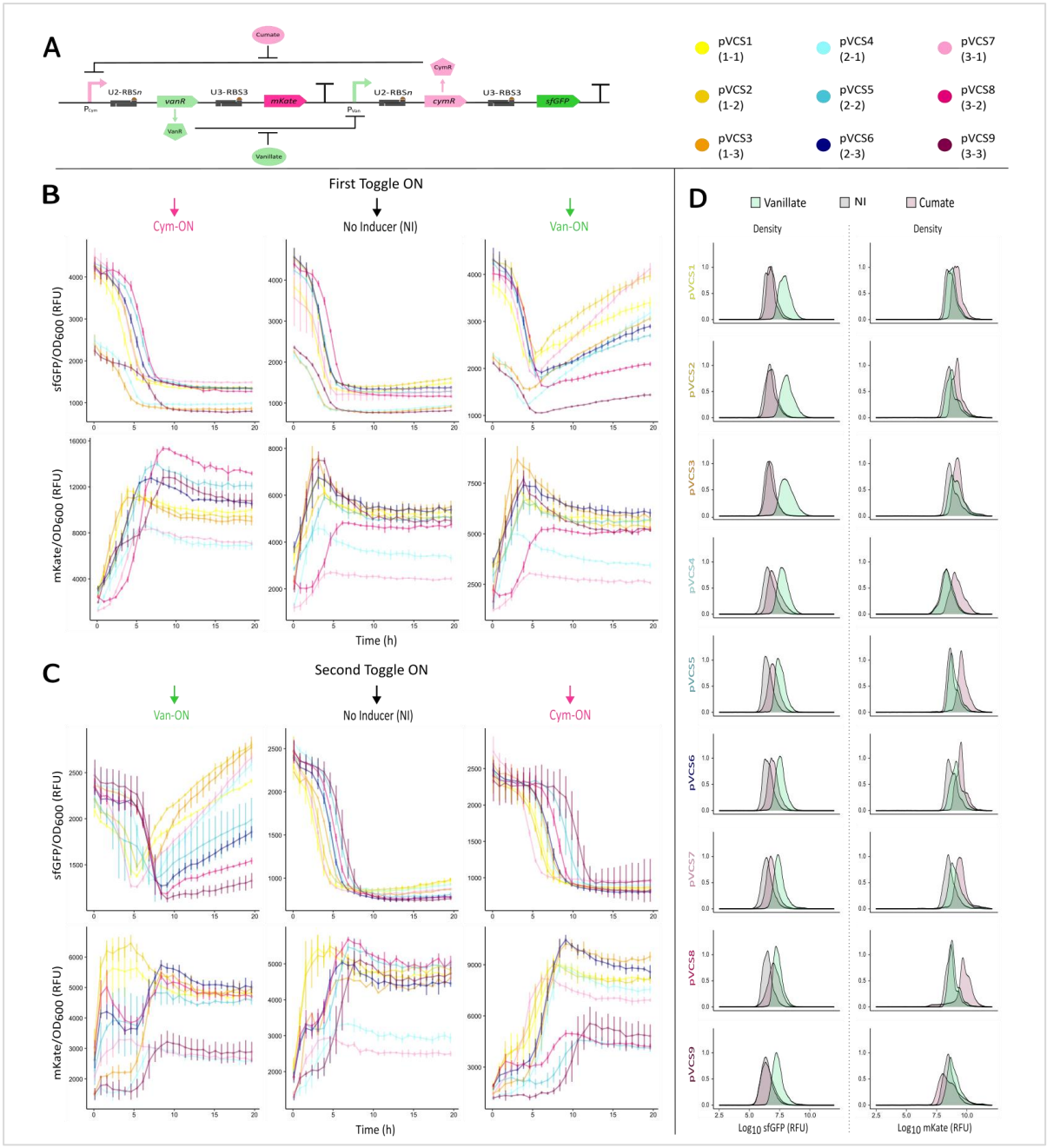

Fig. 8. Toggle switch fluorescence dynamics in *P. putida* as observed through a toggling assay and according fluorescence distribution. (A) Toggle scheme and colour coding scheme of plasmids varying in RBS combinations. (B) The switches were toggled from initial OFF state (no inducer) to ON state (First Toggle ON) with 0.75 mM vanillate and cumate, respectively. Normalized sfGFP and mKate fluorescence signals are shown (n=4) including error bars indicating standard deviation. (C) Washed and diluted cells were toggled to their respective opposite state (Second Toggle ON) using the same inducer concentrations (n=4). (D) Population density plots across induced states (0.75 mM Van, 0.75 mM Cym, NI) based on sfGFP and mKate measurements are shown for each plasmid carrying strain (n=4), while 20000 events were recorded per sample.

Table 8. Summary of estimated performance metrics based on fluorescence output measured during the first toggle event in *P. putida* (First Toggle ON). Rate = maximum rate of fluorescence (h^{-1}), F_{ss} = maximum fluorescence steady-state intensity at stationary growth phase (RFU) (rounded), Dynamic Range = F_{ss} ratio between induced (ON) and non-induced (OFF) state. All parameters are reported with standard deviations.

	Vanillate			Cumate			No Inducer		Dynamic Range	
	sfGFP		mKate	sfGFP	mKate		sfGFP	mKate	Vanillate	Cumate
	Rate	F_{ss}	F_{ss}	F_{ss}	Rate	F_{ss}	F_{ss}	F_{ss}	sfGFP	mKate
pVCS1	0.05 ± 0.00	3300 ± 100	5700 ± 100	1300 ± 20	0.40 ± 0.03	9900 ± 200	1500 ± 50	5300 ± 200	2.27 ± 0.09	1.88 ± 0.09
pVCS2	0.07 ± 0.00	3900 ± 100	5400 ± 200	1400 ± 20	0.36 ± 0.02	9500 ± 10	1600 ± 40	5100 ± 70	2.47 ± 0.07	1.88 ± 0.03
pVCS3	0.07 ± 0.01	3000 ± 50	6000 ± 200	900 ± 40	0.71 ± 0.04	9200 ± 300	900 ± 30	5500 ± 200	3.34 ± 0.08	1.68 ± 0.05
pVCS4	0.1 ± 0.00	3000 ± 100	3600 ± 30	1000 ± 30	0.61 ± 0.07	7000 ± 300	900 ± 20	3500 ± 100	3.37 ± 0.17	2.01 ± 0.05
pVCS5	0.04 ± 0.01	2600 ± 30	5700 ± 50	1400 ± 200	0.33 ± 0.02	12300 ± 300	1300 ± 30	5000 ± 30	2.08 ± 0.03	2.43 ± 0.06
pVCS6	0.04 ± 0.00	2800 ± 70	6100 ± 200	1400 ± 10	0.33 ± 0.02	10900 ± 100	1400 ± 40	5400 ± 200	2.04 ± 0.04	2.02 ± 0.05
pVCS7	0.08 ± 0.00	3900 ± 100	2700 ± 70	1500 ± 20	0.55 ± 0.06	7500 ± 30	1300 ± 100	2400 ± 50	3.09 ± 0.27	3.05 ± 0.07
pVCS8	0.03 ± 0.00	2100 ± 40	5200 ± 80	1300 ± 20	0.49 ± 0.02	13900 ± 200	1200 ± 20	4700 ± 70	1.75 ± 0.04	2.94 ± 0.07
pVCS9	0.03 ± 0.00	1400 ± 20	5200 ± 30	800 ± 30	0.71 ± 0.03	11400 ± 500	800 ± 20	5000 ± 100	1.77 ± 0.05	2.30 ± 0.15

Table 9. Summary of estimated performance metrics based on fluorescence output measured during the second toggle event in *P. putida* (Second Toggle ON). Rate = maximum rate of fluorescence (h^{-1}), F_{ss} = maximum fluorescence steady-state intensity at stationary growth phase (RFU) (rounded), Dynamic Range = F_{ss} ratio between induced (ON) and non-induced (OFF) state. All parameters are reported with standard deviations.

	Vanillate			Cumate			No Inducer		Dynamic Range	
	sfGFP		mKate	sfGFP	mKate		sfGFP	mKate	Vanillate	Cumate
	Rate	F_{ss}	F_{ss}	F_{ss}	Rate	F_{ss}	F_{ss}	F_{ss}	sfGFP	mKate
pVCS1	0.10 ± 0.01	2300 ± 10	4800 ± 90	900 ± 10	0.41 ± 0.01	8200 ± 200	900 ± 30	4700 ± 100	2.48 ± 0.1	1.74 ± 0.05
pVCS2	0.10 ± 0.01	2700 ± 40	4900 ± 80	900 ± 20	0.45 ± 0.1	8100 ± 200	1000 ± 10	4900 ± 50	2.85 ± 0.05	1.66 ± 0.05
pVCS3	0.10	2700	4900	800 ± 10	0.45 ± 0.05	9400 ± 300	900	4500	2.73	2.13
pVCS4	0.09 ± 0.01	2500 ± 80	2700 ± 90	900 ± 20	0.52 ± 0.03	7800 ± 300	900 ± 20	3000 ± 80	2.68 ± 0.06	2.64 ± 0.06
pVCS5	0.06 ± 0.00	1900 ± 200	4600 ± 40	900 ± 20	0.34 ± 0.05	4400 ± 200	800 ± 20	5000 ± 100	2.41 ± 0.29	0.86 ± 0.05
pVCS6	0.05 ± 0.01	1800 ± 60	5100 ± 100	800 ± 30	0.40 ± 0.03	9200 ± 300	800 ± 10	4500 ± 200	2.29 ± 0.07	2.05 ± 0.09
pVCS7	0.08 ± 0.01	2500 ± 70	2800 ± 60	1000 ± 20	0.40 ± 0.04	7100 ± 100	900 ± 10	2500 ± 30	2.94 ± 0.08	2.80 ± 0.05
pVCS8	0.05 ± 0.01	1500 ± 100	4800 ± 100	800 ± 20	0.36 ± 0.1	4400 ± 100	800 ± 10	5100 ± 100	1.84 ± 0.14	0.89 ± 0.01
pVCS9	0.02 ± 0.00	1300 ± 80	2900 ± 300	1300 ± 700	0.42 ± 0.03	5500± 1200	800 ± 20	4700 ± 100	1.73 ± 0.09	1.16 ± 0.23

4.3.2 RBS Combinations impact Induction Kinetics

All nine toggle switches previously demonstrated the ability to attain and switch between two stable induction states in *P. putida*, according to a single inducer concentration. To further examine induction kinetics across the combinatorial RBS landscape and under varying inducer concentrations, an induction assay was performed. The toggle switches were exposed to increasing concentrations of the respective inducer and fluorescence response was measured to generate device-specific induction curves.

Examining the induction curves reveals that all nine toggle switches display the expected output according to their ON-state: sfGFP fluorescence was measured when induced with vanillate, and mKate fluorescence output was generated upon cumate induction (Fig. 9). However, some irregularities can be observed when considering the fluorescence output of the respective OFF-state. Contrary to the expectations, some toggle switches show increasing fluorescence output in the presence of the gene cassette's antagonistic inducer. This is particularly observed in mKate response upon increasing vanillate concentration for pVCS6, pVCS8, and pVCS9. Consequently, the different RBS strengths appear to impact induction kinetics displayed by the toggle switch.

To further quantify and verify variation in induction performance across the combinatorial RBS landscape in *P. putida*, the Hill function was fitted to each induction curve. The returned parameters C, β, and K describe induction characteristics, while n is used as a fitting parameter. Across all toggle switches, a range of performance parameters were obtained, further underlining the impact of different RBS strengths on the performance profile of the genetic circuits (Table 10).

All nine toggle switches displayed basal fluorescence expression in absence of inducer, expressed by parameter C. Maximum fluorescence intensity at steady state is estimated by performance parameter β, indicating maximal expression level of the toggle switch. When induced with cumate, plasmids pVCS2 (1-2), pVCS6 (2-3), pVCS8 (3-2), and pVCS9 (3-3) display some of the highest β values, while simultaneously exhibiting some of the highest leakage levels. Vanillate induction results in β values ranging from 800 ± 10 RFU to 4900 ± 70 RFU on average, while some of the highest sfGFP intensities were recorded in pVCS2 (1-2), pVCS3 (1-3), pVCS4 (2-1) and pVCS7 (3-1). Surprisingly, these toggle switches comprise the opposite combination of RBS strengths, yet exhibiting highest maximal expression upon vanillate induction. It is pertinent to note that the leaky expression of the antagonistic gene

cassette upon induction, as displayed by some toggle switches, potentially impacts maximum expression levels.

The activation coefficient K reflects the concentration of the respective inducer required to reach half maximum expression. Upon cumate induction, K is increasing with increasing RBS strength regulating *cymR* expression, suggesting that translational efficiency correlates to RBS strength and leads to higher CymR abundance. Simultaneously, the lowest K values are displayed by toggle switches comprising a weak RBS upstream of *cymR* (pVCS1, pVCS4, pVCS7). Accordingly, when induced with vanillate, pVCS1 (1-1), pVCS2 (1-2), and pVCS3 (1-3) show the lowest K value of 0.08, while all switches hold a weak RBS regulating *vanR* expression. While these findings may imply that K is primarily influenced by the RBS located upstream of *vanR* rather than by the strength of the RBS regulating *cymR*, this pattern is not applicable for the remaining plasmids that show altering K values with varying strength of RBS controlling for *cymR*. Consequently, the variation in performance metrics as displayed across the combinatorial RBS landscapes suggest a clear impact of RBS strength on performance of the genetic circuit in *P. putida*.

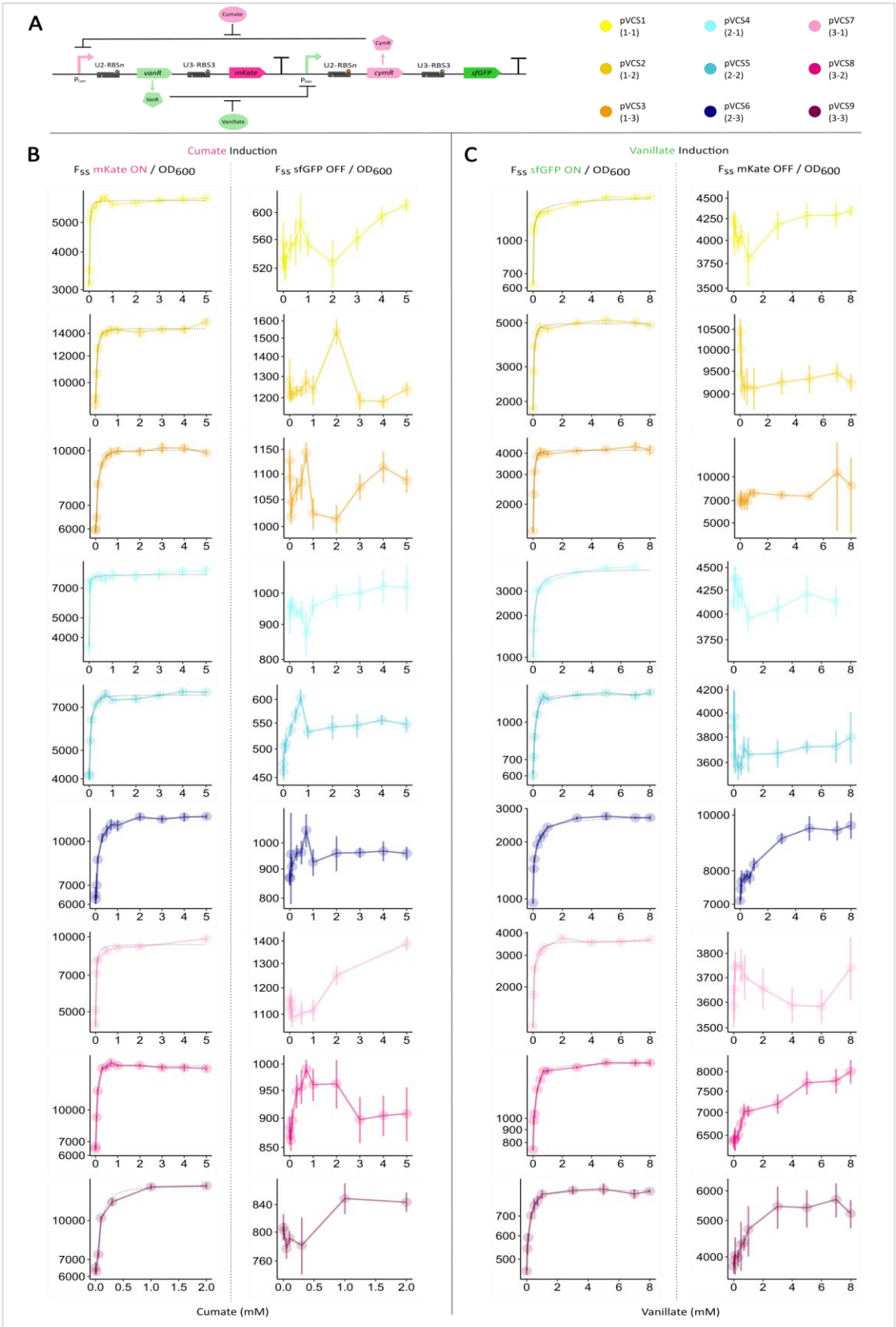

Fig. 9. Toggle switch induction kinetics vary with different RBS combinations in *P. putida*. (A) Toggle scheme and colour coding scheme of plasmids varying in RBS combinations. (B) Cumate and (C) vanillate induction curves with parameter fitted Hill function (dashed line) and the respective opposing fluorescence signal are shown (n=8). Fluorescence signals recorded at steady-state are plotted on a log-transformed Y-axis and are standardized and normalized to OD_{600}. Error bars show standard deviation.

Table 10. Estimated and empirical performance parameters obtained by fitting the Hill function to the respective induction curve in *P. putida* toggle switches. K=activation coefficient (mM) (estimated), β=maximal expression level (RFU) (empirical, rounded), n=Hill coefficient (estimated), C=basal expression level (RFU) (estimate, rounded). All parameters are *reported with standard deviations.*

	Cumate Induction				Vanillate Induction			
	K	β	n	C	K	β	n	C
pVCS1	0.03 ± 0.00	6000 ± 90	1.57 ± 0.16	3100 ± 80	0.08 ± 0.02	1500 ± 50	0.56 ± 0.09	600 ± 10
pVCS2	0.07 ± 0.01	14100 ± 500	2.06 ± 0.47	8700 ± 300	0.08 ± 0.00	4900 ± 70	1.31 ± 0.21	1800 ± 30
pVCS3	0.11 ± 0.02	9900 ± 200	1.68 ± .016	5900 ± 200	0.08 ± 0.02	4000 ± 200	1.55 ± 0.40	1400 ± 50
pVCS4	0.01 ± 0.01	8500 ± 500	0.53 ± 0.07	3600 ± 400	0.26 ± 0.04	4100 ± 100	0.98 ± 0.08	1000 ± 20
pVCS5	0.07 ± 0.01	7900 ± 100	1.46 ± 0.22	4000 ± 200	0.15 ± 0.02	1200 ± 30	1.52 ± 0.13	600 ± 30
pVCS6	0.17 ± 0.03	12200 ± 200	1.25 ± 0.21	6200 ± 200	0.23 ± 0.02	2600 ± 40	0.76 ± 0.05	1000 ± 20
pVCS7	0.04 ± 0.01	9800 ± 200	1.60 ± 0.98	4400 ± 200	0.11 ± 0.01	3600 ± 100	1.10 ± 0.15	1200 ± 20
pVCS8	0.08 ± 0.00	15900 ± 500	2.14 ± 0.24	6500 ± 100	0.19 ± 0.02	1600 ± 40	1.05 ± 0.10	800 ± 20
pVCS9	0.11 ± 0.01	13700 ± 400	1.77 ± 0.53	6200 ± 300	0.19 ± 0.03	800 ± 10	1.17 ± 0.27	500 ± 20

4.3.3 Maintenance and Expression of pVCS impacts Growth Dynamics

As demonstrated in preliminary tests (4.1.3), introducing the toggle device in the *P. putida* host significantly reduced the specific growth rate of pVCS-carrying strains compared to the WT counterpart ($p < 0.001$). To further assess how growth is affected in each induction state, a growth assay was performed, in which a single inducer concentration was added to toggle the pVCS series to the respective induction state. OD_{600} values were measured generating growth curves for each toggle switch (Fig. 10B).

A brief examination of the growth curves indicates changes in growth patterns across the RBS landscape and induction states. Based on these growth curves, the maximum specific growth rate (μ) and carrying capacity (A) was estimated, to quantify growth behavior and determine distinct growth dynamics across the RBS combinations (Table 11). The results suggest that growth behavior is influenced by both, the induction state, and the RBS strength in the toggle switches. On average, toggle switches displayed higher μ values in absence of inducer (0.42 ± 0.03) compared to the cumate (0.35 ± 0.02) and vanillate (0.38 ± 0.03) induced state, suggesting that expression of the gene cassettes or inducer toxicity has an impact on growth dynamics in the toggle switches. In absence of inducer or upon cumate induction, pVCS9 (3-3) exhibits the lowest μ values, while in the presence of vanillate, the specific growth rate of pVCS3 (1-3) is most diminished.

To further assess if inverting the toggle switch affects growth dynamics in the toggle switches, the inducer was washed out and the pVCS series was toggled to their respective opposite state by adding the corresponding inducer (Fig. 10C). Based on measured OD_{600} curves, μ and A were estimated to quantify growth behavior. The findings reveal varying growth parameters across induction state and RBS combination (Table 12). On average, cumate induction is still associated with slightly lower μ values (0.37 ± 0.02), no growth diminishing effect can be observed upon vanillate induction (0.4 ± 0.03), compared to the non-induced state (0.4 ± 0.02). Interestingly, pVCS9 is not displaying the lowest μ value within the cumate and NI induction state as observed in the first toggle event. Accordingly, pVCS3, as most of the pVCS series exhibit increased μ values upon vanillate induction in the second toggle event. These findings verify the impact of the induction state and the RBS combination.

Furthermore, the growth assay aims to assess the extent of a growth burden caused by varying RBS strengths and the respective induction state. To quantify growth burden in a non-induced state, growth rates were compared between the toggle switches and the *P. putida* WT, indicated by $\Delta\mu_{NI}$. Growth burdens in absence of inducer range from -21.6 ± 4.8 to -37.1 ± 4.6 %, with pVCS9 (3-3) displaying the highest proportional decrease in growth rate (Fig. 10D). Growth impairments upon vanillate and cumate induction were quantified by comparing growth rates between non-induced and induced switches, resulting in $\Delta\mu_{Cym}$ and $\Delta\mu_{Van}$, respectively. While vanillate induction results in an average growth burden of -9.3 ± 4.7 %, growth rates are averagely reduced by -17.1 ± 3.7 % when induced with cumate. The highest growth burden upon vanillate induction is shown by pVCS3 (1-3) (Fig. 10E), while in the cumate-induced state, growth behavior appears to be most affected in pVCS6 (2-3) (Fig. 10F). The results suggest a varying extent of growth burdens across induction states and toggle switches, emphasizing again the impact of different RBS combinations on growth dynamics.

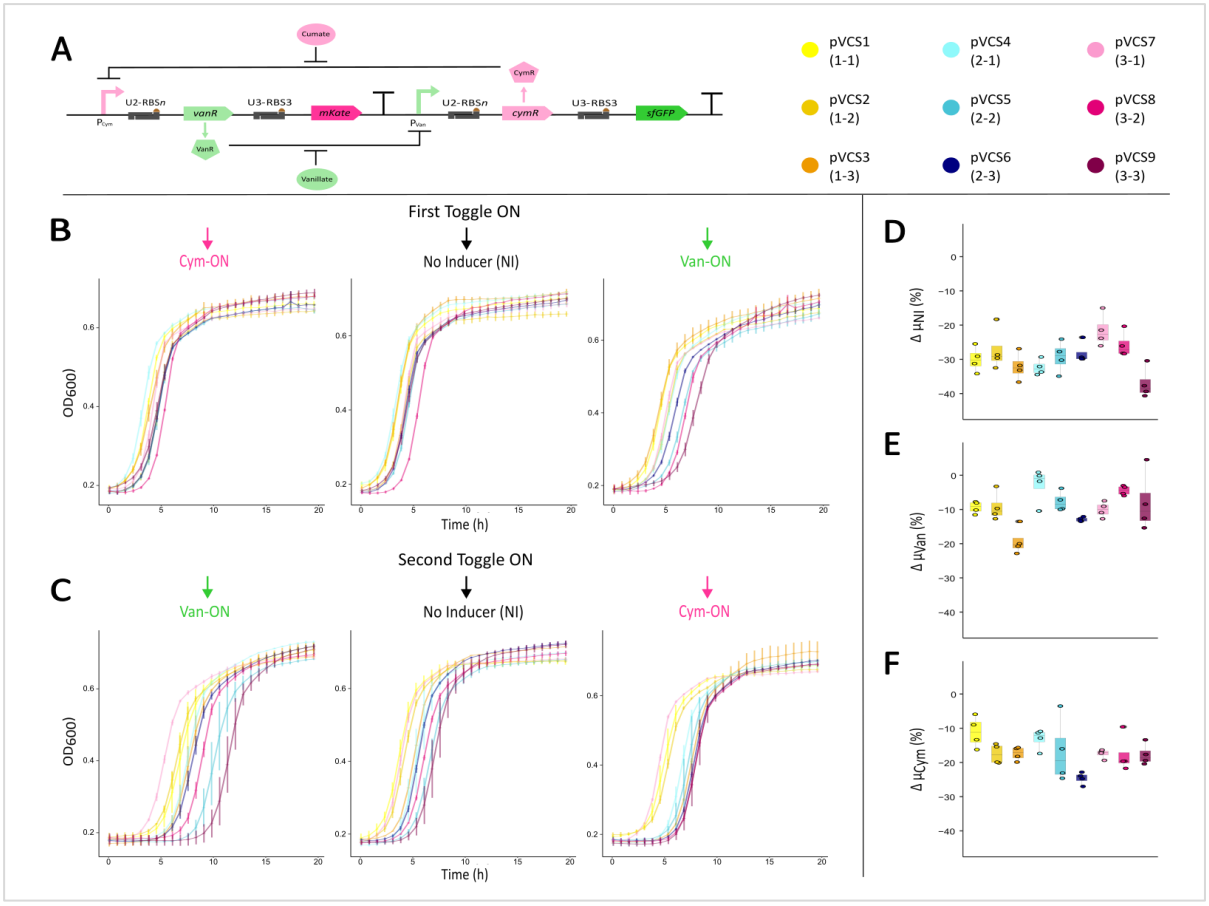

Fig. 10. Growth dynamics displayed by toggle switches in *P. putida* and the extent of growth burdens vary across RBS combinations and inducer. (A) Toggle scheme and colour coding scheme of plasmids varying in RBS combinations are introduced. (B) OD_{600} curves of switches as recorded during the toggle assay: First toggled from initial OFF state (no inducer) to ON state (First Toggle ON) and then (C) to the respective opposite state (n=4). Error bars show standard deviation. (D) Growth burden exhibited by the plasmid bearing strains in the absence of inducer compared to WT counterpart (n=4). (E) Growth burden of plasmid bearing strains as a result of vanillate and (F) cumate induction compared to non-induced state (n=4).

Table 11. Summary of estimated growth metrics based on OD_{600} output measured during the first toggle event *P. putida* (First Toggle ON)μ = maximum specific growth rate (h^{-1}), A = carrying capacity (OD_{600}). All parameters are reported with standard deviations.

	Vanillate		Cumate		No Inducer	
	μ	A	μ	A	μ	A
pVCS1	0.38 ± 0.01	0.65 ± 0.01	0.37 ± 0.02	0.67 ± 0.01	0.42 ± 0.02	0.68 ± 0.01
pVCS2	0.39 ± 0.01	0.63 ± 0.00	0.36 ± 0.01	0.65 ± 0.00	0.43 ± 0.01	0.65 ± 0.01
pVCS3	0.32 ± 0.01	0.67 ± 0.01	0.33 ± 0.01	0.68 ± 0.00	0.40 ± 0.00	0.70 ± 0.01
pVCS4	0.39 ± 0.01	0.66 ± 0.01	0.35 ± 0.01	0.69 ± 0.00	0.40 ± 0.02	0.70 ± 0.01
pVCS5	0.39 ± 0.00	0.64 ± 0.01	0.33 ± 0.01	0.65 ± 0.01	0.42 ± 0.01	0.67 ± 0.00
pVCS6	0.37 ± 0.01	0.64 ± 0.00	0.32 ± 0.00	0.67 ± 0.01	0.43 ± 0.01	0.67 ± 0.01
pVCS7	0.42 ± 0.00	0.64 ± 0.01	0.38 ± 0.01	0.64 ± 0.00	0.46 ± 0.01	0.67 ± 0.01
pVCS8	0.42 ± 0.00	0.67 ± 0.00	0.36 ± 0.01	0.68 ± 0.01	0.44 ± 0.00	0.69 ± 0.00
pVCS9	0.33 ± 0.01	0.67 ± 0.01	0.31 ± 0.01	0.70 ± 0.00	0.37 ± 0.00	0.68 ± 0.00

Table 12. Summary of estimated growth metrics based on OD_{600} output measured during the second toggle event in *P. putida* (Second Toggle ON). μ = maximum specific growth rate (h^{-1}), A = carrying capacity (OD_{600}). All parameters are reported with standard deviations.

	Vanillate		Cumate		No Inducer	
	μ	A	μ	A	μ	A
pVCS1	0.37 ± 0.01	0.68 ± 0.00	0.36 ± 0.01	0.68 ± 0.00	0.38 ± 0.02	0.67 ± 0.01
pVCS2	0.36 ± 0.00	0.67 ± 0.00	0.34 ± 0.01	0.67 ± 0.00	0.39 ± 0.02	0.67 ± 0.01
pVCS3	0.39 ± 0.00	0.71 ± 0.03	0.37 ± 0.00	0.70 ± 0.01	0.43	0.70
pVCS4	0.42 ± 0.01	0.67 ± 0.01	0.38 ± 0.00	0.71 ± 0.00	0.43 ± 0.00	0.68 ± 0.00
pVCS5	0.40 ± 0.01	0.69 ± 0.01	0.41 ± 0.02	0.67 ± 0.00	0.37 ± 0.01	0.67 ± 0.01
pVCS6	0.41 ± 0.00	0.69 ± 0.00	0.36 ± 0.01	0.70 ± 0.01	0.41 ± 0.01	0.71 ± 0.01
pVCS7	0.41 ± 0.00	0.66 ± 0.00	0.36 ± 0.01	0.68 ± 0.01	0.41 ± 0.01	0.68 ± 0.00
pVCS8	0.41 ± 0.01	0.68 ± 0.00	0.39 ± 0.02	0.68 ± 0.01	0.38 ± 0.01	0.68 ± 0.01
pVCS9	0.43 ± 0.02	0.68 ± 0.01	0.38 ± 0.01	0.70 ± 0.01	0.41 ± 0.00	0.71 ± 0.01

4.4 Performance Profiles displayed by the pVCS Series cluster along Host Context

The performance of genetic circuits is dependent on the host environment in which they operate (Cardinale & Arkin, 2012). This phenomenon acknowledges that the same genetic circuit may exhibit different performance characteristics when incorporated into distinct host organisms, referred to as the chassis-effect (Chan et al., 2023). In previous assays, the performance of the toggle switch across the combinatorial RBS design space has been explored in context of each host, underlining the impact of different combinations of RBS strengths on toggle switch behavior. Through the comparison of selected performance parameters obtained from the induction assay, the behavior of toggle switches is assessed across different bacterial hosts, aiming to elucidate a potential chassis-effect on device performance.

Induction performance parameters were chosen to demonstrate the sampled expression space in a host-dependent context for each inducer. The activation coefficient K is indicative of the devices' sensitivity, while the DR, expressing the difference between basal and maximum fluorescence signal, reflects the responsiveness of the toggle switch. The results suggest a substantial difference in performance characteristics across the induction states and between the host species (Fig. 11). Upon cumate induction, all toggle switches in *P. putida* display a low responsiveness and varying sensitivity, compared to the *E. coli* host, whose toggle switches are mainly varying in responsiveness, while most are exhibiting relative high sensitivity (Fig. 11A). Outstanding devices include *P. putida* pVCS6 showing the lowest sensitivity and low responsiveness, *E. coli* pVCS1 characterized by a highly sensitive performance combined with a high DR, and *E. coli* pVCS3, displaying high responsiveness and low sensitivity. Within the vanillate induced performance space, most *E. coli* toggle switches vary predominantly in their responsiveness, while exhibiting some variation in sensitivity (Fig. 11B). Contrary, toggle devices in *P. putida* display a similar DR, while mainly varying in their sensitivity. Of all devices, *E. coli* pVCS4 and pVCS7 display the highest level of responsiveness combined with high sensitivity, while *P. putida* pVCS4 performs with the highest DR, while exhibiting lowest sensitivity.

Assessing the inducer-dependent expression space suggests that the variation of toggle switch performance within the explanatory parameters is characteristic for each host. To further examine and illustrate this, PCA was performed to condense the variability in toggle switch performance observed within each device and host into a low-dimensional space (Fig. 11C). The PCA results are presented in the two-dimensional space of a biplot, which is spanned by

the principal components. These are the variables that explain the maximum variability of the original data set according to the selected performance parameters (K, β and C). The observed variance among the toggle switch performances noticeably partitions between the host species, visually demonstrating a clear chassis-effect regardless of RBS design space (Fig. 11C). Each host displays its own characteristic performance space, while the pVCS series appears to behave more similarly in *P. putida* compared to *E. coli* and the observed variance appears to largely correlate with the activation coefficient. In contrast, the toggle switches display more variability in context of the *E. coli* host, indicating a wider expression space. These results emphasize that performance characteristics exhibited by the toggle switches differ not only across the combinatorial RBS landscape, but are more strongly driven by the host context.

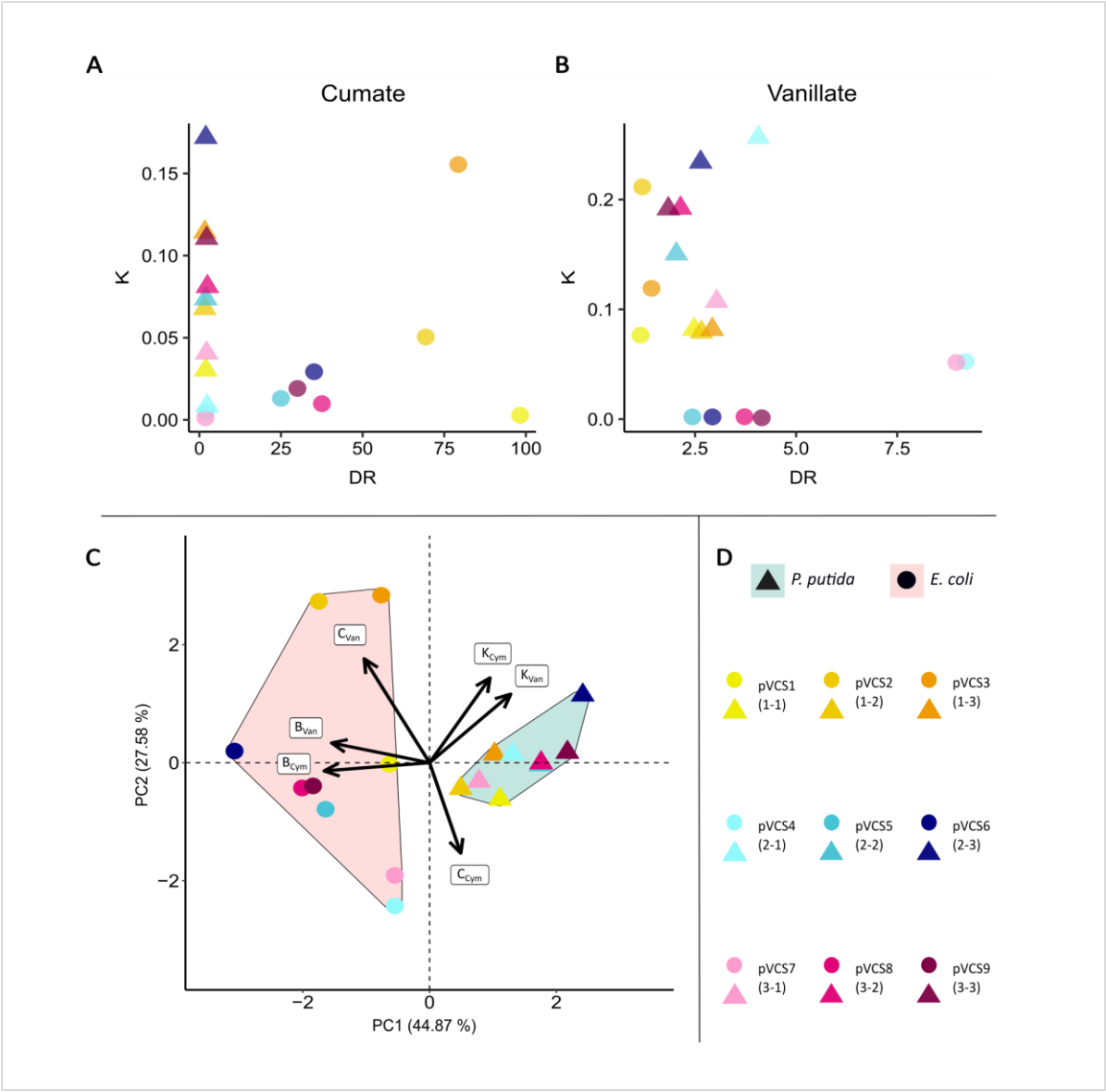

Fig. 11. **Device performance in the sampled expression space partitions between *E. coli* and *P. putida* host species, demonstrating a clear chassis-effect.** Host-specific performance of the pVCS series within the expression space spanned by the activation coefficient (K) and the dynamic range (DR) for (A) cumate and (B) vanillate. (C) Observed variance between toggle switch performances in the host-specific context according to multiple performance parameters, as returned through PCA. Principal components (PC) represent variables that explain maximal variance between the devices, while the respective proportion of the total variance is specified. Variables were scaled to account for dimensional homogeneity. The arrows suggest the direction of increase of a given performance parameter. (D) Colour and shape coding scheme of the pVCS series in their respective host-context.

5 Discussion

Tuning gene expression levels is a crucial aspect in optimizing the performance of genetic circuits. However, indiscriminate enhancement of all expression levels may not necessarily yield optimal performance parameters (Zelcbuch et al., 2013). Achieving balanced expression levels of individual genes is critical to ensure the desired functionality of a genetic device, while simultaneously mitigate growth-inhibitory or interfering effects within the circuit elements. As synthetic devices grow in complexity, the application of combinatorial optimization strategies to fine-tune gene expression becomes increasingly vital (Naseri & Koffas, 2020). This thesis demonstrates how different combinations of RBS strengths, regulating expression of transcriptional repressors, can impact the performance of a genetic toggle switch. Thereby, the results highlight the importance of modifying RBSs as an efficient combinatorial strategy to fine-tune gene expression at the translational level driving the output properties of a synthetic construct.

5.1 Translation Initiation Efficiency as subject to mRNA sequence

RBS strengths are associated with the rate at which ribosomes are recruited to bind to the RBS sequence and initiate translation of the mRNA transcript. The efficiency of the 30S initiation complex formation varies depending on the mRNA sequence and is determined by a multitude of molecular interactions. These include hybridization of the 16S rRNA to the SD-sequence of the RBS, spacing, the start codon of the protein coding sequence, and the presence of mRNA secondary structures. The choice of start codon has been found to affect translation initiation with the codon AUG experimentally verified to exhibit enhanced translation efficiency compared to other start codons (Ringquist et al., 1992; Vellanoweth & Rabinowitz, 1992). AUG has therefore been the start codon of choice for many cloned genes, including the protein coding sequences within the toggle switch designs. Spacing describes the distance between RBSs and the start codon. While different spacing optima have been experimentally verified to enhance translation rates (Ringquist et al., 1992; Salis et al., 2009; Vellanoweth & Rabinowitz, 1992). However, given the consistent spacing and choice of start codon AUG for all protein coding sequence within the pVCS series, their potential impact on modulating translation initiation is not elaborated upon within the confines of this work.

Unfolding of the mRNA is crucial in the translation initiation process, ensuring accessibility for the ribosome to form the translation initiation complex, hence correlating with the protein expression level (de Smit & van Duin, 1990). The presence of secondary structures imposes a

thermodynamic barrier that the ribosome must overcome to bind the mRNA transcript, hence, more stable secondary structures lead to decreased translational efficiencies (Studer & Joseph, 2006). Depending on the UTR upstream of the RBS, varying structural elements participating in mRNA unfolding are present and facilitate accessibility (Seo et al., 2013). Consequently, the occurrence of secondary structures and the presence of differing structural elements depending on the genetic context may account for the varying translation initiation rates predicted by the OSTIR tool.

A critical process for driving translation initiation is the hybridization of the SD sequence in the RBS to the anti-SD sequence of the 16S rRNA in the ribosomal subunit. Thereby, the level of complimentary, corresponding to the strength of the molecular interactions, contributes to the formation and stabilization of the translation initiation complex, potentially contributing to mRNA unfolding and thus determining translational efficiency (Salis et al., 2009; Studer & Joseph, 2006). Furthermore, the length of the SD sequence was proposed to regulate the translational procedure, since short sequence are suggested to form a weak translation initiation complex due to less efficient binding to the anti-SD sequence, while long SD sequences bind too tightly preventing the ribosome from leaving the initiation site and proceed with elongation (Komarova et al., 2002; Vimberg et al., 2007). Although the anti-SD sequence within the 16S rRNA was found to be a conserved region across bacterial species (Salis et al., 2009; Shine & Dalgarno, 1974), indicating the significance of molecular interactions between SD and anti-SD sequences, certain species utterly lack the SD sequence (Tzareva et al., 1994). Consequently, alternative SD-independent strategies have been identified, such as translational enhancer elements within mRNA sequences (Stenström & Isaksson, 2002; Vimberg et al., 2007) and the ribosomal protein S1, promoting mRNA unfolding and capable of compensating for weak or absent SD sequences (Tzareva et al., 1994; Vellanoweth & Rabinowitz, 1992). However, these mechanisms, when concurrent, may be masked by the strong effects of SD sequence-based interactions (Komarova et al., 2002).

In this work only the translation initiation process is considered as it is the rate-limiting step, although it is worth noting that inefficiency in translation elongation or termination can also have an impact on gene expression and feed back on the initiation process (Hersch et al., 2014). For example, the occurrence of internal SD-like motifs within a protein coding sequence can cause translational pausing, caused by hybridization attempts between the anti-SD sequence and the SD-like feature in the protein coding sequence (Li et al., 2012). The resulting decrease

in translation elongation rate can reduce the amount of ribosomes available for translation initiation.

5.2 Misinterpretation of the Hill Coefficient (n)

Numerous biochemical reactions involve complex molecular mechanisms that are generally not comprehensively known. Applying the hill function generates a simplified model to characterize complex non-linear dynamics. The equation was established by A. V. Hill to describe binding interactions between oxygen and hemoglobin. Applying the function allows to quantify binding affinity between ligand and macromolecule and the number of binding sites that need to interact with a ligand to induce functional effects (Hill, 1913). Although the latter can be inferred from the Hill coefficient n, the accuracy of this estimate suffers considerably when molecules with multiple binding sites are involved in a reaction. As of today it is recognized that only in the case of extreme positive cooperativity and simultaneous binding of ligands, the Hill coefficient can provide a minimum estimate (Weiss, 1997). However, these prerequisites are considered physically implausible in common biochemical reactions. Hence, the relevance of the hill coefficient shifted towards indication of general cooperativity at ligand binding sites (Ang et al., 2013). However, detailed knowledge of the molecular binding interactions between the inducer and the corresponding TF is lacking. Subsequently, it is not possible to assume a condition of extreme positive cooperativity. The Hill coefficient n, as estimated from induction experiments in this work, hence, should be considered as an empirical value and further interpretations are not advisable.

5.3 Toggle Performance as driven by the Host-Context

The findings of this work reveal an underlying chassis-effect that drives toggle switch performance in a host-dependent context: Regardless of RBS combinations, the toggle switches displayed distinct host-specific performance spaces with a broad range of observed parameters. Each host provides a unique environment in which a given genetic device will be operating alongside numerous endogenous processes that potentially interfere with device performance. These interferences can be indirect through competition over shared cellular resources or direct cross-talk interactions between components of the synthetic device and the host cell, impeding the functionality of the genetic circuit (Cardinale & Arkin, 2012).

The performance of a genetic device is inevitably coupled to the physiological state of the cell as it dictates the availability of indispensable cellular resources required for the transcriptional and translational machinery. During cellular proliferation, protein biosynthesis stands as the most energy-intensive process, with ribosomal translation estimated to consume approximately 50% of the energy in a rapidly growing bacterial cell (Li et al., 2014). The maintenance of exogenous plasmids is hence competing with endogenous cellular processes for these resources, limiting the capability of biosynthesis, which in turn, impedes growth dynamics and impacts device performance (Boo et al., 2019; Klumpp et al., 2009; Vind et al., 1993). Furthermore, the (enhanced) expression of heterologous pathways can lead to accumulation of toxic compounds, inhibiting cell growth. The extent of growth burdens imposed by the toggle switches differ between the hosts, with *P. putida* being more affected than *E. coli.* Differences in plasmid copy number (PCN) associated with the hosts may account for this observation. As the number of plasmids to be maintained increases, so does the metabolic burden, while upon induction, these growth inhibitions are further intensified (Rouches et al., 2022). Although PCN is regulated by the replication system of the plasmid, varying PCN have been observed across different host organisms, harboring plasmids with identical origins of replication (Chan et al., 2023; Jahn et al., 2016).

As gene expression in the genetic device directly corresponds to the availability of cellular resources, mainly RNAPs, tRNAs and ribosomes, variations in abundance of these crucial components can account for the observed differences in performance (Hanson & Coller, 2018; Qian et al., 2017). Furthermore, the availability of ribosomes is known to correlate with the bacterial growth rate, with slower-growing cells exhibiting a reduction in the abundance of ribosomal proteins (Klumpp et al., 2009; Milne et al., 1975). Considering that maintaining and inducing the toggle switch imposes a greater growth burden in *P. putida* compared to *E. coli*, it is plausible that *P. putida* could display a lower ribosome count, affecting the performance of the toggle switch. This could be tested in future experiments, for example by quantifying rRNA amounts through qPCR and thereby estimating ribosome counts. The occurrence of competition for limited resources among the gene cassettes of the toggle switch might typically be disregarded, given that the expression of one gene cassette theoretically entails repression of the opposing cassette. However, the toggle switches in *P. putida* exhibit a higher level of leakage compared to *E. coli* upon vanillate induction, suggesting that resource competition among both gene cassettes could indeed transpire and limit the devices' performance.

Despite the presence of transcriptional repressors or in the absence of the cognate inducers, respectively, a number of promoters in the toggle switches retained a basal level of transcriptional activity, as observed by corresponding fluorescence signals. Although genetic switches are reported to be stochastically driven towards one site of the gene cassette (Wu et al., 2013), leakage commonly arises when expression systems are introduced into novel host contexts (Carrillo Rincón & Farny, 2023; Tas et al., 2021). Particularly notable was the leakage of P_{Cym} in the presence of the antagonistic inducer vanillate in *P. putida*. Several factors inherent to the host-specific context may account for this phenomenon, including a stronger operation of P_{Cym}, a higher PCN in *P. putida*, or cross-talk with other endogenous components enhancing transcriptional activity (Martin-Pascual et al., 2021; Tas et al., 2021). Furthermore, incompatibility of the P_{Van} promoter, leading to insufficient synthesis of CymR, could impair control over P_{Cym}. Strategic modifications to the promoter structure such as sigma factor optimization (Carrillo Rincón & Farny, 2023) or alterations to the -35 and -10 sites (Chen et al., 2018) can mitigate promoter leakage and reinforce tight control over gene expression.

Furthermore, codon usage bias could account for alterations in toggle switch performance between multiple species. Thereby, the host exhibits non-random variability in its codon usage, which corresponds to the host-specific tRNA pool (Hanson & Coller, 2018). Although codon usage bias is mainly suggested to affect translation elongation rate, it can feed back to translation initiation efficiency, for example if ribosome collisions and queues occur and diminish abundance of free ribosomes (Mitarai et al., 2008). Hence, host-individual codon optimization of a synthetic device is proposed to be an effective strategy to ensure robust operation in the respective host and further enhance translation efficiency.

5.4 The Importance of the Chassis-Effect for Expanding the Design Space

Furthermore, this work emphasizes the significance of host-specific performance characterization when designing a genetic circuit. The context in which the device operates heavily influences its behavior and is unpredictable when viewed solely from the sequence-centric perspective of the device (Tas et al., 2021). On the one side, contextual dependencies can limit the accuracy of prediction and complicate the design of novel genetic devices that are reliably operating across multiple hosts (Kushwaha & Salis, 2015). Approaches to achieve interoperability across multiple hosts aim to minimize host-circuit interaction by creating circuit-specific regulatory networks using orthogonal components. For instance, Darlington et

al. described the design of an orthogonal translational network, which expresses synthetic 16S rRNA to decouple host-translational from device-translational activities (Darlington et al., 2018). Decoupling from the intrinsic machinery of the host can also serve as an effective strategy to reduce competition for cellular resources, thereby diminishing the growth burden (Boo et al., 2019). However, the attempts of improving general interoperability and minimizing growth inhibition are only preventing the performance variability to a certain extent (Qian et al., 2017). Despite the restrictions in terms of reliability and prediction of circuit performance, the chassis-effect, on the other hand, presents an interesting opportunity for expanding the devices' functionality. Considering multiple hosts allows access to an enlarged design space, which facilitates the selection of an optimal device for tailored applications according to its intrinsic properties. This makes the host-context a crucial design parameter for empowering synthetic biodesign and optimizing performance space (Tas et al., 2021). Future efforts should focus on exploring and characterizing the performance space of genetic devices in context of multiple hosts to enlarge functionality and the design space, while applying fine-tune strategies to improve reliability, efficiency, and predictability of the circuits. Additionally, the context focus can be expanded upon environmental dependencies, affecting the host metabolism and thus the performance space (Cardinale & Arkin, 2012). These endeavors are promising steps for innovative context-dependent design that allows the reliable operation of a synthetic device in accordance to the intended applicative framework.

6 Conclusion

In the realm of synthetic biology, achieving precise control over protein expression stands as a fundamental aspect in ensuring robust and reliable operation of genetic circuits. This work focuses on tuning gene expression at the translational level through varying RBS combinations regulating for the production of transcriptional repressors within a genetic toggle switch. Fluorescence and OD_{600} was measured to determine performance metrics and identify differences in toggle switch behavior across the pVCS series. The results highlight the efficacy of modulating RBS strength as a means to fine-tune the performance of a genetic toggle switch. Through the combinatorial adjustment of RBS strengths, a two-dimensional performance space emerges, displaying diverse performance metrics across the pVCS series. Furthermore, this work assesses toggle switch behavior across multiple species to elucidate the influence of host context on the performance. The findings address the remarkable variability of the observed performance landscape in relation to the host context, emphasizing the pivotal role of the chassis-effect in shaping toggle switch behavior independent of RBS context. Despite the challenges posed by the attendant reliability and predictability issues in genetic devices due to contextual dependencies, considering these context effects offer opportunities for expanding device functionality. Gaining access to an enlarged performance space facilitates the selection of an optimal device exhibiting desired properties tailored to specific applications. While the host-context serves as a critical design parameter in shaping the performance space, modifying RBS strengths emerges as an effective design strategy to further fine-tune this performance space.

7 References

Alon, U. (2006). *An Introduction to Systems Biology: Design Principles of Biological Circuits*. CRC Press.

Anderson, J. C., Voigt, C. A., & Arkin, A. P. (2007). Environmental signal integration by a modular AND gate. *Molecular Systems Biology*, *3*(1), 133. https://doi.org/10.1038/msb4100173

Ang, J., Harris, E., Hussey, B. J., Kil, R., & McMillen, D. R. (2013). Tuning Response Curves for Synthetic Biology. *ACS Synthetic Biology*, *2*(10), 547–567. https://doi.org/10.1021/sb4000564

Anton, B. P., & Raleigh, E. A. (2016). Complete Genome Sequence of NEB 5-alpha, a Derivative of Escherichia coli K-12 DH5α. *Genome Announcements*, *4*(6), 10.1128/genomea.01245-16. https://doi.org/10.1128/genomea.01245-16

Belda, E., van Heck, R. G. A., José Lopez-Sanchez, M., Cruveiller, S., Barbe, V., Fraser, C., Klenk, H.-P., Petersen, J., Morgat, A., Nikel, P. I., Vallenet, D., Rouy, Z., Sekowska, A., Martins dos Santos, V. A. P., de Lorenzo, V., Danchin, A., & Médigue, C. (2016). The revisited genome of Pseudomonas putida KT2440 enlightens its value as a robust metabolic chassis. *Environmental Microbiology*, *18*(10), 3403–3424. https://doi.org/10.1111/1462-2920.13230

Benner, S. A., & Sismour, A. M. (2005). Synthetic biology. *Nature Reviews Genetics*, *6*(7), Article 7. https://doi.org/10.1038/nrg1637

Boo, A., Ellis, T., & Stan, G.-B. (2019). Host-aware synthetic biology. *Current Opinion in Systems Biology*, *14*, 66–72. https://doi.org/10.1016/j.coisb.2019.03.001

Cardinale, S., & Arkin, A. P. (2012). Contextualizing context for synthetic biology – identifying causes of failure of synthetic biological systems. *Biotechnology Journal*, *7*(7), 856–866. https://doi.org/10.1002/biot.201200085

Carrillo Rincón, A. F., & Farny, N. G. (2023). Unlocking the strength of inducible promoters in Gram-negative bacteria. *Microbial Biotechnology*, *16*(5), 961–976. https://doi.org/10.1111/1751-7915.14219

Casini, A., Storch, M., Baldwin, G. S., & Ellis, T. (2015). Bricks and blueprints: Methods and standards for DNA assembly. *Nature Reviews Molecular Cell Biology*, *16*(9), 568–576. https://doi.org/10.1038/nrm4014

Chan, D. T. C., Baldwin, G. S., & Bernstein, H. C. (2023). Revealing the Host-Dependent Nature of an Engineered Genetic Inverter in Concordance with Physiology. *BioDesign Research*, *5*, 0016. https://doi.org/10.34133/bdr.0016

Chen, Y., Ho, J. M. L., Shis, D. L., Gupta, C., Long, J., Wagner, D. S., Ott, W., Josić, K., & Bennett, M. R. (2018). Tuning the dynamic range of bacterial promoters regulated by ligand-inducible transcription factors. *Nature Communications*, *9*(1), 64. https://doi.org/10.1038/s41467-017-02473-5

Cherry, J. L., & Adler, F. R. (2000). How to make a Biological Switch. *Journal of Theoretical Biology*, *203*(2), 117–133. https://doi.org/10.1006/jtbi.2000.1068

Darlington, A. P. S., Kim, J., Jiménez, J. I., & Bates, D. G. (2018). Dynamic allocation of orthogonal ribosomes facilitates uncoupling of co-expressed genes. *Nature Communications*, *9*(1), 695. https://doi.org/10.1038/s41467-018-02898-6

de Smit, M. H., & van Duin, J. (1990). Secondary structure of the ribosome binding site determines translational efficiency: A quantitative analysis. *Proceedings of the National Academy of Sciences*, *87*(19), 7668–7672. https://doi.org/10.1073/pnas.87.19.7668

De Wannemaeker, L., Mey, F., Bervoets, I., Ver Cruysse, M., Baldwin, G. S., & De Mey, M. (2023). Standardization of Fluorescent Reporter Assays in Synthetic Biology across the Visible Light Spectrum. *ACS Synthetic Biology*, *12*(12), 3591–3607. https://doi.org/10.1021/acssynbio.3c00386

Eaton, R. W. (1997). p-Cymene catabolic pathway in Pseudomonas putida F1: Cloning and characterization of DNA encoding conversion of p-cymene to p-cumate. *Journal of Bacteriology*, *179*(10), 3171–3180. https://doi.org/10.1128/jb.179.10.3171-3180.1997

Elbeik, T., Surtihadi, J., Destree, M., Gorlin, J., Holodniy, M., Jortani, S. A., Kuramoto, K., Ng, V., Valdes, R., Valsamakis, A., & Terrault, N. A. (2004). Multicenter Evaluation of the Performance Characteristics of the Bayer VERSANT HCV RNA 3.0 Assay (bDNA). *Journal of Clinical Microbiology*, *42*(2), 563–569. https://doi.org/10.1128/jcm.42.2.563-569.2004

Ellis, T., Wang, X., & Collins, J. J. (2009). Diversity-based, model-guided construction of synthetic gene networks with predicted functions. *Nature Biotechnology*, *27*(5), 465–471. https://doi.org/10.1038/nbt.1536

Elowitz, M. B., & Leibler, S. (2000). A synthetic oscillatory network of transcriptional regulators. *Nature*, *403*(6767), Article 6767. https://doi.org/10.1038/35002125

Farasat, I., Kushwaha, M., Collens, J., Easterbrook, M., Guido, M., & Salis, H. M. (2014). Efficient search, mapping, and optimization of multi-protein genetic systems in diverse bacteria. *Molecular Systems Biology*, *10*(6), 731. https://doi.org/10.15252/msb.20134955

Fedr, R., Kahounová, Z., Remšík, J., Reiterová, M., Kalina, T., & Souček, K. (2023). Variability of fluorescence intensity distribution measured by flow cytometry is influenced by cell size and cell cycle progression. *Scientific Reports*, *13*(1), 4889. https://doi.org/10.1038/s41598-023-31990-1

Frank, S. A. (2013). Input-output relations in biological systems: Measurement, information and the Hill equation. *Biology Direct*, *8*(1), 31. https://doi.org/10.1186/1745-6150-8-31

Gardner, T. S., Cantor, C. R., & Collins, J. J. (2000). Construction of a genetic toggle switch in Escherichia coli. *Nature*, *403*(6767), Article 6767. https://doi.org/10.1038/35002131

Gilbert, E. S., Walker, A. W., & Keasling, J. D. (2003). A constructed microbial consortium for biodegradation of the organophosphorus insecticide parathion. *Applied Microbiology and Biotechnology*, *61*(1), 77–81. https://doi.org/10.1007/s00253-002-1203-5

Gompertz, B. (1815). *On the Nature of the Function Expressive of the Law of Human Mortality, and on a New Mode of Determining the Value of Life Contingencies.* https://doi.org/10.1098/rspl.1815.0271

Haines, M. C., Carling, B., Marshall, J., Shenshin, V. A., Baldwin, G. S., Freemont, P., & Storch, M. (2022). basicsynbio and the BASIC SEVA collection: Software and vectors for an established DNA assembly method. *Synthetic Biology*, *7*(1), ysac023.

Hanson, G., & Coller, J. (2018). Codon optimality, bias and usage in translation and mRNA decay. *Nature Reviews Molecular Cell Biology*, *19*(1), Article 1. https://doi.org/10.1038/nrm.2017.91

Hersch, S. J., Elgamal, S., Katz, A., Ibba, M., & Navarre, W. W. (2014). Translation Initiation Rate Determines the Impact of Ribosome Stalling on Bacterial Protein Synthesis*. *Journal of Biological Chemistry*, *289*(41), 28160–28171. https://doi.org/10.1074/jbc.M114.593277

Hill, A. V. (1913). The Combinations of Haemoglobin with Oxygen and with Carbon Monoxide. I. *The Biochemical Journal*, *7*(5), 471–480. https://doi.org/10.1042/bj0070471

Jahn, M., Vorpahl, C., Hübschmann, T., Harms, H., & Müller, S. (2016). Copy number variability of expression plasmids determined by cell sorting and Droplet Digital PCR. *Microbial Cell Factories*, *15*(1), 211. https://doi.org/10.1186/s12934-016-0610-8

Jeschek, M., Gerngross, D., & Panke, S. (2016). Rationally reduced libraries for combinatorial pathway optimization minimizing experimental effort. *Nature Communications*, *7*(1), 11163. https://doi.org/10.1038/ncomms11163

Jiang, T., Teng, Y., Li, C., Gan, Q., Zhang, J., Zou, Y., Desai, B. K., & Yan, Y. (2023). Establishing Tunable Genetic Logic Gates with Versatile Dynamic Performance by Varying Regulatory Parameters. *ACS Synthetic Biology*, *12*(12), 3730–3742. https://doi.org/10.1021/acssynbio.3c00554

Kaczmarczyk, A., Vorholt, J. A., & Francez-Charlot, A. (2013). Cumate-Inducible Gene Expression System for Sphingomonads and Other Alphaproteobacteria. *Applied and Environmental Microbiology*, *79*(21), 6795–6802. https://doi.org/10.1128/AEM.02296-13

Kaczmarczyk, A., Vorholt, J. A., & Francez-Charlot, A. (2014). Synthetic vanillate-regulated promoter for graded gene expression in Sphingomonas. *Scientific Reports*, *4*(1), Article 1. https://doi.org/10.1038/srep06453

Kærn, M., Elston, T. C., Blake, W. J., & Collins, J. J. (2005). Stochasticity in gene expression: From theories to phenotypes. *Nature Reviews Genetics*, *6*(6), 451–464. https://doi.org/10.1038/nrg1615

Khalil, A. S., & Collins, J. J. (2010). Synthetic biology: Applications come of age. *Nature Reviews Genetics*, *11*(5), 367–379. https://doi.org/10.1038/nrg2775

Khan, N., Yeung, E., Farris, Y., Fansler, S. J., & Bernstein, H. C. (2020). A broad-host-range event detector: Expanding and quantifying performance between Escherichia coli and

Pseudomonas species. *Synthetic Biology*, *5*(1), ysaa002. https://doi.org/10.1093/synbio/ysaa002

Klumpp, S., Zhang, Z., & Hwa, T. (2009). Growth Rate-Dependent Global Effects on Gene Expression in Bacteria. *Cell*, *139*(7), 1366–1375. https://doi.org/10.1016/j.cell.2009.12.001

Komarova, A. V., Tchufistova, L. S., Supina, E. V., & Boni, I. V. (2002). Protein S1 counteracts the inhibitory effect of the extended Shine-Dalgarno sequence on translation. *RNA*, *8*(9), 1137–1147.

Kunjapur, A. M., & Prather, K. L. J. (2019). Development of a Vanillate Biosensor for the Vanillin Biosynthesis Pathway in E. coli. *ACS Synthetic Biology*, *8*(9), 1958–1967. https://doi.org/10.1021/acssynbio.9b00071

Kushwaha, M., & Salis, H. M. (2015). A portable expression resource for engineering cross-species genetic circuits and pathways. *Nature Communications*, *6*(1), Article 1. https://doi.org/10.1038/ncomms8832

Laursen, B. S., Sørensen, H. P., Mortensen, K. K., & Sperling-Petersen, H. U. (2005). Initiation of Protein Synthesis in Bacteria. *Microbiology and Molecular Biology Reviews*, *69*(1), 101–123. https://doi.org/10.1128/MMBR.69.1.101-123.2005

Li, G.-W., Burkhardt, D., Gross, C., & Weissman, J. S. (2014). Quantifying Absolute Protein Synthesis Rates Reveals Principles Underlying Allocation of Cellular Resources. *Cell*, *157*(3), 624–635. https://doi.org/10.1016/j.cell.2014.02.033

Li, G.-W., Oh, E., & Weissman, J. S. (2012). The anti-Shine–Dalgarno sequence drives translational pausing and codon choice in bacteria. *Nature*, *484*(7395), 538–541. https://doi.org/10.1038/nature10965

Liu, R., Bassalo, M. C., Zeitoun, R. I., & Gill, R. T. (2015). Genome scale engineering techniques for metabolic engineering. *Metabolic Engineering*, *32*, 143–154. https://doi.org/10.1016/j.ymben.2015.09.013

Lorenz, R., Bernhart, S. H., Höner zu Siederdissen, C., Tafer, H., Flamm, C., Stadler, P. F., & Hofacker, I. L. (2011). ViennaRNA Package 2.0. *Algorithms for Molecular Biology*, *6*(1), 26. https://doi.org/10.1186/1748-7188-6-26

Lu, T. K., Khalil, A. S., & Collins, J. J. (2009). Next-generation synthetic gene networks. *Nature Biotechnology*, *27*(12), 1139–1150. https://doi.org/10.1038/nbt.1591

Martin-Pascual, M., Batianis, C., Bruinsma, L., Asin-Garcia, E., Garcia-Morales, L., Weusthuis, R. A., van Kranenburg, R., & Martins dos Santos, V. A. P. (2021). A navigation guide of synthetic biology tools for *Pseudomonas putida*. *Biotechnology Advances*, *49*, 107732. https://doi.org/10.1016/j.biotechadv.2021.107732

Meyer, A. J., Segall-Shapiro, T. H., Glassey, E., Zhang, J., & Voigt, C. A. (2019). Escherichia coli "Marionette" strains with 12 highly optimized small-molecule sensors. *Nature Chemical Biology*, *15*(2), Article 2. https://doi.org/10.1038/s41589-018-0168-3

Milne, A. N., Mak, W. W., & Wong, J. T. (1975). Variation of ribosomal proteins with bacterial growth rate. *Journal of Bacteriology*, *122*(1), 89–92. https://doi.org/10.1128/jb.122.1.89-92.1975

Mitarai, N., Sneppen, K., & Pedersen, S. (2008). Ribosome Collisions and Translation Efficiency: Optimization by Codon Usage and mRNA Destabilization. *Journal of Molecular Biology*, *382*(1), 236–245. https://doi.org/10.1016/j.jmb.2008.06.068

Morabbi Heravi, K., Lange, J., Watzlawick, H., Kalinowski, J., & Altenbuchner, J. (2015). Transcriptional Regulation of the Vanillate Utilization Genes (vanABK Operon) of Corynebacterium glutamicum by VanR, a PadR-Like Repressor. *Journal of Bacteriology*, *197*(5), 959–972. https://doi.org/10.1128/jb.02431-14

Na, D., & Lee, D. (2010). RBSDesigner: Software for designing synthetic ribosome binding sites that yields a desired level of protein expression. *Bioinformatics*, *26*(20), 2633–2634. https://doi.org/10.1093/bioinformatics/btq458

Naseri, G., & Koffas, M. A. G. (2020). Application of combinatorial optimization strategies in synthetic biology. *Nature Communications*, *11*(1), 2446. https://doi.org/10.1038/s41467-020-16175-y

Ow, D. S.-W., Nissom, P. M., Philp, R., Oh, S. K.-W., & Yap, M. G.-S. (2006). Global transcriptional analysis of metabolic burden due to plasmid maintenance in *Escherichia coli* DH5α during batch fermentation. *Enzyme and Microbial Technology*, *39*(3), 391–398. https://doi.org/10.1016/j.enzmictec.2005.11.048

Qian, Y., Huang, H.-H., Jiménez, J. I., & Del Vecchio, D. (2017). Resource Competition Shapes the Response of Genetic Circuits. *ACS Synthetic Biology*, *6*(7), 1263–1272. https://doi.org/10.1021/acssynbio.6b00361

Reeve, B., Hargest, T., Gilbert, C., & Ellis, T. (2014). Predicting Translation Initiation Rates for Designing Synthetic Biology. *Frontiers in Bioengineering and Biotechnology*, *2*. https://www.frontiersin.org/articles/10.3389/fbioe.2014.00001

Ringquist, S., Shinedling, S., Barrick, D., Green, L., Binkley, J., Stormo, G. D., & Gold, L. (1992). Translation initiation in Escherichia coli: Sequences within the ribosome-binding site. *Molecular Microbiology*, *6*(9), 1219–1229. https://doi.org/10.1111/j.1365-2958.1992.tb01561.x

Roots, C. T., Lukasiewicz, A., & Barrick, J. E. (2021). OSTIR: Open source translation initiation rate prediction. *Journal of open source software*, *6*(64), 3362. https://doi.org/10.21105/joss.03362

Rouches, M. V., Xu, Y., Cortes, L. B. G., & Lambert, G. (2022). A plasmid system with tunable copy number. *Nature Communications*, *13*(1), 3908. https://doi.org/10.1038/s41467-022-31422-0

Salis, H. M. (2011). The ribosome binding site calculator. *Methods in Enzymology*, *498*, 19–42. https://doi.org/10.1016/B978-0-12-385120-8.00002-4

Salis, H. M., Mirsky, E. A., & Voigt, C. A. (2009). Automated design of synthetic ribosome binding sites to control protein expression. *Nature Biotechnology*, *27*(10), Article 10. https://doi.org/10.1038/nbt.1568

Seo, S. W., Yang, J.-S., Kim, I., Yang, J., Min, B. E., Kim, S., & Jung, G. Y. (2013). Predictive design of mRNA translation initiation region to control prokaryotic translation efficiency. *Metabolic Engineering*, *15*, 67–74. https://doi.org/10.1016/j.ymben.2012.10.006

Shine, J., & Dalgarno, L. (1974). The 3′-Terminal Sequence of Escherichia coli 16S Ribosomal RNA: Complementarity to Nonsense Triplets and Ribosome Binding Sites. *Proceedings of the National Academy of Sciences of the United States of America*, *71*(4), 1342–1346.

Silva-Rocha, R., Martínez-García, E., Calles, B., Chavarría, M., Arce-Rodríguez, A., de las Heras, A., Páez-Espino, A. D., Durante-Rodríguez, G., Kim, J., Nikel, P. I., Platero, R., & de Lorenzo, V. (2013). The Standard European Vector Architecture (SEVA): A coherent platform for the analysis and deployment of complex prokaryotic phenotypes. *Nucleic Acids Research*, *41*(D1), D666–D675. https://doi.org/10.1093/nar/gks1119

Stenström, C. M., & Isaksson, L. A. (2002). Influences on translation initiation and early elongation by the messenger RNA region flanking the initiation codon at the 3′ side. *Gene*, *288*(1), 1–8. https://doi.org/10.1016/S0378-1119(02)00501-2

Storch, M., Casini, A., Mackrow, B., Fleming, T., Trewhitt, H., Ellis, T., & Baldwin, G. S. (2015). BASIC: A New Biopart Assembly Standard for Idempotent Cloning Provides Accurate, Single-Tier DNA Assembly for Synthetic Biology. *ACS Synthetic Biology*, *4*(7), 781–787. https://doi.org/10.1021/sb500356d

Strasser, M., Theis, F. J., & Marr, C. (2012). Stability and Multiattractor Dynamics of a Toggle Switch Based on a Two-Stage Model of Stochastic Gene Expression. *Biophysical Journal*, *102*(1), 19–29. https://doi.org/10.1016/j.bpj.2011.11.4000

Studer, S. M., & Joseph, S. (2006). Unfolding of mRNA Secondary Structure by the Bacterial Translation Initiation Complex. *Molecular Cell*, *22*(1), 105–115. https://doi.org/10.1016/j.molcel.2006.02.014

Tas, H., Grozinger, L., Stoof, R., de Lorenzo, V., & Goñi-Moreno, Á. (2021). Contextual dependencies expand the re-usability of genetic inverters. *Nature Communications*, *12*(1), 355. https://doi.org/10.1038/s41467-020-20656-5

Thanbichler, M., Iniesta, A. A., & Shapiro, L. (2007). A comprehensive set of plasmids for vanillate- and xylose-inducible gene expression in Caulobacter crescentus. *Nucleic Acids Research*, *35*(20), e137. https://doi.org/10.1093/nar/gkm818

Thiel, K., Mulaku, E., Dandapani, H., Nagy, C., Aro, E.-M., & Kallio, P. (2018). Translation efficiency of heterologous proteins is significantly affected by the genetic context of RBS sequences in engineered cyanobacterium Synechocystis sp. PCC 6803. *Microbial Cell Factories*, *17*(1), 34. https://doi.org/10.1186/s12934-018-0882-2

Tzareva, N. v., Makhno, V. i., & Boni, I. v. (1994). Ribosome-messenger recognition in the absence of the Shine-Dalgarno interactions. *FEBS Letters*, *337*(2), 189–194. https://doi.org/10.1016/0014-5793(94)80271-8

Vellanoweth, R. L., & Rabinowitz, J. C. (1992). The influence of ribosome-binding-site elements on translational efficiency in Bacillus subtilis and Escherichia coli in vivo. *Molecular Microbiology*, *6*(9), 1105–1114. https://doi.org/10.1111/j.1365-2958.1992.tb01548.x

Vimberg, V., Tats, A., Remm, M., & Tenson, T. (2007). Translation initiation region sequence preferences in Escherichia coli. *BMC Molecular Biology*, *8*(1), 100. https://doi.org/10.1186/1471-2199-8-100

Vind, J., Sørensen, M. A., Rasmussen, M. D., & Pedersen, S. (1993). Synthesis of Proteins in *Escherichia coli* is Limited by the Concentration of Free Ribosomes. *Journal of Molecular Biology*, *231*(3), 678–688. https://doi.org/10.1006/jmbi.1993.1319

Waks, Z., & Silver, P. A. (2009). Engineering a Synthetic Dual-Organism System for Hydrogen Production. *Applied and Environmental Microbiology*, *75*(7), 1867–1875. https://doi.org/10.1128/AEM.02009-08

Weiss, J. N. (1997). The Hill equation revisited: Uses and misuses. *The FASEB Journal*, *11*(11), 835–841. https://doi.org/10.1096/fasebj.11.11.9285481

Wu, M., Su, R.-Q., Li, X., Ellis, T., Lai, Y.-C., & Wang, X. (2013). Engineering of regulated stochastic cell fate determination. *Proceedings of the National Academy of Sciences*, *110*(26), 10610–10615. https://doi.org/10.1073/pnas.1305423110

Zelcbuch, L., Antonovsky, N., Bar-Even, A., Levin-Karp, A., Barenholz, U., Dayagi, M., Liebermeister, W., Flamholz, A., Noor, E., Amram, S., Brandis, A., Bareia, T., Yofe, I., Jubran, H., & Milo, R. (2013). Spanning high-dimensional expression space using ribosome-binding site combinatorics. *Nucleic Acids Research*, *41*(9), e98. https://doi.org/10.1093/nar/gkt151

Appendix

Appendix A: Sequences

Table 13. Sequences of DNA modules used in this work.

Gene/Part	Sequence
P_{Van}	ATTGGATCCAATTGACAGCTAGCTCAGTCCTAGGTACCATTGGATCCAAT
P_{Cym}	AACAAACAGACAATCTGGTCTGTTTGTATTATGGAAAATTTTTCTGTATAATAGAT TCAACAAACAGACAATCTGGTCTGTTTGTATTAT
P_{J23104}	TTGACAGCTAGCTCAGTCCTAGGTATTGTGCTAGC
mKate	ATGTCAGAATTAATTAAAGAAAATATGCACATGAAATTATATATGGAAGGTACTG TCAACAATCATCATTTCAAATGCACATCCGAAGGTGAAGGTAAACCATATGAAGG CACACAAACAATGCGCATCAAAGCAGTTGAAGGTGGACCCCTGCCCTTTGCGTTT GACATTCTCGCAACGAGCTTTATGTACGGGTCTAAAACTTTTATCAATCACACCCA AGGCATTCCTGACTTTTTTAAACAGTCCTTTCCTGAAGGCTTTACCTGGGAACGTG TAACAACTTATGAAGATGGCGGTGTACTTACAGCAACTCAAGATACGAGTTTACA AGATGGCTGTCTGATTTACAATGTTAAAATCCGTGGCGTAAATTTCCCGAGTAAC GGACCCGTAATGCAAAAAAAAACTCTTGGTTGGGAAGCATCAACAGAAACCTTA TATCCTGCGGACGGTGGCTTAGAAGGACGCGCAGACATGGCACTGAAATTAGTTG GAGGCGGTCATTTAATCTGCAACCTGAAAACAACCTATCGTTCCAAAAAACCCGC TAAAAACCTTAAAATGCCTGGAGTATACTATGTTGATCGTCGCTTAGAACGTATT AAAGAAGCTGATAAAGAAACCTACGTTGAACAACATGAAGTAGCCGTAGCCCGT TATTGTGACCTTCCGTCGAAATTAGGACATCGTTGA
sfGFP	ATGCGTAAAGGCGAAGAGCTGTTCACTGGTGTCGTCCCTATTCTGGTGGAACTGG ATGGTGATGTCAACGGTCATAAGTTTTCCGTGCGTGGCGAGGGTGAAGGTGACGC AACTAATGGTAAACTGACGCTGAAGTTCATCTGTACTACTGGTAAACTGCCGGTA CCTTGGCCGACTCTGGTAACGACGCTGACTTATGGTGTTCAGTGCTTTGCTCGTTA TCCGGACCATATGAAGCAGCATGACTTCTTCAAGTCCGCCATGCCGGAAGGCTAT GTGCAGGAACGCACGATTTCCTTTAAGGATGACGGCACGTACAAAACGCGTGCG GAAGTGAAATTTGAAGGCGATACTCTGGTAAACCGCATTGAGCTGAAAGGCATTG ACTTTAAAGAAGACGGCAATATCCTGGGCCATAAGCTGGAATACAATTTTAACAG CCACAATGTTTACATCACCGCCGATAAACAAAAAAATGGCACTAAAGCGAATTTT AAAATTCGCCACAACGTGGAGGATGGCAGCGTGCAGCTGGCTGATCACTACCAG CAAAACACTCCAATCGGTGATGGTCCTGTTCTGCTGCCAGACAATCACTATCTGA GCACGCAAAGCGTTCTGTCTAAAGATCCGAACGAGAAACGCGATCATATGGTTCT GCTGGAGTTCGTAACCGCAGCGGGCATCACGCATGGTATGGATGAACTGTAC
VanR	ATGGACATGCCTCGTATTAAACCGGGTCAGCGTGTTATGATGGCACTGCGTAAAA TGATTGCAAGCGGTGAAATCAAAAGTGGTGAACGTATTGCAGAAATTCCGACCGC AGCAGCACTGGGTGTTAGCCGTATGCCGGTTCGTATCGCACTGCGTTCACTGGAA CAAGAAGGTCTGGTTGTTCGTCTGGGTGCACGTGGTTATGCAGCCCGTGGTGTTA GCAGCGATCAGATTCGTGATGCAATTGAAGTTCGTGGTGTTCTGGAAGGTTTTGC AGCACGTCGTCTGGCAGAACGTGGTATGACCGCAGAAACCCATGCACGTTTTGTT GTACTGATTGCAGAAGGTGAAGCACTGTTTGCAGCCGGTCGCCTGAATGGTGAAG ATCTGGATCGTTATGCCGCATATAATCAGGCATTTCATGATACCCTGGTTAGCGCA GCAGGTAATGGTGCAGTTGAAAGCGCACTGGCACGTAATGGTTTTGAACCGTTTG CAGCAGCCGGTGCACTGGCCCTGGATCTGATGGACCTGTCTGCCGAATATGAACA TCTGCTGGCAGCACATCGTCAGCATCAGGCAGTTCTGGATGCAGTTAGCTGTGGT GATGCCGAAGGTGCAGAACGTATTATGCGTGATCATGCACTGGCAGCAATTCGTA

	ATGCAAAAGTTTTTGAAGCAGCAGCAAGCGCAGGCGCACCGCTGGGTGCAGCAT GGTCAATTCGTGCAGATTGA
CymR	ATGAGCCCGAAACGTCGTACCCAGGCAGAACGTGCAATGGAAACCCAGGGTAAA CTGATTGCAGCAGCACTGGGTGTTCTGCGTGAAAAAGGTTATGCAGGTTTTCGTA TTGCAGATGTTCCGGGTGCAGCCGGTGTTAGCCGTGGTGCACAGAGCCATCATTT TCCGACCAAACTGGAACTGCTGCTGGCAACCTTTGAATGGCTGTATGAGCAGATT ACCGAACGTAGCCGTGCACGTCTGGCAAAACTGAAACCGGAAGATGATGTTATTC AGCAGATGCTGGATGATGCAGCAGAATTTTTTCTGGATGATGATTTTAGCATCGG CCTGGATCTGATTGTTGCAGCAGATCGTGATCCGGCACTGCGTGAAGGTATTCAG CGTACCGTTGAACGTAATCGTTTTGTTGTTGAAGATATGTGGCTGGGTGTGCTGGT GAGCCGTGGTCTGAGCCGTGATGATGCCGAAGATATTCTGTGGCTGATTTTTAAC AGCGTTCGTGGTCTGGTAGTTCGTAGCCTGTGGCAGAAAGATAAAGAACGTTTTG AACGTGTGCGTAATAGCACCCTGGAAATTGCACGTGAACGTTATGCAAAATTCAA ACGTTGA
UTR2	TGTTACTATTGGCTGAGATAAGGGTAGCAGAA
UTR3	GTATCTCGTGGTCTGACGGTAAAATCTATTGT
RBS1	ATCACACAGGACTA
RBS2	AAAGAGGGGAAATA
RBS3	AAAGAGGAGAAATA
pBBR1	CTACCGGCGCGGCAGCGTTACCCGTGTCGGCGGCTCCAACGGCTCGCCATCGTCC AGAAAACACGGCTCATCGGGCATCGGCAGGCGCTGCTGCCCGCGCCGTTCCCATT CCTCCGTTTCGGTCAAGGCTGGCAGGTCTGGTTCCATGCCCGGAATGCCGGGCTG GCTGGGCGGCTCCTCGCCGGGGCCGGTCGGTAGTTGCTGCTCGCCCGGATACAGG GTCGGGATGCGGCGCAGGTCGCCATGCCCCAACAGCGATTCGTCCTGGTCGTCGT GATCAACCACCACGGCGGCACTGAACACCGACAGGCGCAACTGGTCGCGGGGCT GGCCCCACGCCACGCGGTCATTGACCACGTAGGCCGACACGGTGCCGGGGCCGTT GAGCTTCACGACGGAGATCCAGCGCTCGGCCACCAAGTCCTTGACTGCGTATTGG ACCGTCCGCAAAGAACGTCCGATGAGCTTGGAAAGTGTCTTCTGGCTGACCACCA CGGCGTTCTGGTGGCCCATCTGCGCCACGAGGTGATGCAGCAGCATTGCCGCCGT GGGTTTCCTCGCAATAAGCCCGGCCCACGCCTCATGCGCTTTGCGTTCCGTTTGCA CCCAGTGACCGGGCTTGTTCTTGGCTTGAATGCCGATTTCTCTGGACTGCGTGGCC ATGCTTATCTCCATGCGGTAGGGGTGCCGCACGGTTGCGGCACCATGCGCAATCA GCTGCAACTTTTCGGCAGCGCGACAACAATTATGCGTTGCGTAAAAGTGGCAGTC AATTACAGATTTTCTTTAACCTACGCAATGAGCTATTGCGGGGGGGTGCCGCAATG AGCTGTTGCGTACCCCCCTTTTTTAAGTTGTTGATTTTTAAGTCTTTCGCATTTCGC CCTATATCTAGTTCTTTGGTGCCCAAAGAAGGGCACCCCTGCGGGGTTCCCCCAC GCCTTCGGCGCGGCTCCCCCTCCGGCAAAAAGTGGCCCCTCCGGGGCTTGTTGAT CGACTGCGCGGCCTTCGGCCTTGCCCAAGGTGGCGCTGCCCCCTTGGAACCCCCG CACTCGCCGCCGTGAGGCTCGGGGGGCAGGCGGGCGGGCTTCGCCCTTCGACTGC CCCCACTCGCATAGGCTTGGGTCGTTCCAGGCGCGTCAAGGCCAAGCCGCTGCGC GGTCGCTGCGCGAGCCTTGACCCGCCTTCCACTTGGTGTCCAACCGGCAAGCGAA GCGCGCAGGCCGCAGGCCGGAGGCTTTTCCCCAGAGAAAATTAAAAAAATTGAT GGGGCAAGGCCGCAGGCCGCGCAGTTGGAGCCGGTGGGTATGTGGTCGAAGGCT GGGTAGCCGGTGGGCAATCCCTGTGGTCAAGCTCGTGGGCAGGCGCAGCCTGTCC ATCAGCTTGTCCAGCAGGGTTGTCCACGGGCCGAGCGAAGCGAGCCAGCCGGTG GCCGCTCGCGGCCATCGTCCACATATCCACGGGCTGGCAAGGGAGCGCAGCGAC CGCGCAGGGCGAAGCCCGGAGAGCAAGCCCGTAGGGGG
Km^R	TTGTGTCTCAAAATCTCTGATGTTACATTGCACAAGATAAAAATATATCATCATGA ACAATAAAACTGTCTGCTTACATAAACAGTAATACAAGGGGTGTTATGAGCCATA

TTCAGCGTGAAACGAGCTGTAGCCGTCCGCGTCTGAACAGCAACATGGATGCGGA
TCTGTATGGCTATAAATGGGCGCGTGATAACGTGGGTCAGAGCGGCGCGACCATT
TATCGTCTGTATGGCAAACCGGATGCGCCGGAACTGTTTCTGAAACATGGCAAAG
GCAGCGTGGCGAACGATGTGACCGATGAAATGGTGCGTCTGAACTGGCTGACCG
AATTTATGCCGCTGCCGACCATTAAACATTTTATTCGCACCCCGGATGATGCGTGG
CTGCTGACCACCGCGATTCCGGGCAAAACCGCGTTTCAGGTGCTGGAAGAATATC
CGGATAGCGGCGAAAACATTGTGGATGCGCTGGCCGTGTTTCTGCGTCGTCTGCA
TAGCATTCCGGTGTGCAACTGCCCGTTTAACAGCGATCGTGTGTTTCGTCTGGCCC
AGGCGCAGAGCCGTATGAACAACGGCCTGGTGGATGCGAGCGATTTTGATGATG
AACGTAACGGCTGGCCGGTGGAACAGGTGTGGAAAGAAATGCATAAACTGCTGC
CGTTTAGCCCGGATAGCGTGGTGACCCACGGCGATTTTAGCCTGGATAACCTGAT
TTTCGATGAAGGCAAACTGATTGGCTGCATTGATGTGGGCCGTGTGGGCATTGCG
GATCGTTATCAGGATCTGGCCATTCTGTGGAACTGCCTGGGCGAATTTAGCCCGA
GCCTGCAAAAACGTCTGTTTCAGAAATATGGCATTGATAATCCGGATATGAACAA
ACTGCAATTTCATCTGATGCTGGATGAATTTTTCTAATAATTAATTG

Table 14. Sequences of primers used in this work.

Primer	Sequence
LMP-F	CGTGGAAACACTATTATCTGGTGGG
LMP-R	CCCACCAGATAATAGTGTTTCCACG
LMS-R	CCGAAGTTACACCAGATTGGACTG
UTR2-R	GCTACCCTTATCTCAGCCAATAG
UTR3-R	GATTTTACCGTCAGACCACGAG

Appendix B: Toggle Switch Verification via Gel Electrophoresis

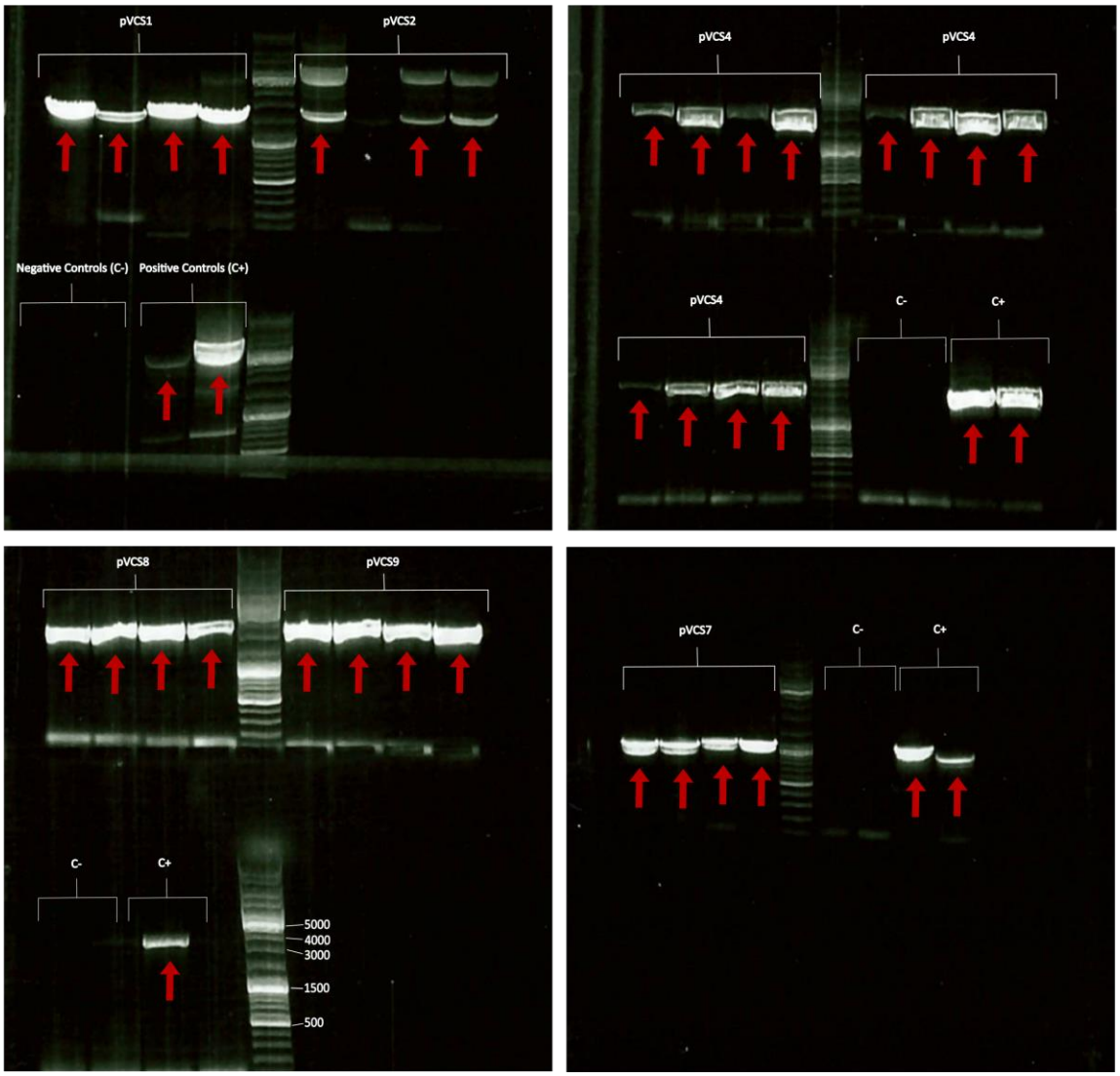

Fig. 12. Verification of correct transformation of the pVCS series into *P. putida* via gel electrophoresis. A minimum of 4 colonies were tested for each plasmid via colony PCR and subsequent gel electrophoresis. The DNA ladder (bottom left) allows for determination of band sizes (unit: base pairs). Red arrows indicate positive colony samples carrying the pVCS plasmid with an expected size of ca. 3600 bp. An extracted pVCS plasmid sample and a successfully transformed colony served each as positive controls (C+), while a plasmid lacking colony and a plasmid DNA lacking sample were used each as negative controls (C-).

Appendix C: Preliminary Ethanol Toxicity Test

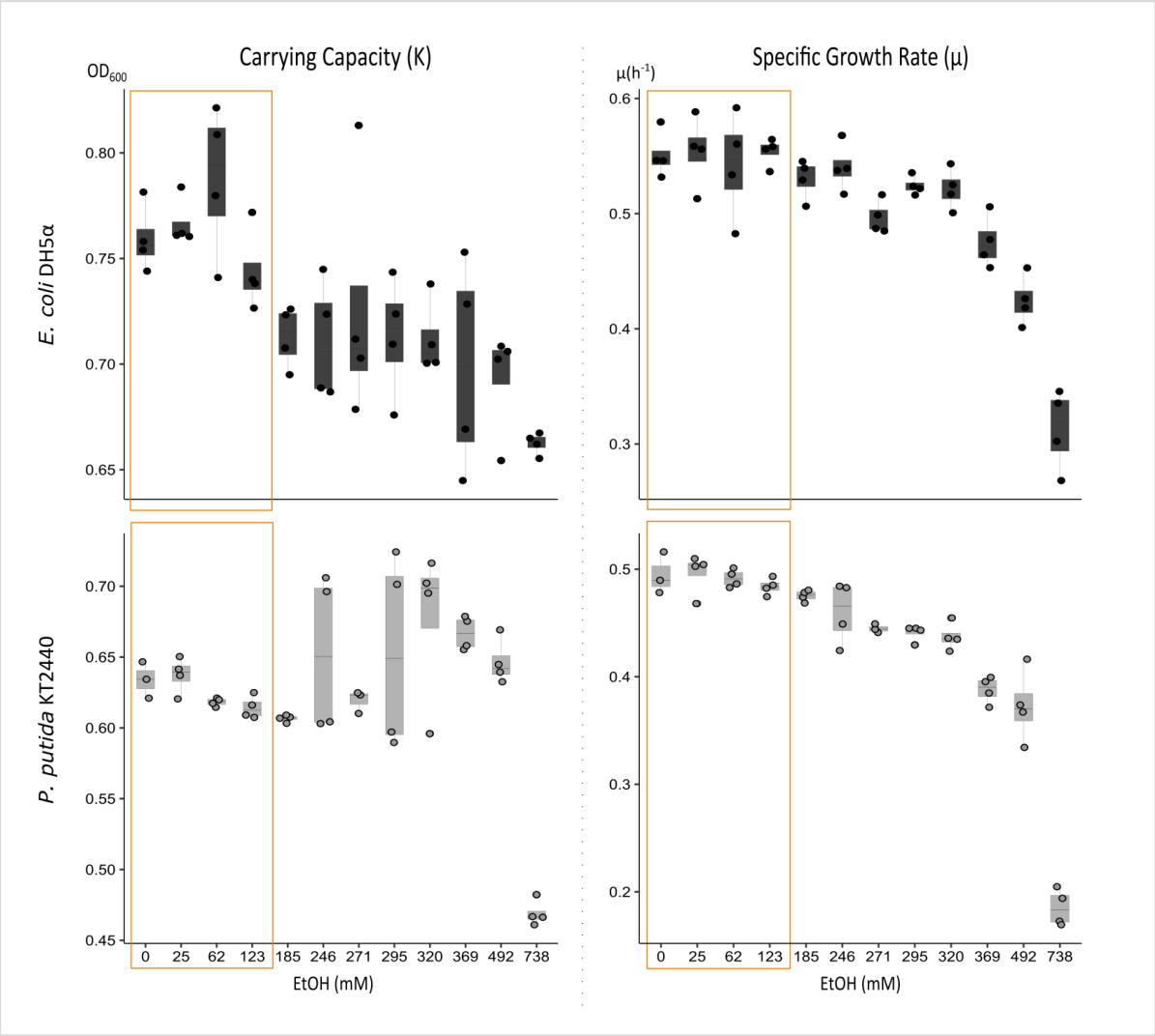

Fig. 13. The concentration range of Ethanol used in this work shows no growth inhibiting effects on the WT host organisms. OD_{600} values were measured during incubation of WT strains exposed to different concentrations of EtOH under standardized conditions (n=4). Carrying capacity (K) and specific growth rate (μ) were calculated for *P. putida* WT (grey) and *E. coli* (black). The concentration range of EtOH used in this work is marked orange and is not associated with growth diminishing effects.

Appendix D: Preliminary RBS Strength Verification

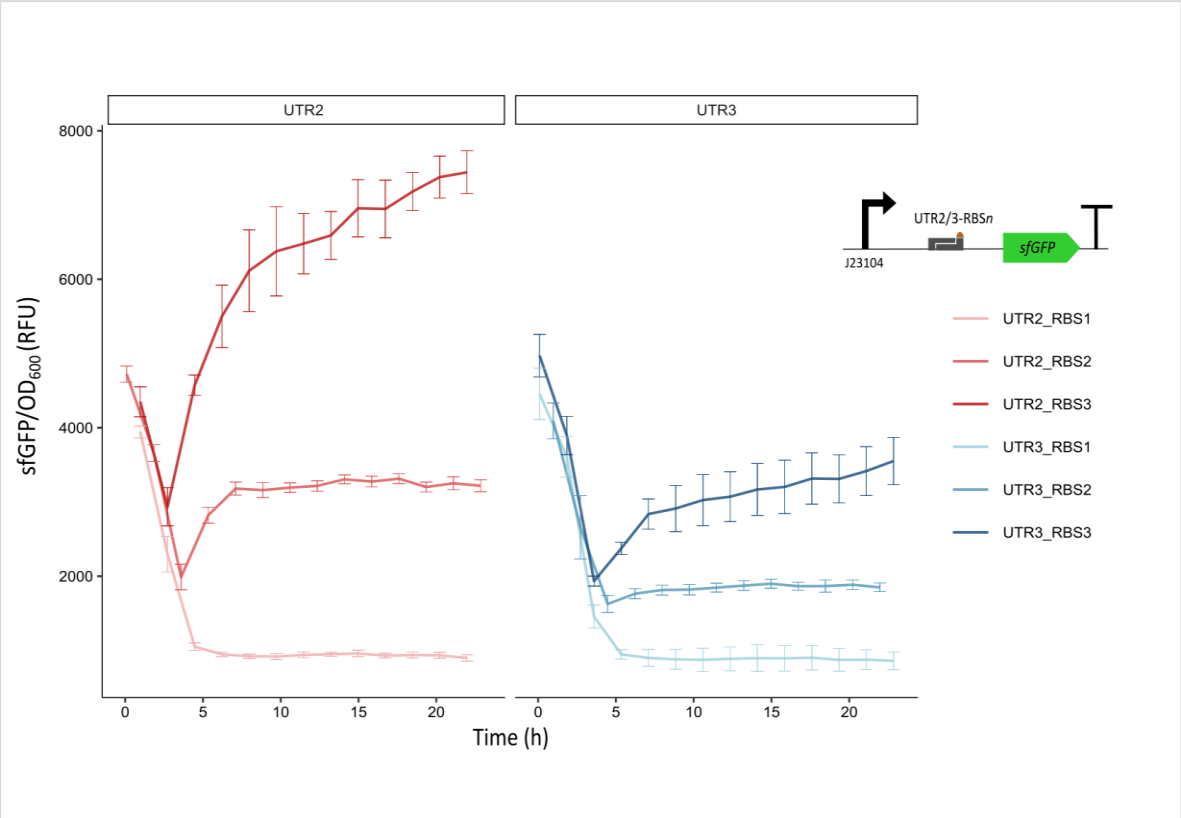

Fig. 14. Fluorescence intensities increase with increasing RBS strengths, while varying across UTR. A preliminary construct was assembled to verify pre-defined RBS strengths by linking a constitutive promoter (J23104) to each RBS variant including the respective untranslated region (UTR) and a sfGFP fluorescence reporter. Fluorescence was measured under standardized conditions (n=8) and normalized against OD_{600}. Error bars show standard deviation.